Fast determination of gasoline related compounds in groundwater by differential ion mobility spectrometry

Dissertation

zur Erlangung des akademischen Grades eines

Doktors der Naturwissenschaften

– Dr. rer. nat. –

vorgelegt von

Feng Liang

geboren in Jiangsu, V.R. China

Fakultät für Chemie

der

Universität Duisburg-Essen

2014

Die vorliegende Arbeit wurde im Zeitraum von 10,2010 bis 9,2013 im Arbeitskreis von PD. Dr. Ursula Telgheder am Fakultät für Chemie der Universität Duisburg-Essen durchgeführt.

Tag der Disputation: 27.05.2014

Gutachter: PD. Dr. Ursula Telgheder

            PD. Dr. Wolfgang Schrader

Vorsitzender: Prof. Dr. Elke Sumfleth

Abstract

Groundwater can be contaminated when e.g. gasoline tanks leak. The analysis for gasoline related compounds in groundwater is generally done on lab using standard methods. Due to sampling and lab analysis, groundwater monitoring is time consuming and expensive. It is very important to develop methods to fast monitor before lab analysis. Although the technologies developed for rapid on-site analysis of gasoline contaminated groundwater exist in commercial market, they still face the technical limitation to distinguish the gasoline from complex matrices.

Different ion mobility spectrometry (DMS) can separate different gasoline related compounds dependent on the mobilities of chemical compounds at high and low electric fields. Coupled to micro gas chromatography column, DMS can distinguish the target gasoline compounds from the complicated gasoline matrix and the surrounding environment in short time. In this work, a fast method based on GC-DMS for the detection of gasoline related compounds in groundwater has been developed.

The gasoline related compounds benzene, toluene, ethylbenzene and xylene (BTEX) were selected as fingerprint substances. A short column MXT-5 was utilized for separating the target compounds (BTEX) in groundwater. The analysis time is less than 2 min.

In order to improve the detection limits and the sensitivity, a krypton UV lamp is utilized as ionization source instead of ^{63}Ni. After optimizing the operation condition, The detection limits of BTEX determined by GC-UV-DMS are 0,15 mg/L for toluene, 0,12 mg/L for ethylbenzene, 0,15 mg/L for m-xylene, 0,16 mg/L for p-xylene, 0,16 mg/L for o-xylene, respectively, which are 30 to 330 fold lower than those obtained by GC-^{63}Ni-DMS. However, the detection limit of benzene is 0,08 mg/L, which is above the MCL recommended by WHO.

Finally, the GC-UV-DMS is used to analyze the concentrations of BTEX in 17 real groundwater samples collected from contaminated sites. In comparison with

the reference method, the results of EXT obtained by this GC-UV-DMS are in good agreement with those obtained by reference method. To simulate the on field condition, a simulation system is built up. Temperature and matrix components influence the diffusion of BTEX in groundwater.

The results reveal that the method based on GC-UV-DMS is feasible to be applied as a fast system to monitor the groundwater.

Content

1. Introduction

1.1Groundwater contamination by gasoline

Groundwater is the most abundant source of readily available freshwater in the world, excluding polar caps and glaciers, making up 97% of all freshwater. Groundwater fulfills different functions and is widely used for food production, irrigation and industrial cooling. The groundwater is one of the most important resources for drinking water. In European Union (EU), about 75% of EU residents are depending on groundwater for their water supply [1]. Besides use to support human activity, groundwater also plays a significant role in supporting and enabling ecosystem functions. It is well known that groundwater supports surface water flows and their dependent aquatic and terrestrial ecosystem.

In early times, it was thought that groundwater have sufficient protection by soils and rocks which overlay groundwater. However, through natural and human activity, the groundwater source is at risk of contamination from a variety of pollutants such as physical, chemical, and biological contaminants. One of contamination of groundwater is hydrocarbons, which enter the environment through improper use, waste disposal and leaking storage facilities. Petroleum based fuels such as gasoline and diesel are one of the best known classes of groundwater contaminants. In 1971, a gasoline pipeline in Pennsylvania, United States broke and several hundred gallons of gasoline released into the groundwater. From then, contaminant of groundwater by petroleum products has appeared as a new environmental challenge. Until 2012, over 470,000 confirmed releases of petroleum based fuels from leaking underground storage tanks have been recorded in USA[2]. In Europe, as shown in Figure 1.1, main pollutants for soil and groundwater are mineral oil, aromatic hydrocarbons (mainly BTEX) and polycyclic aromatic hydrocarbons (PAH) (total about 53%), higher than the heavy metals pollution 37,3%. Furthermore, in some European countries, the percentages of mineral oil contaminations are

higher to 67,9% in Czech Republic, 52% in Italy and 45% in Luxembourg, respectively[1]. For the purposes of assessing groundwater chemical status, the groundwater quality standards have been established in Directive 2000/60/EC [3]. Contamination of groundwater with gasoline occurs at many sites, particularly those associated with petrochemical industry such as former gaswork sites, landfills and petroleum stations.
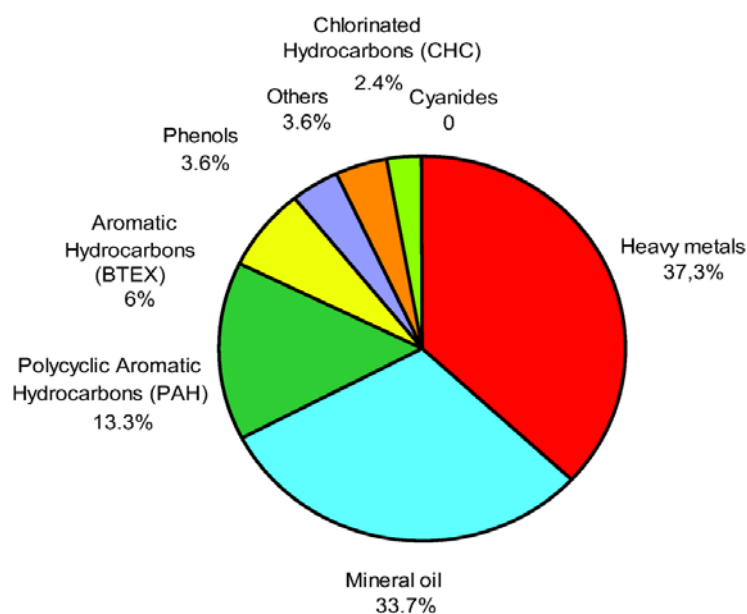
Figure 1.1: Overview of contaminants affecting soil and groundwater in Europe [1]

1.2 Emerging sensor technologies for monitoring VOCs in groundwater

The groundwater monitoring is important for characterization, assessment and remediation of contaminated groundwater. For example, during a remedial investigation, groundwater samples are collected and analyzed to determine the types of contaminants present and the horizontal and vertical extent of those contaminants. The resulting data provide much of the information necessary to determine an effective remedial approach. Once a remedy is selected and operational, ground water monitoring is used to determine the progress of remediation and to ensure the remedy is operating effectively.

It is still a big challenge to monitor groundwater. In many countries, groundwater quality monitoring has been a neglected point in overall

environmental surveillance, even in European Community and other industrialized countries. The capital costs and monitoring techniques associated with dedicated, customer-built, monitoring networks are the significant challenges to overcome.

EC Water Framework Directive (2000/60/EC) and its associated daughter Groundwater Pollution Protection Directive (2006/118/EC) enforce the need for systematic monitoring and periodic assessment of groundwater quality, for management and protection measurements, and for evaluation of their effectiveness to further appropriate monitoring. In order to evaluate the current technologies, it is very important to establish the currently used procedures for sampling and analysis of groundwater.

VOC is one major of organic pollutants in groundwater. Analysis is generally lab basis done using gas chromatography (GC) coupled with mass spectrometry (MS) or other detectors like photoionization detector (PID) and an electrolytic conductivity detector (ECD). EPA 8260b and 8021b are more widely used [4, 5]. These lab methods are capable of detecting the more prevalent VOCs such as BTEX (benzene, toluene, ethylbenzene, and xylenes), trichloroethylene and halogenated hydrocarbons, when coupled with special methods to extract the substances from the water. The detection limits of GC methods are low to ppt[6]. However, the costs of these methods 8260b and 8021b are high and the analysis time is long (in the range of week). For example, based on the analytical costs $120 per sample for VOCs testing, the cost of testing samples from 30 wells with traditional lab methods is approximately $3600 [7]. The whole monitor procedure of 30 wells by traditional sampling and measurement at one site will cost approximately $10,000 to $15,000.

The development of method that can be used to monitor and characterize VOCs in water, which can provide cheap and reliable information about contamination, is required. Therefore, the effective sensor based instruments for groundwater monitoring are very useful to achieve this target. These sensor technologies can

distinguish the target analytes from other background chemicals, semi or quantify the concentration of analytes, and easy operation by user. Several main characteristics of sensor based technologies are: sensitivity, reliability, selectivity and speed[8]. All sensors should have been sensitive enough to detect VOCs in groundwater. Ideally, the detection limit for a particular compound should be lower than the legal maximum contaminant levels (MCLs). Practically, the sensors with detection limit higher than the MCL still provide meaningful results. Furthermore, the concentrations at a site may vary in a large range from ppt level to the high level. The results of these sensors should be reliable. The concentration determination from a particular sample or from samples with the same actual concentrations should be consistent with minimal variation. Additionally, the concentrations monitored by the technique should be closed to the actual concentrations of the sample being measured. A variety of contaminants may be contained in groundwater at hazardous waste sites. The sensor should be able to distinguish the target analytes from the other contaminants. Speed is also considered as one important factor for sensor to monitor groundwater. The instruments should be able to spend appropriate time to work. For long term monitoring, the time can be long if the device is fixed in place. Otherwise, if the device is moved from one well to another in a single sampling event, the analysis would be more frequent and the analysis time is required in the order of seconds or minutes.

Even though a number of technologies are currently being developed for in-situ sampling and analysis of VOCs in groundwater, each technology faces the technical problems such as distinguishing the target analyte from other substances in the surrounding environment and then accurately quantifying the amount. The following technologies partly overcome these technical problems but are still in various stages of development. A brief description and current efforts on techniques such as chemiresistor, surface acoustic wave sensors, and fiber optic sensor and quartz crystal microbalances will be present as follows.

Chemiresistors are comprised of a conductive polymer film applied to a micro-fabricated circuit[9]. When the analyte contacts with the polymer, it swells and changes the resistance leading to an electrical response. Each sensor includes an array of these resistors with different polymers. Mathematical analysis of the signals from each resistor is used to determine the concentrations of components within the sample. Because the vapor is used to be analyzed, the vapor phase concentration must be converted into an aqueous or liquid phase concentration using Henry's Law. In laboratory conditions, the sensor detection limit is approximately 0.1% of the saturated vapor pressure. For example, the detection limit for trichloroethylene translates to an aqueous concentration of approximately 1.000µg/L (compared to the MCL of 5 µg/L) and the detection limit of xylene is approximately 2.000 µg/L(compared to MCL of 10.000 µg/L) [10].

Chemiresistor has several advantages such as small size, low power usage and good sensitivity to various chemicals. In comparison with other standard electrochemical sensors, another advantage of chemiresistor is that it can work properly without liquid. A big drawback for chemiresistor is that it may not be able to discriminate the target compounds from the unknown complicated mixtures of chemicals. Durability of polymers in subsurface environments is uncertain when polymers react strongly to water vapor [11].

Surface Acoustic Wave Sensors (SAWS) utilize the piezoelectric effect to translate an electric signal into a mechanical wave [12]. The mechanical wave propagates through the material to another transducer which converts the wave back to an electrical signal. Surface acoustic wave devices specifically use the Rayleigh wave transverse and surface wave in operation. Normally, SAWS consist of an input and output transducer, a chemical adsorbent film on a quartz piezoelectric substrate. An acoustic wave launched by input transducer travels through the chemical film and is detected by an output transducer at a very high frequency 100 MHz. The velocity and attenuation of the signal are sensitive to

the viscoelasticity as well as the mass of the thin film, which can allow for the identification of the contaminant. After analysis, the chemical film can release chemicals from the device by heating. SAWS can detect chlorinated hydrocarbons, ketones, saturated hydrocarbons, aromatic hydrocarbons, organophosphates, and water. As well as chemiresistor, SAWS have a lot of advantage like good sensitivity to various chemicals, small size, low power consumptions, low detection limits for various chemicals. However, SAWS may not be able to discriminate target analytes among unknown mixtures of chemicals. The durability is very sensitive for water vapor.

Fiber Optic Sensors are a class of sensors that use optical fibers to detect chemical pollutants [13]. A light source generates light. Then the light is sent through an optical fiber. After scanning the sample, the light returns through the optical fiber and is captured by a photo detector. There are three general classes of fiber optic sensors. The first class of fiber optic sensors consist of an optic sensor coupled with a chemically interaction thin film attached to the tip. When the contaminant binds to the film, the concentration will be reflected by the color of the film, the refractive index, or the fluorescing intensity of film. The second type is completely passive. The light, which is reflected or emitted by the contaminant, is analyzed. The refractive index of the material at the tip of the optical fiber can be used to determine the phases. The third type of fiber optic sensors involves injection a reagent near the sensor. This reagent can react either chemically or biologically with the pollutants. Based on the amount of reaction products, the concentration of a contaminant can be obtained.

Detection limits of different type fiber optic sensors vary largely. As an example, the detection limits are 0,38 ppm for benzene, 0,30 ppm for toluene, 0,10 ppm for ethylbenzene and 0,13 ppm for xylenes [13]. Furthermore, a fiber optic probe based on lasers has been developed with detection in approximately 1 μg/L range for BTEX. Currently, the technology based on mid-infrared fiberoptic sensors can analyse concentrations of 5 to 10 various VOCs(including TCE,

tetrachloroethylene, and BTEX) in a single sample with detection limits of approximately 100 μg/L. Efforts with various lasers and membranes are focused on increasing the sensitivity to allow for detection in the 1 to 10 μg/L range. Another sensor has been developed with detection capability low to approximately 50 to 100 μg/L[13].

The advantages of fiber optic sensor are low power consumption; low detection limits for detecting various chemicals, a variable of spectroscopies can be used like Fourier transform infrared spectrometer, UV induced fluorescence spectroscopy. The drawbacks involve: limited ability to transmit light through the optical fiber over long distances; concentration range sensitivity may be limited; some organic contaminants are not easily differentiated using UV-visible spectroscopy or IR; the chemically sensitive coatings of sensors will degrade with time.

Quartz Crystal Microbalances (QCMs) coated with various polymers that selectively absorb the chemicals of interest are used in sensor technology [14]. The mass at the surface of the QCM changes, when the chemicals adsorb to the polymer. The resonant frequency can be measured electronically affecting by the mass on the QCM. In order to detect different compounds, different polymers can be developed. Like the chemiresistor technology, a single sensor includes multiple QCMs and chemometrics of the resulting signals is used to determine the concentrations and constituents of the sample. After calibration with specific standards, a variety of VOCs can be detected.

The vapors of target contaminants are selected and isolated from the surrounding groundwater by permeable membrane. For example, chlorinated compounds in vapor phase enter the chamber and adsorb to the polymers, and therefore, create a QCM response. The concentration of chlorinated pollutants is correlated to the aqueous or liquid phase concentration. If the device is moved to a different location, the time for equilibration is needed[15].

Ueyama et al. developed a water monitoring system based on polymer coated QCM chemical sensor, which can detect the oil in contaminated river water with threshold odor number less than three [14]. The detecting time was less than 5 min depending on the oil kindness and the sensitivity was kept steady for longer than 6 months with 400 detections of diesel and heavy oil. Dickert reported that the xylene isomers could be detected with an accuracy of about 1% in the range of 0-200 ppm by QCM [16]. They nearly eliminated the residual water cross-sensitivity of the sensor coatings, which allows effective work place or environmental monitoring of toxic compounds with fast response levels. A VOCs detecting sensor based on QCM was developed for the detection of toluene and p-xylene by Matsuguchi[15].

Bourgeois et al. demonstrated that a chemical sensor array can rapidly identify the presence of organic compounds (such as diesel) in a wastewater matrix [17]. Another advantage of QCMs is that it may be possible to discriminate the kind of pollutants. As reported by Ueyama, the response curve shape depends on the kinds of oil, which means the analysis of response curves might lead to the estimation of the kind of oil [14]. The data for the first several minutes are necessary for effective discrimination. The long-term performance is one of the key properties of a water monitoring system. The QCMs have a long life time. The development of a combined system, such as QCM and surface-plasma resonance (SPR) or other electrochemical measurement system would lead to next generation of sensing devices capable of providing a lot of additionally useful information in comparison to an individual technique [18, 19].

There are still several technical problems of QCMs to overcome. In many cases, the changes in temperature and humidity will lead to variation in the organic content of wastewater, which is detected. This shows the difficulty of establishing an independent relationship between the response of signal and pollutants content in samples. The calibration of the instrument using data acquired under wide ranging conditions is needed.

Differential ion mobility spectrometer (DMS) is a technique to identify and to detect ions at the ambient pressure. The ions have field dependent mobility in strong electric fields above 10.000 V/cm. Based on the nonlinear field dependence of the coefficient of mobility in high electric fields, DMS is fundamentally different from conventional low field techniques such as time of flight ion mobility spectrometry (IMS). It was found to be one of the most viable candidates for fast monitoring groundwater because of its simplicity and portability. DMS has been developed in the past for applications in a lot of fields. The historical development, principles and theory of DMS and the main applications of DMS on environmental monitoring will be presented in the following part.

1.3 History of differential ion mobility spectrometry development

In 1973, Mason and Daniel first described the phenomenon about ions nonlinear mobility in strong electric fields [20]. In the 1980's, M Gorshkov first proposed the method to use the differential mobility approach for ion separation in Soviet Union. Several years later, Buryakov et al. developed practical implementation of DMS [21].

There are two geometry types of the separation cell used for DMS: 1) a pair of cylindrical (or curved) electrodes and 2) a pair of flat planar electrodes.

The main milestones of development on cylindrical version are listed as follows: In 1995, Carnahan et al. reported the first commercial prototype of cylindrical design of DMS at *Proceeding of an Fourth International Workshop on IMS*, Cambridge, UK [22]. In 1999, Purves succeed to use DMS as an ion pre-filter for atmospheric pressure ionization mass spectrometry and called this system as FAIMS [23]. In 2000, Ionalytics company commercialized FAIMS and Thermofisher purchased Ionalytics in 2005.

Another type of DMS with planar electrode was developed in Soviet Union in the late 1980's[24]. In 2000, Miller et al. developed the first prototype of a micromachined DMS sensor (Figure 1.2) [25]. In 2005, Sacks et al. reported a

silicon microfabricated column with microfabricated differential mobility spectrometer for GC analysis of VOCs[26]. The prototypes of DMS coupled with GC were designed and built up. In 2006, MicroAnalyzer, a GC-DMS system combining sophisticated pre-concentration, flash thermal desorption, GC temperature ramping, and DMS separation and detection in a compact, portable and field deployable package, was commercialized by Sionex. In 2009, Shvartsburg utilized a multichannel (47 channels) microchip with 35 μm gaps in FAIMS (Figure 1.3)[27].

From the beginning of DMS, this technology made huge progress and applications of DMS/FAIMS grow rapidly[24]. At the early stage, the separation of ion species at a strong electrical field was observed and considered as interesting physical phenomena. Later, this method was exploited to a powerful and useful analytical device with varied application. Particularly, miniaturization and easy operation of DMS resulted in the attraction of more and more interest. The amount of publications increases each year, and the scientific community of ion mobility spectrometry broadens largely.
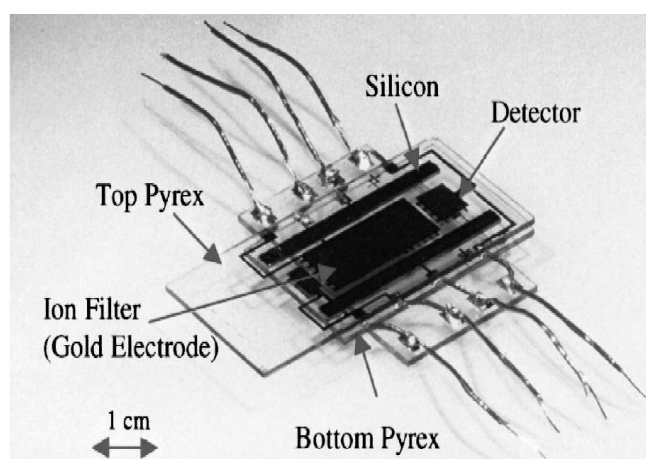
Figure 1.2: Photograph of a micromachined field asymmetric ion mobility spectrometer [25]
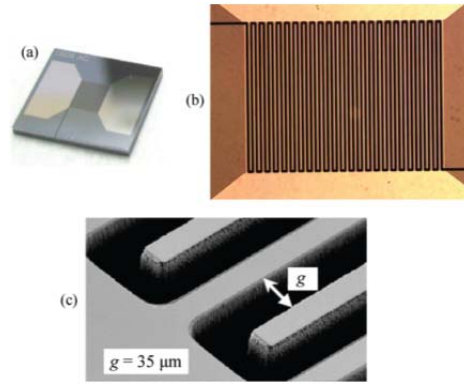
Figure 1.3**:** Photograph of the FAIMS microchip (a), its face exhibiting the serpentine channel (b), and electron micrograph showing detail of the gap entrance (c) [27].

1.4 Ion behavior in high electric field

In a low electric field (<10kV/cm) and under standard conditions of a pressure 101,3kPa and temperature 273 K, the mobility coefficient (K, $m^2/(V*s)$) of a singularly charged ions is principally governed by its reduced mass μ (kg) and the collision cross section Ω (m^2). As shown in Mason-Shramp equation (eq.1.1)[20], K can be described with relation to μ and Ω, where e, is the elementary charge constant, k_b is the Boltzmann constant (J/K), T_{eff} is effective temperature of the ion and is approximated to gas temperature and N is the molecular density of neutrals in the gas (the drift gas) supporting the ion ($2,69\times10^{25}$ m^{-3}).

$$K = \frac{3e}{16N} * (\frac{2\pi}{\mu k_b T_{eff}})^{\frac{1}{2}} * \frac{1}{\Omega} \qquad \text{(eq. 1.1)}$$

In higher electrical field (> 10 kV/cm), the effective temperature T_{eff} of the ion increase and can no longer be approximated to the gas temperature. With the increase of temperature, the cluster ion is modified, expand or contract, which result in a change in the collision cross-section parameter (Ω). The Mason-Shramp equation can be modified as follows:

$$K_{eff} = \frac{3e}{16N} * (\frac{2\pi}{\mu k_b T_{eff}})^{\frac{1}{2}} * \frac{1}{\Omega(T_{eff})} \quad \text{(eq. 1.2)}$$

In eq. 1.2, Ω is replaced by the effective ion temperature dependent collision cross section parameter ($\Omega(T_{eff})$).

Therefore, the mobility coefficient K is field dependent by virtue of the influence of the filed on the effective ion temperature and K is molecular specific on the basis of its dependence on Ω. Over a narrow field range, K is approximately proportional to $1/\Omega$. K is dependent on the size of the analyte molecule, from which the cluster ion is produced. In a fixed applied electric field, ion may be separated on their specific fixed mobility coefficient K[28].

When an ion passes through the gap between a pair of electrodes over which an oscillating asymmetric electric field is applied, the mobility of the ion will oscillate between a low field mobility (K_0), which is usually approximated to be representative of the zero field mobility and a high field mobility K(E). The FAIMS or DMS separates ions on the basis of differential mobility of ions in an oscillating asymmetric field.

As described by eq. 1.3, the filed dependency of K(E) is related to K_0, whereby α is the function of the K(E)/K_0 versus E curve

$$K(E) = K_0[1 + \alpha(E)] \text{ (eq. 1.3) [28]}$$

To an approximation over a narrow electric field range (0-30000V/cm), the α-function is closed to a polynomial expandable in even powers over E (eq. 1.4), where the coefficients α_1, α_2, …, α_n are specific to the ion, and more importantly the parent molecule forming the ion.

$$K(E) = K_0[1 + \alpha_1(E)^2 + \alpha_2(E)^4 + \cdots + \alpha_n(E)^{2n}] \text{ (eq. 1.4)}$$

The change in ion mobility under the influence of the high electric field intensity is also related to the gas density N. the eq. 1.4 can be modified to eq. 1.5 as follows:

$$K\left(\frac{E}{N}\right) = K_0\left[1 + \alpha_1\left(\frac{E}{N}\right)^2 + \alpha_2\left(\frac{E}{N}\right)^4 + \cdots + \alpha_n\left(\frac{E}{N}\right)^{2n}\right]$$

or

$$K\left(\frac{E}{N}\right) = K_0\left[1 + \alpha\left(\frac{E}{N}\right)\right] \text{ (eq. 1.5)}$$

where $\alpha\left(\frac{E}{N}\right) = \alpha_1\left(\frac{E}{N}\right)^2 + \alpha_2\left(\frac{E}{N}\right)^4 + \cdots + \alpha_n\left(\frac{E}{N}\right)^{2n}$.

The variation range of K with the electric field is defined by E/N, in which E is the electric field intensity and N is the gas density, namely the number of the gas molecule in unit volume. The unit of E/N is Townsend (Td). It is presumed that the electric field intensity is 1kV/cm, under standard conditions (pressure 101.3 kPa and temperature 273 K), the gas density N will be $2,7 \times 10^{19}$, The value of E/N is about $3,7 \times 10^{-17}$ V/cm^2. It is defined that 1 Td is equal to 1×10^{-17} V/cm^2, then the value of E/N is about 3,7 Td under standard conditions [29].

When E/N is about 40 Td, the ion mobility begins to change when the electrical field intensity increase. When the electrical filed intensity is over a certain value (>10kV/cm), the mobility of the ion will change nonlinearly with the electric field. Depending on the change of mobility, the ions can be sorted to three types *A*, *B* and *C*. With an increase of the electric field, the mobility of ion *A* will also increase. Otherwise, the mobility of ion *C* will decline when the electric field increases. The mobility of ion B will primarily increase and then decrease with the electric field increasing above 10 kV/cm. Generally, most of the ions with small mass to charge ratio (m/z <300) have *A* type mobility and the large molecular will have a behavior of mobility change as type *C*. However, the change in mobility is very complicated and will be related with the size of the ion, the structural rigidity and interaction between ion and molecule. Even today, due to technical difficulties, alpha parameters for atmosphere pressure conditions are available for only a few substances such as amines, chloride, kentones and positive and negative amino acids ions [24],[30],[31],[32].

1.5 Principle of differential ion mobility spectrometry

General principle for planar DMS/FAIMS for the separation of ions with different α is shown on Figure 1.3. When the high electric filed asymmetric waveform is applied to the narrow planar electric plates and the ion is brought into this electrical field by carrier gas, it will undergo oscillations between the two plate electrodes. For example, an ion into the electrical field, the oscillation routes with different α(E/N) values are shown in Figure 1.3. In t_1 of one

vibration period, corresponding with the electric field intensity E_1, these three type ions will move towards the upper plate of the electrode; while within t_2 of the vibration period, corresponding to the low electric field intensity E_2 (Figure 1.4), these three different species of ions will move towards the lower plate electrode; the vibration direction is vertical to the plate electrode.

During the t_1 and t_2, the ion can be approximated as a uniform motion. The velocities of the ion during t_1 and t_2 are supposed to v_1 and v_2 respectively. The time can be described as eq. 1.6 [24].
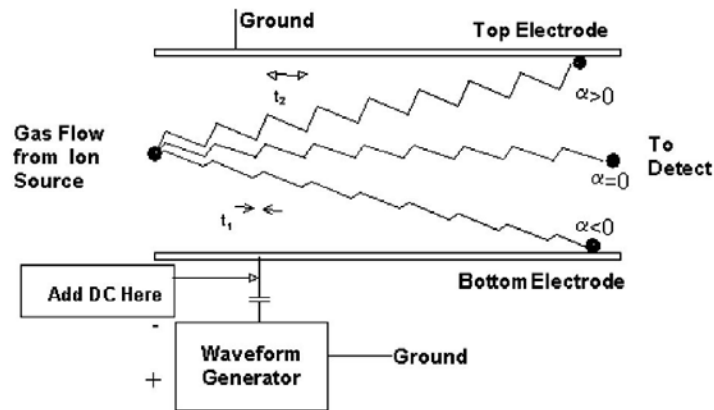

Figure 1.3: schematic of a differential ion mobility spectrometry and motion track of the ions with different α [33]
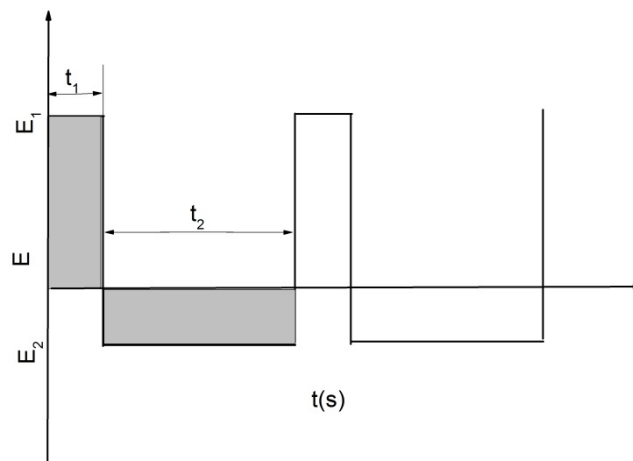

Figure 1.4: electric field of asymmetric rectangular waveform [24]

$$\Delta t = \frac{2mv_1}{qE_1} = \frac{2mK}{q} \qquad \text{(eq. 1.6)}$$

Where, q is the charge of the ion, K is the mobility of the ion and m is the mass of the ion. Compared with the radio frequency asymmetry waveform voltage period, Δt can be ignored.

As shown in Figure 1.4, the field is designed to satisfy the condition $E_1t_1=E_2t_2$, which means the integral peak above and below the time axis are equal.

If the $\alpha(E/N)=0$ ($K(E_1)=K(E_2)$), displacement of ions during the high and low portions of the applied field will be equal and opposite as described follows:

$$v_1t_1=v_2t_2=K(E_1)E_1t_1=K(E_2)E_2t_2 \qquad \text{(eq. 1.7)}$$

The sum in displacement of the ions during on period of the separation field will be zero.

If ion mobility significantly depends on electric filed strength ($\alpha(E/N)\neq0$), the displacement of ions during a period of the separation field will be not zero.

$$K(E_1)E_1t_1\neq K(E_2)E_2t_2 \qquad \text{(eq. 1.8)}$$

If $\alpha(E/N) > 0$, then the ions will be displaced towards the upper electrode at a distance ΔKE_1t_1. The extent of displacement depends on field waveform (ratio t_1/t_2), field amplitude (E_1), and ion mobility dependence (α_1). If $\alpha(E/N) < 0$, then the ions will be displaced towards the lower electrode.

When the net displacement per period of asymmetric filed is zero, the ions of analyte can pass through the gap between the electrodes. A displaced ion can be restored to the center of the gap by adding a low strength DC electric field (the compensation field, C) on the asymmetric waveform. Different ions with differing displacement, which depend on mobility in the high field condition, can pass through the gap at different compensation fields. Each particular ion can be characterized by using various strengths of C. Therefore, a scan of C will allow a complete measurement of ion species and the resultant scan of C with time will be referred as mobility scan due to C related with mobility.

From above, it can be concluded that the ion drift spectrometer can function as continuous ion filter. When the compensation voltage is set for a specific ion, only this ion can pass through the gap of electrodes, while others will be

neutralized by the electrode and remain in drift region. The DMS spectrogram of the ion can characterize all ions in the drift region when C is swept through a certain range.

Mathematical description of the DMS method is briefly presented below. The DMS field must satisfy the following conditions [34]:

Zero offset

$$\frac{1}{T}\int_0^T Sf(t)dt \equiv S\langle f(t)\rangle = 0 \qquad \text{(eq. 1.9)}$$

Asymmetry

$$\langle f^3\rangle = \int_0^T f^3(t)dt \neq 0 \qquad \text{(eq. 1.10)}$$

High frequency

$$F \gg \frac{\langle |f|\rangle SK}{2d} \qquad \text{(eq. 1.11)}$$

High strength

$$\frac{E_{BD}}{2} < S < E_{BD} \qquad \text{(eq. 1.12)}$$

Where $f(t)$ is a periodic normalized $\{max[f(t)] = 1\}$ function describing the separation waveform, S is the separation filed peak amplitude, E_{BD} is the break down electric field strength, T and F are separation field period and frequency, d is the distance between DMS electrodes, K is the approximate ion mobility coefficient for the analyte, and triangular brackets denote averaging over one period of separation field.

The net displacement per period of asymmetric field is zero after inputting a low strength DC electric field C, which can be present as follows,

$$l = \int_0^T v(t)\, dt = \int_0^T K(\frac{E}{N})(Sf(t) + C)\, dt = 0 \qquad \text{(eq. 1.13)}$$

To solve for C, eq. 1.5 is substituted into eq. 1.13

$$\int_0^T K_0\left(1 + \alpha\left(\frac{E}{N}\right)\right)(Sf(t) + C)dt = 0 \qquad \text{(eq. 1.14)}$$

it can be transformed to eq. 15

$$\langle\left(1 + \alpha\left(\frac{E}{N}\right)\right)(Sf(t) + C)\rangle = 0 \qquad \text{(eq. 1.15)}$$

Expanding alpha function by Taylor's theorem in terms of the small parameter C/S yields a first order approximation for the compensation field C.

$$C = \frac{S\langle \alpha f \rangle}{1+\langle \alpha \rangle + S\langle \alpha' f \rangle} \qquad \text{(eq. 1.16)}$$

The value of this compensation electric field can be predicated precisely when the alpha parameter for the ion species, the waveform $f(t)$, and the amplitude of the asymmetric waveform S are known. α is the alpha dependence and α' is the derivative with respect to E/N. triangular brackets mean the average over a period of the separation field. Dependent on this theory, the alpha function will be calculated as follows.

1.6 Alpha function calculation

According to Krylov et al, the method is described to represent the function of $\alpha(E/N)$ [32]. This method could be used for different asymmetric waveforms of different designs of IMS drift tubes whether linear, cylindrical, or planar FAIMS. The function of $\alpha(E/N)$ can be given as a polynomial expansion into a series of electric field strength E degrees as shown in following equation:

$$\alpha(E) = \sum_{n=1}^{\infty} \alpha_{2n} E^{2n} \quad \text{(eq. 1.17)}$$

Substituting this equation to eq.1.16, the eq. 1.17 can be obtained, where an uneven polynomial function is divided by an even polynomial function. Therefore, an odd degree polynomial is placed after the sign to approximate experimental results:

$$C = \frac{\sum_{n=1}^{\infty} \alpha_{2n} S^{2n+1} <f^{2n+1}(t)>}{1+\sum_{n=1}^{\infty}(2n+1)\alpha_{2n}S^{2n}<f^{2n}(t)>} \equiv \sum_{n=1}^{\infty} c_{2n+1} S^{2n+1} < f^{2(n-k)} > \text{ (eq. 1.18)}$$

This allows the comparison of the expected coefficient (approximated) and values of alpha parameter as shown as follows:

$$c_{2n+1} = \alpha_{2n} < f^{2n+1} > - \sum_{k=1}^{n-1}(2(n-k)+1)c_{2k+1}\alpha_{2(n-k)} < f^{2(n-k)} > \text{ (eq. 1.19)}$$

Alternatively, alpha parameters can be calculated by inverting the formula using an approximation of the experimental results:

$$\alpha_{2n} = \frac{1}{<f^{2n+1}>}\{c_{2n+1} + \sum_{k=1}^{n-1}(2(n-k)+1)c_{2k+1}\alpha_{2(n-k)}\langle f^{2(n-k)}\rangle\} \text{ (eq. 1.20)}$$

Principally, any number of polynomial terms (e.g. 2n) can be determined from the above eq. 1.20. However, a practical limit exists. The number of polynomial terms in the experimental results of the approximation c_{2n+1} should be higher than the expected number of alpha coefficients α_{2n}. Since the size of n depends on the experimental error, the power of the approximation of the experimental curves C(S) cannot be increased without limit. Usually N experimental points of $C_i(S_i)$ exist for the same ion species and experimental data can be approximated by the polynomial using a conventional least square's method. Finally, increasing the number of series terms above the point where the fitted curves are located within the experimental error bars is unreasonable. Practically, two or three terms are sufficient to provide a good approximation as shown in prior literature[30].

The error in measurements must be determined in order to measure the order of a polynomial for alpha. The sources of error in these experiments (with known or estimated error) are

1. Error associated with measurement and modeling of the separation field amplitude (about 5%)

2. Error in C(S) from a first order approximation of eq. 1.9 and 1.10 (about 3%)

3. Error in measuring the compensation voltage (about 2%). The approximate combined error may be 10% and there is therefore no gain with approximations beyond two polynomial terms; thus, alpha can be expressed as $\alpha\left(\frac{E}{N}\right) = \alpha_2\left(\frac{E}{N}\right)^2 + \alpha_4\left(\frac{E}{N}\right)^4$ with a level of accuracy as good as permitted by the measurements.

Modern software usually provided the possibility to approximate experimental data by polynomial function $C = c_3 S^3 + c_5 S^5$ according to eq. 1.18. A standard least squares method (regression analysis) was used to approximate or model the experimental findings. For N experimental points with $C_i(S_i)$ and for

$C=c_3S^3+c_5S^5$ a function $y=c_3+c_5x$ can be defined where $y=C/S^3$; $x=S^2$ so c_5 and c_3 are given as follows:

$$c_5 = \frac{\sum_{i=1}^{N} x_i \sum_{i=1}^{N} y_i - N \sum_{i=1}^{N} x_i y_i}{\left(\sum_{i=1}^{N} x_i\right)^2 - N \sum_{i=1}^{N} x_i} \quad \text{(eq.1.21)}$$

$$c_3 = \frac{1}{N}\left(\sum_{i=1}^{N} y_i - c_5 \sum_{i=1}^{N} x_i\right) \quad \text{(eq. 1.22)}$$

Through substituting experimental values for c_3 and c_5, the derived values for α_2 and α_4 can be found as follows:

$$\alpha_2 = \frac{c_3}{\langle f^3 \rangle} \quad \text{(eq. 1.23)}$$

$$\alpha_4 = \frac{c_5 + 3c_3\alpha_2\langle f^2 \rangle}{\langle f^5 \rangle} \quad \text{(eq. 1.24)}$$

This formula is valid for any waveform and may be described by form factors $<f^2(t)><f^3(t)><f^5(t)>$; these can be calculated analytically or numerically.

1.7 Ionization theory for DMS (^{63}Ni and UV)

In this thesis, two ionization techniques are used by DMS. One is the radioactive source and another is UV lamp. The efficiency of targets ions ionized by these two techniques are different due to the different mechanisms. The theories of these two ionization ways are detailed as follows.

1.7.1 Radioactive ionization theory (^{63}Ni)

When a β ray, an electron of modestly high energy, passes through a gas at an atmospheric pressure, its energy is dissipated primarily by inelastic collisions with the orbital electrons of the gas molecules. The decelerating primary electron leaves a track of slow positive ions and secondary electrons via direct and indirect ionization processes, some of which have sufficient energy to leave small tracks of their own[35]. In the absence of a strong electric field, secondary electrons are thermalized after a few collisions of the ions. The room temperature's chemistry of ion-molecule reactions and electron attachment becomes the most interestin aspect of the entire process. While the physical period of ionization and thermalization is over in 10^{-9} s, the chemical period may

continue to evolve for a second or more, until the charge cloud is finally destroyed by the following three ways[35].

1. the recombination of positively and negatively charged species
2. diffusion of charged species to the walls
3. physical removal by bulk flow of the gas

^{63}Ni emits β particles of energies forming a continuous distribution from 0 to 67 MeV[36]. The β particles lose energy during collision with the drift gas. For instance, the average energy loss per ion pair formed in N_2 is 35 eV, with ionization occurring as long as the energy of the β particle remains above the ionization potential of N_2 (IE 15,58 eV). The process is summarized as follows:

$$N_2 + \beta \rightarrow N_2^+ + \beta' + e^- \quad \text{(eq. 1.25)}$$
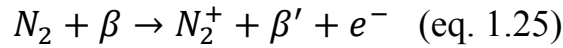
β' is a β particle of reduced energy following the reaction, and e$^-$ is the electron produced upon ionization of the N_2. The N_2^+ initiates a series of reactions, subsequently leading to the formation of three positive reactant ion species, $(H_2O)_nH^+$, $(H_2O)_nNO^+$, and $(H_2O)_nNH_4^+$.

The formation of $(H_2O)_nH^+$ was studied by Good et al[37] and is shown as follows:

$$N_2^+ + 2N_2 \rightarrow N_4^+ + N_2 \quad \text{(eq. 1.26)}$$

$$N_4^+ + H_2O \rightarrow 2N_2 + H_2O^+ \quad \text{(eq.1.27)}$$

$$H_2O^+ + H_2O \rightarrow H_3O^+ + OH \quad \text{(eq. 1.28)}$$

$$H_3O^+ + H_2O + N_2 \rightarrow (H_2O)_2H^+ + N_2 \quad \text{(eq. 1.29)}$$

$$(H_2O)_2H^+ + H_2O + N_2 \leftrightarrow (H_2O)_3H^+ + N_2 \quad \text{(eq. 1.30)}$$

$$(H_2O)_3H^+ + H_2O + N_2 \leftrightarrow (H_2O)_4H^+ + N_2 \quad \text{(eq. 1.31)}$$

…… ..
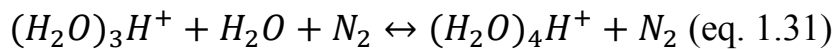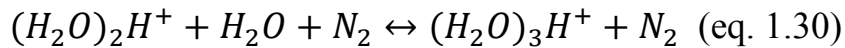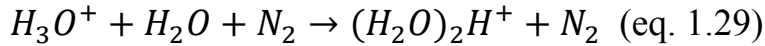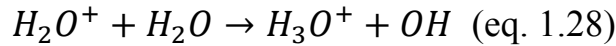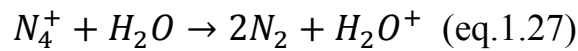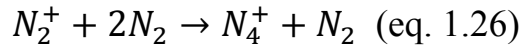
The number of cluster waters, n, in $(H_2O)_nH^+$ is a function of the temperature and the partial pressure of water in the gas. At source pressures of 0,5 to 3,5 torr, with trace water concentrations of 0,3 to 10 mtorr, n=2,3 or 4 predonmiated. Sumner et al presented the cluster contained 5 to 8 water molecules at 298 Kelvin degrees, 700 torr, and 5 torr partial water pressure [38]. Carroll et al

reported that the $(H_2O)_nH^+$ ion peak contained n=2 or 3 water molecules in a ratio of approximately 7:3 at 433 Kelvin degrees, ambient pressure, and 5×10^{-3} torr partial water pressure[39].

The mechanism for the formation of the $(H_2O)_nNO^+$ reactant ion has been hypothesized based on processer known to occur in the atmosphere[40]. As described above, N_2^+ and OH are produced and they initiated the following reactions leading to the hydrated nitric oxide ions:

$$N_2^+ + OH \rightarrow OH^+ + N_2 \text{ (eq. 1.32)}$$

$$OH^+ + H_2O \rightarrow H_3O^+ + O \text{ (eq. 1.33)}$$

$$N_2^+ + O \rightarrow NO^+ + N \text{ (eq. 1.34)}$$

$$NO^+ + H_2O + N_2 \rightarrow (H_2O)NO^+ + N_2 \text{ (eq. 1.35)}$$
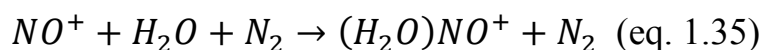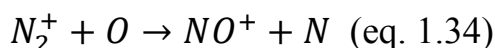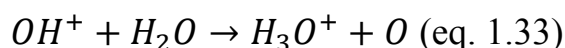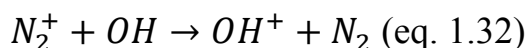
Carroll et al observed NO^+ and $(H_2O)NO^+$ as the predominant species[39].

The final reactant ion, $(H_2O)_nNH_4^+$, n=0 or 1[39], is probably obtained via proton transfer from the $(H_2O)_nH^+$ reactant ion to NH_3 contaminants from the atmosphere.

$$NH_3 + (H_2O)_nH^+ \rightarrow NH_4^+ + nH_2O \text{ (eq. 1.36)}$$

$$NH_4^+ + H_2O + N_2 \rightarrow (H_2O)NH_4^+ + N_2 \text{ (eq. 1.37)}$$
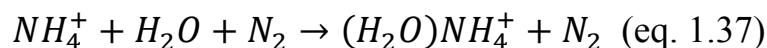
There are four basic ion-molecule reactions to the formation of positive product ions: 1) proton transfer reaction, 2) charge transfer reactions, 3) electrophilic addition, 4) hydride transfer[41]. The reactions are described as following equations:

1) Proton transfer reactions (when the proton affinity (PA) of the sample molecule is greater than that of the reactant ions.)

$$(H_2O)_nH^+ + M \rightarrow MH^+ + nH_2O \text{ (eq. 1.38)}$$

$$(H_2O)_nNH_4^+ + M \rightarrow MH^+ + NH_3 + nH_2O \text{ (eq. 1.39)}$$

2) Charge transfer reactions:

$$(H_2O)_nNO^+ + M \rightarrow M^+ + NO + nH_2O \text{ (eq. 1.40)}$$

3) Electrophilic addition:

$$(H_2O)_nNO^+ + M \rightarrow MNO^+ + nH_2O \text{ (eq. 1.41)}$$

4) Hydride transfer:

$$(H_2O)_n NO^+ + M \rightarrow [M-H]^+ + HNO + nH_2O \quad \text{(eq. 1.42)}$$

The major negative reactive ions $(H_2O)_nO_2^-$, and thermal electrons selectively ionize molecular species of high electron affinity by one of three ways: 1) Associative electron capture, 2) Dissociative electron capture, 3) Proton abstraction[42].

1) Associative electron capture

$$AB + e^- \rightarrow AB^- \quad \text{(eq. 1.43)}$$

2) Dissociative electron capture

$$AB + e^- \rightarrow A + B^- \quad \text{(eq. 1.44)}$$

3) Proton abstraction

$$ABH + e^- \rightarrow AB^- + H^+ e^- \quad \text{(eq. 1.45)}$$
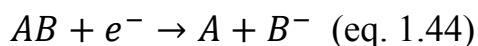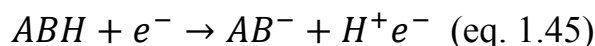
1.7.2 Atmosphere pressure photo ionization (APPI) theory

Photoionization occurs when the interaction of a photon beam produced by a discharge lamp with the vapors of analytes of interest. There are several steps of this progress [43]. First, an electronically excited molecule (M*) is formed when the molecule (M) absorbs a photon (E=hv):

$$M + hv \rightarrow M^* \quad \text{(eq.1.46)}$$
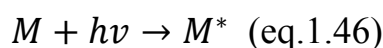
If $hv > IE$ (IE is the ionization energy), the molecule releases an energetic electron with energy $Ee^-_{(max)}$=hv-IE_M and the corresponding odd-electron cation M^{+} yields (a phenomenon typically occurring with molecules with conjugated double bonds, such as aromatic compounds[44]).

$$M^* \rightarrow M^{\cdot+} + e^- \quad \text{(eq.1.47)}$$
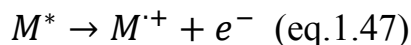
At atmospheric pressure, the ion's free pathway is 65 nm[44]. Therefore, M^{+} with an unpaired electron has a tendency to react in collisional environments[45]. Moreover, molecules with low IE and/or high proton affinity will dominate the positive ion spectra due to their high collision frequency[46].

However, when the IE>$h\nu$, M* may undergo a de-excitation process, such as photodissociation [47], photon emission[48], or collisional quenching[49] with a non-excited molecule (C):

$$M^* \rightarrow A + B \quad \text{(eq. 1.48)}$$

$$M^* \rightarrow M + h\nu \quad \text{(eq. 1.49)}$$

$$M^* + C \rightarrow M + C^* \quad \text{(eq. 1.50)}$$
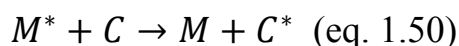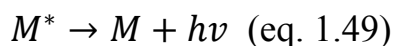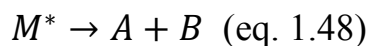
In such cases, the use of a preferentially ionized substance, called a dopant (D), has been proposed to promote the ionization of M:

$$D + h\nu \rightarrow D^{\cdot+} \quad \text{(eq. 1.51)}$$
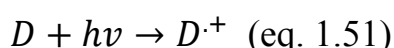
The dopant is added to large quantities compared to the analytes, and it acts as an intermediate between the photons and the analytes. The dopant must therefore produce ions with high recombination energy and/or a low proton affinity. The ionization mechanism depends on the PA values of the involved molecules (dopant, solvent, analyte) and on their capacity to capture an electron in the gas phase, called electron affinity (EA) [50]. Two mechanisms can occur, namely charge transfer [51]and proton transfer [52]:

If EA$_D$>EA$_M$,

$$D^{\cdot+} + M \rightarrow D + M^{\cdot+} \quad \text{(eq. 1.52)}$$

If PA$_M$>PA$_{[D-H]*}$,

$$D^{\cdot+} + M \rightarrow [D - H]^{\cdot} + [M + H]^{+} \quad \text{(eq. 1.53)}$$
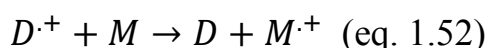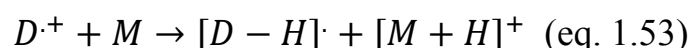
However, a dopant molecule can react only once. The dopant can also be used to improve the ionization yield of the analyte because photons cannot penetrate deeply into the dense mixture of gases[53](the photon beam produced by a krypton lamp loses 50% of its intensity each 1,5mm[54]). Therefore, the probability for direct ionization of analytes, present in small proportion compared to solvent molecules, is very low.

1.8 Environmental applications of differential ion mobility spectrometry

There are a large number of applications of DMS in different fields, including chemical weapons detection, explosive tracing, biologically active molecules separation, pharmaceutical inspection and pollutants monitoring. In the following section, based on the literatures, the applications of DMS on the environmental monitoring, including gas, water, bacteria and toxic chemicals monitoring will be overviewed.

In 2005, Sacks and co-worker exploited a microfabricated silicon chip coated with a dimethyl polysiloxane stationary phase being used as GC separation[26]. They coupled this chip to a microfabricated differential ion mobility spectrometer by a heated transfer line. A unique feature of this device is that both positive and negative ions are detected from a single experiment. The combined microfabricated column and detector is evaluated for the analysis of VOCs with a variety of functionalities. The DMS can detect the compounds which are not resolved by GC.

Limero et al reported that Sionex MicroAnalyzer^{TM} is used to analyze the common trace VOCs in the International Space Station [55]. The Sionex microAnalyzer™ is an ideal replacement for the Volatile Organic Analyzer (VOA). The MicroAnalyzer has a volume of less than one-tenth of a cubic foot and it relies on GC and DMS for accurate analysis of atmospheric contaminants. Moreover, MicroAnalyzer retains or exceeds the VOA's capability for detecting trace levels of air contaminants. It is small, low cost, and uses minimal spacecraft resources.

Shellie et al introduced a portable, fast gas chromatographic approach that employs a standard capillary column and DMS detection to analyze sulfur free odorants. This approach is based on a resistively heated, temperature programmable silicon micromachined GC. A complete analysis can be conducted in less than 70s. In the range from 0,5 to 5 ppm, the repeatability is

less than 3% RSD(n=20) and the detection limits for the target compounds are low to 50 ppb (v/v) [56].

Daniele Evers et al detected and quantified the natural contaminants of wine by portable GC-DMS (Microanalyzer, Sionex). They identified and quantified some natural and volatile contaminants of wine such as geosmin, 2-methylisoborneol, 1-octen-3-ol, 1-octen-3-one, and pyrazine through a very fast run cycle in less than 10 min. The detection of all target compounds at concentrations is below 5 ng/L (except 1-octen-3-ol), which is below the human olfactory threshold [57].

Eiceman et al applied DMS equipped with a photo discharge lamp at 10,6 eV continuously to monitor VOCs in ambient air inside a building and in an open space near the union of I-10 and I-25 at Las Cruces, New Mexico [58]. Air was drawn directly and analyzed by DMS without enrichment or preparation. The DMS results were consistent with VOCs from traffic on major city thoroughfare adjacent to the building. In-field studies near two interstate highways demonstrated that DMS response could be correlated to traffic patterns and exhibited diurnal trends. These findings demonstrated the concept and practice of DMS as continuous monitors for VOCs as airborne vapors in buildings and on site.

Moreover, the GC-DMS device was also evaluated as a smart smoke alarm by Eiceman[59]. In this work, chemical composition of vapors from different fuel sources such as cotton, paper, grass and engine were identified by both GC-MS and GC-DMS. The orthogonal separation provided by DMS combined with the separation capabilities of GC yields maps of retention time *vs.* compensation voltage. Topographic plots from GC-DMS analysis of all samples demonstrated that information in the mobility scan provides distinctiveness for each sample. Incompletely combusted hydrocarbons from the internal combustion engine appeared in a narrow band of CV from -2 to 2 V, as well as cotton exhibited unique peaks in the 3D. These findings suggested that a GC-DMS instrument

operating at ambient pressure in air might result in a compact and convenient fuel specific smoke alarm at a reasonable cost.

Shnayderman et al applied differential ion mobility spectrometry to identify bacteria at the species level [60]. The VOCs released from bacterial culture were identified both by solid phase microextraction/conventional headspace GC methods and by GC-DMS. The orthogonal separation capacities of the DMS permitted better discrimination of the markers and simplification of the spectra.

Eiceman reported that DMS was used with pyrolysis GC to chemically characterize bacteria through three-dimensional plot ion intensity, compensation voltage from differential mobility spectra, and chromatographic retention time [61]. They identified more than 70 chemicals in the headspace above the bacterial colonies and distinguished spores from viable bacterial production by the release of crotonic acid. The other chemicals like lipid A and lipoteichoic acid permitted a particular discrimination between a Gram negative (*E.coli*) bacterium and a Gram positive (*M. Luteus*) bacterium. They improved the method to characterize eight viable bacterial strains and two spores in further work [62].

DMS was used to detect chemical warfare agents like nitro-organic explosive and related compounds as a smart portable device[33]. The CVs of 1,2,3-propanetriol trinitrate, 1,3-dinitrobenzene, 2,6-dinitrotoluene, 2,4,6-trinitrotoluene and pentaerythritol tetranitrate in purified air and in air doped with 1000ppm methylene chloride were scanned. Except for 1,2,3-propanetroil trinitrate and pentaerythritol tetranitrate, other explosives are well separated from CV. Moreover, 2,4,6-trintrotoluene exhibits multiple peaks, as a result of isomers or multimer formation. These results suggested that the DMS could be used for the separation and detection of explosives.

Zalewska et al compared two handheld trace explosive detector types: MO-2M and SABRE 4000. MO-2M is a FAIMS equipped with a ß emitter, tritium, as an ionization source, whereas SABRE 4000 is a conventional detector based on

IMS equipped with radioactive nickel as the ionization source [63]. The detection limits of trinitrotoluene and hexadydro-1,3,5-trinitro-1,3,5-triazine with the MO-2M are 10 and 100 fold lower than with the SABRE detector.

FAIMS combined with multicapillary column (MCC) has been used to detect explosives by Buryakov [64]. Speed of response of this detection with the MCC-FAIMS was 0,7 s. Other similar studies included different mononitrotoluenes and nitrobenzenes effect, the effect of ambient temperature and humidity to the ionization efficiency of explosives were also done [65].

Krylova et al presented the electric field dependence of the mobilities of gas phase protonated monomers [$MH^+(H_2O)_n$] and proton bound dimers [$M_2H^+(H_2O)_n$] of organophosphorus compounds at E/N values between 0 and 140. At moisture values between 1000 and 10000ppm, the value of α(E/N) increases more than 2 fold. This work clearly showed that the concentration of water in the carrier gas stream could cause water bound cluster formation. The process of ion declustering at high E/N values was consistent with the kinetics of ion-neutral collisional periods, and the duty cycle of the waveform applied to the drift tube [66].

Rainsber et al used a thermal desorption solid phase microextraction (SPME) inlet introduction for DMS to determine hydrocarbons in water [67]. The introduction system consists of an SPME holder, aluminum heating block, bare GC capillary and T-union fitting. The hydrocarbons of interest in water are extracted ion the fiber and then the fiber is placed into the inlet. After heating, the analytes are carried into the DMS with air. The detection limits of benzene, toluene and m-xylene were 75, 25 and 5 µg/mL, respectively.

Kanu and Thomas detected benzene in water in the presence of phenol with an active membrane UV photo ionization differential mobility spectrometer [68]. The presence of benzene was identified through the presence of a peak corresponding to a benzene response (CV=-9V and FWHM=1V). These encouraging results indicated that VOCs dissolved in water at low

concentrations (sub ppm) may be reliably determined and identified using DMS with UV photo ionization fitted with an active membrane. The whole procedure to analyze requires less than 180s. The further evaluation of this approach for its suitability of applications relating to: drinking water screening, process validation, contaminated land and water monitoring, are the next steps.

Telgheder et al analyzed BTEX compounds from surface waters using GC-DMS combined with SPME[69]. The method was sensitive to the separation and the detection of benzene, toluene, ethylbenzene, and m-, o- and p-xylenes. The detection limits for these five compounds were in the range from 0,01-1,19 µg/L. Kuklya et al developed an electrospray ^{63}Ni-differential ion mobility spectrometer for the analysis of aqueous samples[70]. With adjusted experimental setup, the detection of model substances (2-hxanone, fluoroactamide, L-nicotine and 1-phenyl-2-thiourea) in the water solutions, in the range of 0,1-50 mg/L, was performed.

Kanu and Thomas used DMS as a potential field deployable device for detect 1,2,4-trichlorobenzene in surface water[71]. Furthermore, they compared SPME-GC-DMS with SPME-DMS. The results suggested that the use of SPME result in a lot of variations. The GC-DMS system was demonstrated to be fit for purpose in that it detected the contaminant at the maximum contaminant level in the surface water. It was cheaper, easier to use and smaller than a typical GC-MS. It is feasible to use this device for routinely water contaminant monitoring.

1.9 The aim of this work

The goal of this work is to develop a fast cheap method based on DMS to on-field detect gasoline related compounds in contaminated groundwater. To achieve this goal, several problems should be overcome. Firstly, gasoline or other petroleum products consist of a number of organic compounds. When the groundwater contaminated by gasoline, it is very difficult to identify and to analyze all organic components of gasoline. Thus, to select some compounds, which have a response for DMS detector, from the complex matrix as makers, is the first step. Secondly, it should be as fast as possible to use the DMS as an on-field device. Normally, the typical lab based method like GC equipped with a conventional capillary column needs more than 10 min to analyze gasoline related compounds. How to shorten the time of separating target compounds by chromatography is one of the key points for developing a fast method. Thirdly, the detection limits for target compounds by DMS should be below or close to the regulated maximum contaminant levels. One way to improve the sensitivity of DMS is to select the ionization source, in which condition the target compounds have high ionization efficiencies. Finally, the optimized new method should be applied to detect the real samples in a simulation on-site condition to prove the feasibility.

Firstly, the main aim is to find some target compounds as markers for gasoline. These fingerprint compounds can be detected by DMS and represent in groundwater contaminated by gasoline. In chapter 2, groundwater spiked with 5 different sorts of gasoline will be analyzed by GC-MS. A NIST formula gasoline containing 22 compounds will be utilized as standard to identify and select the target compounds.

Secondly, the total analysis time for BTEX in groundwater spiked with gasoline is long by conventional GC coupled to DMS. To shorten the analysis time, a short capillary GC column MXT-5 will be used to analyze the target compounds BTEX. Then, this short GC column will be connected into DMS equipped with

a homemade interface. After optimization of the operation condition, the calibration curves and detection limits obtained by GC-^{63}Ni-DMS system will be discussed (chapter 3).

In order to improve the sensitivity of DMS for analyzing BTEX, photo ionization (krypton lamp) will be utilized as an ionization source for DMS instead of radioactive ^{63}Ni. The relation between separation voltage and compensation voltage for ^{63}Ni-DMS and UV-DMS to analyze different ions will be systematically studied. The calibration curves and detection limits of BTEX detected by GC-UV-DMS and GC-^{63}Ni-DMS system will be compared (chapter 4).

Then, the concentrations of BTEX in 17 contaminated groundwater samples from Rotenburg (Wümme) will be analyzed by GC-UV-DMS. The results will be compared with those obtained by the reference method (chapter 5).

Finally, in order to simulate the on-field conditions, the diffusion from BTEX in groundwater to air will be systematically studied by GC-UV-DMS(chapter 6). The influence of various factors (temperature, matrix effect) on diffusion will be evaluated.

1.10 References

1.   EEA. *Overview of contaminants affecting soil and groundwater in Europe.* 2012; Available from: http://www.eea.europa.eu/data-and-maps/figures/overview-of-contaminants-affecting-soil-and-groundwater-in-europe.

2.   Enander, R.T., et al., *Reducing Drinking Water Supply Chemical Contamination: Risks from Underground Storage Tanks.* Risk Analysis, 2012. **32**(12): p. 2182-2197.

3.   *Directive 2006/118/EC of the European Parliament and of the Council on the protection of groundwater against pollution and deterioration*, in *Official Journal of the European Union.* 2006.

4.   EPA, U., *Volatile organic compounds by gas chromatography mass spectrometry (GC/MS) Method 8260 B.* 1996.

5.   EPA, U., *Aromatic and halogenated volatiles by gas chromatography using photoionization and/or electrolytic conductivity detectors. Method 8021B.* 1996.

6.   Almeida, C.M.M. and L.V. Boas, *Analysis of BTEX and other substituted benzenes in water using headspace SPME-GC-FID: method validation.* Journal of Environmental Monitoring, 2004. **6**(1): p. 80-88.

7.   Available from: http://des.nh.gov/organization/commissioner/lsu/documents/water_testing.pdf

8.   Stuetz, R.M., et al., *Monitoring wastewater BOD using a non-specific sensor array.* Journal of Chemical Technology and Biotechnology, 1999. **74**(11): p. 1069-1074.

9.   Rivera, D., et al., *Characterization of the ability of polymeric chemiresistor arrays to quantitate trichloroethylene using partial least squares (PLS): effects of experimental design, humidity, and temperature.* Sensors and Actuators B-Chemical, 2003. **92**(1-2): p. 110-120.

10.   Clifford K. Ho, L.K.M., Chad E. Davis, Michael L. Thomas, Jerome L. Wright, and a.R.C.H. Ara S. Kooser, *Chemiresistor Microsensors for In-Situ Monitoring of Volatile Organic Compounds: Final LDRD Report.* 2003, SAND.

11.   Wilson, D.M., et al., *Chemical Sensors for Portable, Handheld Field Instruments.* Ieee Sensors Journal, 2001. **1**(4): p. 256-274.

12.   Kirschner, J., *Surface Acoustic Wave Sensors (SAWS):Design for Application*, in *SURFACE ACOUSTIC WAVE SENSORS (SAWS): DESIGN FOR FABRICATION. MICROELECTROMECHANICAL SYSTEMS.* 2010.

13.   Devinder Saini, R.L., Michelangelo Virgo, *Measurement of Hydrocarbons in Produced Water Using Fiber Optic Sensor Technology.*, in *API 2001 Produced Water Management Technical Forum & Exhibition.* 2001.

14.   Ueyama, S., K. Hijikata, and J. Hirotsuji, *Water monitoring system for oil contamination using polymer-coated quartz crystal microbalance chemical sensor.* Water Science and Technology, 2002. **45**(4-5): p. 175-180.

15.   Matsuguchi, M. and T. Uno, *Molecular imprinting strategy for solvent molecules and its application for QCM-based VOC vapor sensing.* Sensors and Actuators B-Chemical, 2006. **113**(1): p. 94-99.

16.   Dickert, F.L., O. Hayden, and M.E. Zenkel, *Detection of volatile compounds with mass sensitive sensor arrays in the presence of variable ambient humidity.* Analytical Chemistry, 1999. **71**(7): p. 1338-1341.

17.   Bourgeois, W. and R.M. Stuetz, *Use of a chemical sensor array for detecting pollutants in domestic wastewater.* Water Research, 2002. **36**(18): p. 4505-4512.

18.   Kim, J., et al., *Construction of simultaneous SPR and QCM sensing platform.* Bioprocess and Biosystems Engineering, 2010. **33**(1): p. 39-45.

19.   Sandeep Kumar Vashist, P.V., *Recent Advances in Quartz Crystal Microbalance-Based Sensors.* Journal of Sensors, 2011: p. 1-13.

20.   Edward A. Mason, E.W.M., *Transport Properties of Ions in Gases.* 2005: Wiley.

21.   Buryakov, I.A.K., E. V.; Makas, A. L.; Nazarov, E. G.; Pervukhin, V.V.; Rasulev, U. K. , *Separation of ions according to mobility in strong ac fields.* Sov. Tech. Phys. Lett., 1991. **17**(6): p. 446-447.

22.   B. Carnahan, S.D., V. Kouznetsov, A. Tarassov,, *Development and applications of transverse field compensation ion mobility spectrometer.*, in *Proceeding of the Fourth International Workshop on IMS.* 1995: Cambridge, UK.

23.   Purves, R.W. and R. Guevremont, *Electrospray ionization high-field asymmetric waveform ion mobility spectrometry-mass spectrometry.* Analytical Chemistry, 1999. **71**(13): p. 2346-2357.

24.   Buryakov, I.A., et al., *A New Method of Separation of Multi-Atomic Ions by Mobility at Atmospheric-Pressure Using a High-Frequency Amplitude-Asymmetric Strong Electric-Field.* International Journal of Mass Spectrometry and Ion Processes, 1993. **128**(3): p. 143-148.

25.   Miller, R.A., et al., *A novel micromachined high-field asymmetric waveform-ion mobility spectrometer.* Sensors and Actuators B-Chemical, 2000. **67**(3): p. 300-306.

26.   Lambertus, G.R., et al., *Silicon microfabricated column with microfabricated differential mobility spectrometer for GC analysis of volatile organic compounds.* Analytical Chemistry, 2005. **77**(23): p. 7563-7571.

27.   Shvartsburg, A.A., et al., *Ultrafast Differential Ion Mobility Spectrometry at Extreme Electric Fields in Multichannel Microchips.* Analytical Chemistry, 2009. **81**(15): p. 6489-6495.

28.   Shvertsburg, A.A., *Differential Ion Mobility Spectrometry: Nonlinear Ion Transport and Fundamentals of FAIMS.* 2008, Boca Raton: CRC.

29.   Viehland, L.A. and E.A. Mason, *Transport Properties of Gaseous-Ions over a Wide Energy-Range .4.* Atomic Data and Nuclear Data Tables, 1995. **60**(1): p. 37-95.

30.   Viehland, L.A., et al., *Comparison of high-field ion mobility obtained from drift tubes and a FAIMS apparatus.* International Journal of Mass Spectrometry, 2000. **197**: p. 123-130.

31.   Guevremont, R., et al., *Calculation of ion mobilities from electrospray ionization high-field asymmetric waveform ion mobility spectrometry mass spectrometry.* Journal of Chemical Physics, 2001. **114**(23): p. 10270-10277.

32.   Krylov, E., et al., *Field dependence of mobilities for gas-phase-protonated monomers and proton-bound dimers of ketones by planar field asymmetric waveform ion mobility spectrometer (PFAIMS).* Journal of Physical Chemistry A, 2002. **106**(22): p. 5437-5444.

33.   Eiceman, G.A., et al., *Separation of ions from explosives in differential mobility spectrometry by vapor-modified drift gas.* Analytical Chemistry, 2004. **76**(17): p. 4937-4944.

34.   Krylov, E.V., et al., *Selection and generation of waveforms for differential mobility spectrometry.* Review of Scientific Instruments, 2010. **81**(2).

35.   Carr, T.W., *plasma chromatography.* 1984, New York: Plenum Press. 95.

36.   R.C.Weast, *Handbook of Chemistry and Physics.* 1972: CRC press, Boca Raton.

37.   Good, A., D.A. Durden, and P. Kebarle, *Ion-Molecule Reactions in Pure Nitrogen and Nitrogen Containing Traces of Water at Total Pressures 0.5-4 Torr Kinetics of Clustering Reactions Forming H+(H2o)N.* Journal of Chemical Physics, 1970. **52**(1): p. 212-&.

38.   Sunner, J., M.G. Ikonomou, and P. Kebarle, *Sensitivity Enhancements Obtained at High-Temperatures in Atmospheric-Pressure Ionization Mass-Spectrometry.* Analytical Chemistry, 1988. **60**(13): p. 1308-1313.

39.   Carroll, D.I., et al., *Identification of Positive Reactant Ions Observed for Nitrogen Carrier Gas in Plasma Chromatograph Mobility Studies.* Analytical Chemistry, 1975. **47**(12): p. 1956-1959.

40.   Karasek, F.W. and D.W. Denney, *Detection of Aliphatic N-Nitrosamine Compounds by Plasma Chromatography.* Analytical Chemistry, 1974. **46**(9): p. 1312-1314.

41.   Stlouis, R.H. and H.H. Hill, *Ion Mobility Spectrometry in Analytical-Chemistry.* Critical Reviews in Analytical Chemistry, 1990. **21**(5): p. 321-355.

42.   Krylov, E.V., *Pulses of special shapes formed on a capacitive load.* Instruments and Experimental Techniques, 1997. **40**(5): p. 628-631.

43.   Marchi, I., S. Rudaz, and J.L. Veuthey, *Atmospheric pressure photoionization for coupling liquid-chromatography to mass spectrometry: A review.* Talanta, 2009. **78**(1): p. 1-18.

44.   Kauppila, T.J., R. Kostiainen, and A.P. Bruins, *Anisole, a new dopant for atmospheric pressure photoionization mass spectrometry of low proton affinity, low ionization energy compounds.* Rapid Communications in Mass Spectrometry, 2004. **18**(7): p. 808-815.

45.   Hanold, K.A., et al., *Atmospheric pressure photoionization. 1. General properties for LC/MS.* Analytical Chemistry, 2004. **76**(10): p. 2842-2851.

46.   Carroll, D.I., et al., *Atmospheric-Pressure Ionization Mass-Spectrometry.* Applied Spectroscopy Reviews, 1981. **17**(3): p. 337-406.

47.   Syage, J.A., et al., *Atmospheric pressure photoionization II. Dual source ionization.* Journal of Chromatography A, 2004. **1050**(2): p. 137-149.

48.   Driscoll, J.N. and F.F. Spaziani, *Pid Development Gives New Performance Levels.* Research-Development, 1976. **27**(5): p. 50-&.

49.   Driscoll, J.N. and J.H. Becker, *Industrial-Hygiene Monitoring with a Variable Selectivity Photo-Ionization Analyzer.* American Laboratory, 1979. **11**(11): p. 69-&.

50.   Robb, D.B., T.R. Covey, and A.P. Bruins, *Atmospheric pressure photoionisation: An ionization method for liquid chromatography-mass spectrometry.* Analytical Chemistry, 2000. **72**(15): p. 3653-3659.

51.   Langhorst, M.L., *Photo-Ionization Detector Sensitivity of Organic-Compounds.* Journal of Chromatographic Science, 1981. **19**(2): p. 98-103.

52.   Schmermund, J.T. and D.C. Locke, *Universal Photoionization Detector for Liquid-Chromatography.* Analytical Letters, 1975. **8**(9): p. 611-625.

53.   Kauppila, T.J., A.P. Bruins, and R. Kostiainen, *Effect of the solvent flow rate on the ionization efficiency in atmospheric pressure photoionization-mass spectrometry.* Journal of the American Society for Mass Spectrometry, 2005. **16**(8): p. 1399-1407.

54.   Nazarov, E.G., et al., *Miniature differential mobility spectrometry using atmospheric pressure photoionization.* Analytical Chemistry, 2006. **78**(13): p. 4553-4563.

55.   T. Limero, E.R., P. Cheng, , *Demnostration of the Microanalyzer's Measurement of Commone Trace Volatile Organic Compounds in Spacecraft Atmosphere*, in *International Conference on Environment Systems*. 2008: Warrendale, PA.

56.   Luong, J., et al., *Temperature-Programmable Resistively Heated Micromachined Gas Chromatography and Differential Mobility Spectrometry Detection for the Determination of Non-Sulfur Odorants in Natural Gas.* Analytical Chemistry, 2013. **85**(6): p. 3369-3373.

57.   Camara, M., et al., *Detection and Quantification of Natural Contaminants of Wine by Gas Chromatography-Differential Ion Mobility Spectrometry (GC-DMS).* Journal of Agricultural and Food Chemistry, 2013. **61**(5): p. 1036-1043.

58.   Eiceman, G.A., et al., *Monitoring volatile organic compounds in ambient air inside and outside buildings with the use of a radio-frequency-based ion-mobility analyzer*

with a micromachined drift tube. Field Analytical Chemistry and Technology, 2000. **4**(6): p. 297-308.

59.   Eiceman, G.A., et al., *Discrimination of combustion fuel sources using gas chromatography-planar field asymmetric-waveform ion mobility spectrometry.* Journal of Separation Science, 2003. **26**(6-7): p. 585-593.

60.   Shnayderman, M., et al., *Species-specific bacteria identification using differential mobility spectrometry and bioinformatics pattern recognition.* Analytical Chemistry, 2005. **77**(18): p. 5930-5937.

61.   Schmidt, H., et al., *Microfabricated differential mobility spectrometry with pyrolysis gas chromatography for chemical characterization of bacteria.* Analytical Chemistry, 2004. **76**(17): p. 5208-5217.

62.   Prasad, S., et al., *Analysis of bacterial strains with pyrolysis-gas chromatography/differential mobility spectrometry.* Analyst, 2006. **131**(11): p. 1216-1225.

63.   Zalewska, A., W. Pawlowski, and W. Tomaszewski, *Limits of detection of explosives as determined with IMS and field asymmetric IMS vapour detectors.* Forensic Science International, 2013. **226**(1-3): p. 168-172.

64.   Buryakov, I.A., *Express analysis of explosives, chemical warfare agents and drugs with multicapillary column gas chromatography and ion mobility increment spectrometry.* Journal of Chromatography B-Analytical Technologies in the Biomedical and Life Sciences, 2004. **800**(1-2): p. 75-82.

65.   Buryakov, I.A., *Qualitative analysis of trace constituents by ion mobility increment spectrometer.* Talanta, 2003. **61**(3): p. 369-375.

66.   Krylova, N., et al., *Effect of moisture on the field dependence of mobility for gas-phase ions of organophosphorus compounds at atmospheric pressure with field asymmetric ion mobility spectrometry.* Journal of Physical Chemistry A, 2003. **107**(19): p. 3648-3654.

67.   Rainsberg, M.R. and P.D.B. Harrington, *Thermal desorption solid-phase microextraction inlet for differential mobility spectrometry.* Applied Spectroscopy, 2005. **59**(6): p. 754-762.

68.   Kanu, A.B. and C.L.P. Thomas, *The presumptive detection of benzene in water in the presence of phenol with an active membrane-UV photo-ionisation differential mobility spectrometer.* Analyst, 2006. **131**(9): p. 990-999.

69.   Ursula Telgheder, M.M., Maik A. Jochmann *Determination of volatile organic compounds by solid-phase microextraction—gas chromatography-differential mobility spectrometry.* International Journal for Ion Mobility Spectrometry 2009. **12**(4): p. 123-130.

70.   Kuklya, A., et al., *Development of an electrospray-63Ni-differential ion mobility spectrometer for the analysis of aqueous samples.* Talanta, 2014. **120**(0): p. 173-180.

71.   A.B. Knau, C.L.P.T., *Analysis of Trichlorobenzene in Surface Waters by Differential Mobility Spectrometry.* International Journal of Ion Mobility Spectrometer, 2003. **6**(1): p. 15-20.

2. Fingerprint identification of gasoline related compounds in contaminated groundwater by GC-DMS and MS

2.1 Introduction

Gasoline is a light non-aqueous phase liquid and accumulates as a free phase floating layer on top of the groundwater´s phreatic surface[1]. It is a mixture composed of basically alkanes, C5–C14 olefins, cycloparaffins, aromatics and other additives used as oxygenates to raise the octane number. Although the amount of gasoline that dissolves in water is generally small, most of the water soluble fraction of gasoline will induce harmful effect to the environment and public health. The water soluble fraction of gasoline is a complex mixture ranging from pentane to PAHs, phenols, and nitrogen- and sulfur-containing heterocyclic compounds [2].

Until now, the identification of all gasoline related components in contaminated groundwater is still a great challenging task, due to the complex composition and low concentration. Ted and Held identified and analyzed approximately 50 gasoline range hydrocarbons consisting of paraffin, isoparaffin, (mono-) aromatic, naphthene, and olefin compounds in groundwater by GC-MS [3].

Few gasoline-related compounds were reported to be detected in water by DMS. Kanu and Thomas detected benzene in water in the presence of phenol with an active membrane UV photo ionization DMS [4]. BTEX compounds from surface waters were analyzed using GC-DMS combined with SPME[5, 6]. The method was sensitive to the separation and the detection of benzene, toluene, ethylbenzene, and *m*-, *o*- and *p*-xylenes. The detection limits for these five compounds were in the range from 0,01-1,19 µg/L. Therefore, some challenges should be overcome for application of DMS to detect gasoline contaminated groundwater. First challenge of application of DMS to monitor gasoline contaminated groundwater is how to distinguish the compounds from the complex background. Another challenge is that it is impossible for DMS to

response to all gasoline compounds in groundwater. However, as a fast on-field device, it is unnecessary to detect all gasoline compounds in contaminated groundwater. It is enough to give an alarm to report whether groundwater is contaminated by gasoline or not.

In this chapter, the main aim is to find target compounds as markers for gasoline. These target compounds are sensitive for DMS and represent in groundwater contaminated by gasoline. Firstly, clean groundwater were spiked with 5 different sorts of gasoline and analysed by conventional GC-MS. A NIST formula gasoline containing 22 compounds was used as standard to identify the compounds in gasoline contaminated groundwater. Then, in comparison with the GC-DMS, the organic compounds would be selected from the identified components as fingerprint. Finally, the feasibility of GC-DMS for the monitoring gasoline contamination in groundwater will be discussed.

2.2 Experimental section

2.2.1 Preparation of the samples for GC-DMS and GC-MS analysis

10 ml of the gasoline solution with a concentration of 70 mg/L (otherwise noted) was transferred to a 20 mL headspace-vial and hold for 30 min at 25 ℃. After that, 10 μl from the headspace of the vial was taken with a gas-tide syringe for the GC-DMS or GC-MS analysis.

2.2.2 Identification of the compounds in gasoline by GC- DMS

A Shimadzu GC-2014 gas chromatograph (Shimadzu, Duisburg, Germany) was equipped with a split/splitless injector, a 5% diphenyl-/95% dimethyl-polysiloxane GC column (60 meter, 0,25 mm i.d., 0,25 μm film thicknesses, Restek, Bad Homburg, Germany). The GC oven temperature was held at 35 ℃ for 11 minutes, then ramped to 120℃ with a rate of 5 ℃/min and then ramped to 160 ℃ with 10 ℃/min, and finally held at 160 ℃ for 3 minutes. The temperature for the GC injection port was set to 250 ℃. The 0,5 mL of the

sample was injected from the headspace in the split mode at a splitting ratio of 1:10. Helium was used as carrier gas with a constant flow rate of 1 mL/min.

For the DMS analysis, a SIONEX SVAC spectrometer (Sionex Corporation, Bedford, MA, USA) equipped with a ^{63}Ni ion source of 5 mCi, was used. The sensor temperature was set to 60 ℃. Nitrogen (99,999 %, Air Liquide, Oberhausen, Germany) was used as carrier gas with a flow rate of 300 mL/min. All data were recorded by microDMx^{TM} Expert version 2.4.0 software. The home-made interface between GC and DMS was kept at 80 ℃.

2.2.3 Identification of the compounds in gasoline by GC-MS

The gasoline samples were analyzed using Trace GC Ultra (S+H Analytik, Mönchengladbach, Germany) equipped with a split/splitless injector coupled to a DSQ II single quadrupole mass spectrometer (S+H Analytik) equipped with electron impact ionization source. The temperature programme was as described above. The GC-MS interface temperature was set to 250 ℃ and the ion source temperature was set to 220 ℃. The ionization energy of the ion source was set to 70 eV and the quadrupole was set to scan mode (*m/z*) of 49-180, 6,5 scans/s. Xcalibur 1,4 data system (S+H Analytik) was used for instrument control, data acquisition, and performance evaluation.

2.2.4 Chemicals and sampling

For the identification of fingerprint compounds in gasoline, a reformulated gasoline standard reference material 2294 was purchased from National Institute of Standards and Technology (NIST) (Gaithersburg, USA). The other gasoline samples were collected from local petrol stations. In all experiments the concentration of gasoline in water was 70 mg/L, otherwise noted.

Chemicals in this work such as o-xylene(≥99,0%, Fluka Analytical, Steinheim, Germany), p-xylene(≥99,0%, Fluka analytical, Steinheim, Germany), m-xylene(≥99,0%, Fluka, Steinheim, Germany), benzene(99%, AppliChem, Darmstadt, Germany), ethylbenzene (≥99,0%, Fluka, Steinheim, Germany),

toluene(99,9%, J.T.Baker, Netherland), MTBE (≥99,5%,Merck, Germany), 1,2,4-trimethylbenzene(98%,Aldrich, Germany) and methanol (99,99%, Fisher Scientific, Germany) were used without further purification.

2.2.5 Data analysis

A series of different volumes of saturated analyte vapors (at constant temperature of 25 °C and 1 atmosphere pressure) were analyzed. The amount of analyte was calculated by using of following equation:

$$m = \frac{p_a * v_a * M}{(p_{atm} + p_a) * V_m} \qquad \text{(eq. 2.1)}$$

Where p_a is saturated vapor pressure of analyte , v_a the injection volume, p_{atm} the atmosphere pressure, M the molar mass of analyte, V_m the molar volume (24,465 L/mol at 25 ℃, 1 atm).

All data were analyzed by Origin Lab 9.0G.

2.3 Results and Discussion

2.3.1 Selection of fingerprint compounds in gasoline for DMS analysis

The results from the GC-MS measurements of groundwater spiked with different sorts of gasoline are shown in Figure 2.1. By comparison of a gasoline standard from the NIST (SRM 2294) and mass spectrometric data, 22 compounds were satisfactorily identified (Table 2.1). Gasoline is a refined product of crude oil and some additives. It consists of a mixture of n-alkanes, isoalkanes, cycloalkanes, mono- and di-aromatics, olefins and fuel oxygenates with a boiling point in the range of 30 to 200 °C. It is extremely difficult to identify all the compounds in gasoline. Typical compounds of gasoline, which are of interest in the environmental monitoring, are benzene, toluene, xylene, methane, ethane, propane, and gasoline additives like MTBE[7]. The identified 22 standard compounds cover a wide range of hydrocarbons that are present in gasoline. As shown in Figure 2.1, all of 22 compounds except of MTBE were found in the analyzed groundwater samples spiked with gasoline. In addition, by

comparison of gasoline components in SRM 2294 with the real gasoline samples collected from petroleum stations, several of these 21 components (ethylbenzene, m/p-xylene, o-xylene, 1,3,5-trimethylbenzene, 1,2,4-trimethylbenzene) were found in all three gasolines with high relative abundances, whereas the other standard compounds were found with lower relative abundances. Though, several peaks with high relative abundance appear during the initial 15 min in the chromatogram of all three real gasolines. The identification of these peaks was not possible due to limit of standards. Moreover, the peaks appearing during the first 15 min indicate the compounds with relatively high volatility, which may not stay in groundwater for a long period of time after the water contamination.Therefore, it is not necessary to identify these peaks because they cannot be used as an indicator of gasoline. In view of this, it should be feasible to use the moderately volatile compounds with high relative abundances, e.g. ethylbenzene, m/p-xylene, o-xylene, 1,3,5-trimethylbenzene, 1,2,4-trimethylbenzene, as a fingerprint to monitor gasoline in groundwater by DMS.

In order to check the feasibility to use the moderatedly volatile compounds as fingerprint to monitor gasoline in groundwater by DMS, the groundwater spiked with gasoline were analysed by both GC-MS and GC-DMS. The GC-DMS / GC-MS combined chromatogram of groundwater, spiked with a gasoline sample (Super 95, ARAL), is shown in Figure 2.2. During this measurement it was observed that with the increase of retention time, the compensation voltage for the compound detection is approximate to 0 V. This phenomenon can be explained by the fact that the large molecules with a longer retention time have lower differential mobility and hence, need lower compensation voltage[8].

A DMS with a radioactive ^{63}Ni ionization source was used for the ions generation. The positive analyte ions, detected in the positive mode, are mainly ionized by the reactant ions (RIP) such as $H^+(H_2O)_n$ produced in the presence of water traces[9, 10]. If the proton affinities of the analytes are above that of water, then these compounds are able to form the analyte ions, otherwise no significant

formation of analyte ions can be expected. Compounds, investigated in this work (toluene, ethylbenzene, xylene and trimethlybenzene) have electron-donating methyl- or ethyl-groups providing these compounds with high proton affinities[5]. For this reason, the selected alkyl-substituted aromatic compounds are very likely to form the product ions by proton-transfer ionization pathway and therefore, should be good detectable with the DMS.
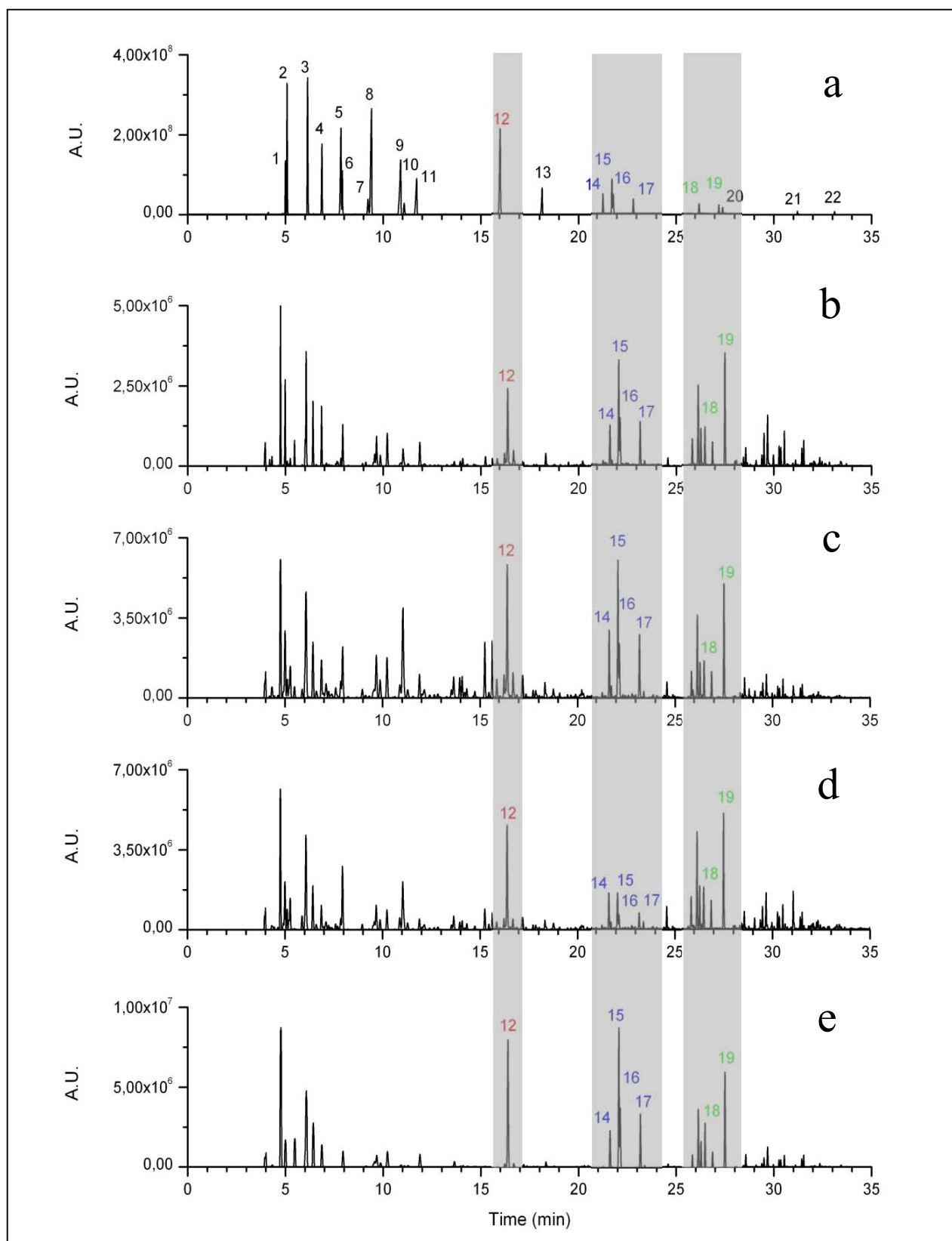
Figure 2.1 GC-MS chromatograms of groundwater spiked with: (a) NIST gasoline (SRM 2294), (b) Aral gasoline, (c) Shell gasoline, (d) Star gasoline and (e) Gasoline without additives

Table 2.1 Molecular weight(MW), retention times of the compounds identified in a groundwater sample spiked with NIST SRM 2294 standard

Peak No.	Substance	MW (g/mol)	Rt[min]
1	1-penten	70,13	4,12
2	n-pentane	72,15	4,99
3	MTBE	88,15	5,08
4	n-hexane	86,18	6,13
5	2,4-dimethylpentane	100,20	6,87
6	2,3-dimethyl-2-butene	84,20	7,84
7	benzene	78,11	7,91
8	cyclohexane	84,16	9,32
9	2,2,4-trimethylpentane	114,23	9,41
10	1-heptene	98,19	10,90
11	n-heptane	100,21	11,08
12	toluene	92,14	11,72
13	octane	114,22	16,03
14	ethylbenzene	106,17	18,14
15	m-xylene	106,16	21,30
16	p-xylene	106,16	21,76
17	o-xylene	106,16	21,83
18	1,3,5-trimethylbenzene	120,20	22,84
19	1,2,4-trimethylbenzene	120,20	26,21
20	n-decane	142,29	27,20
21	1,2,4,5-tetramethylbenzene	134,22	27,39
22	naphthalene	128,17	31,21
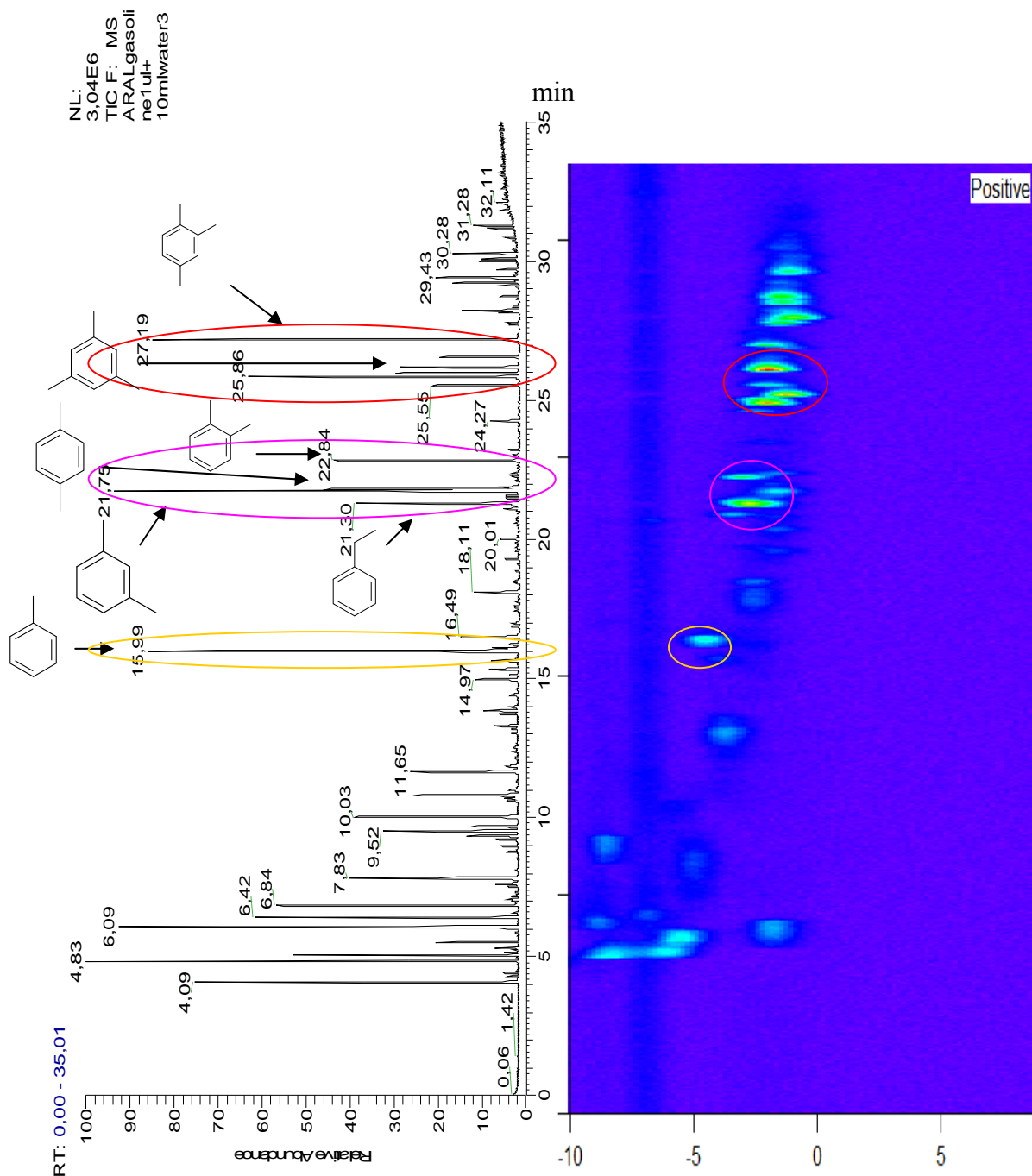
Figure 2.2 Groundwater spiked with gasoline (Super, Aral) by GC DMS(left) and MS(right). The DMS parameters were: sensor temperature of 60°C, flow rate of 300 ml/min, RF-voltage of 1000 V (20 kV/cm)

As shown in Figure 2.2, the peaks of m- and p-xylene are not completely resolved from each other during the gas chromatography step. As it was mentioned above, the DMS is able to separate compounds in a very short period of time based on a difference in the mobility coefficients in high and low electric fields. This ability gives an opportunity to achieve a separation of the

compounds, which were not resolved during the gas chromatography step. Hence, the identification of these compounds on the basis of the retention time and the compensation voltage could be achieved.

2.3.2 Optimization of DMS parameters for the detection of selected fingerprint compounds

To optimize the DMS parameters, a group of compounds (ethylbenzene, m-/p-xylene, o-xylene) with close retention times was selected. The electric field, the carrier gas flow rate and the sensor temperature were chosen as optimisation parameters.

The electric field, created by the asymmetrical RF-voltage, is the most important parameter for the DMS selectivity and sensitivity. In a high electric field, the ion clusters formation is reduced and the ions get a higher mobility[11]. This leads to the dispersion of the analysed compounds along the electric field that results in reduction in signal intensities (see Figure 2.3b). There are two reasons which may explain this phenomenon. Firstly, when at higher voltage field, both reactant and pronated ions are much easier to decluster. Another reason is that less target ions can pass through the electrical plates when a higher separation voltage is used. For example, protonated ethylbenzene decluster when the separation voltage increases. The equation for declustering is as shown in equation 2.2:
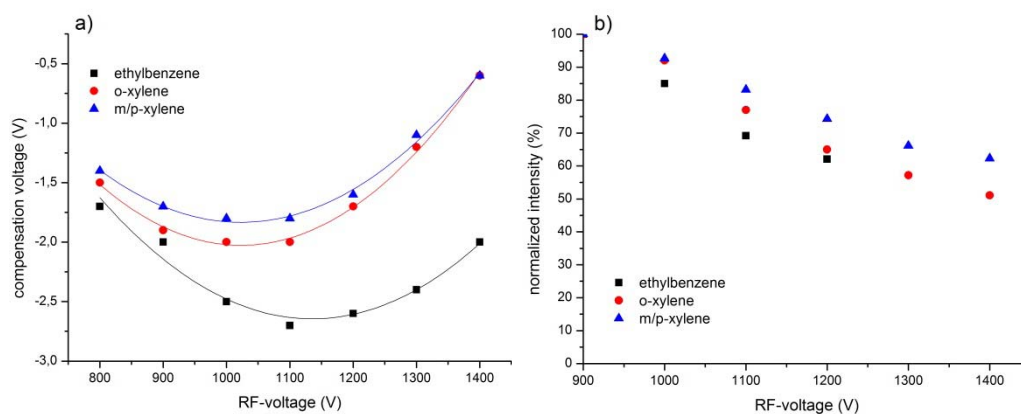

Figure 2.3 Dependences of the compensation voltage (**a**) and normalized signal intensities (**b**) of ethylbenzene, o-xylene and m/p-xylene on the RF-voltage

$$[\text{ethylbenzene}]H^+ \rightarrow \text{ethylbenzene} + H^+ \quad \text{(eq. 2.2)}$$

As shown in Figure 2.3a, the separation of the ethylbenzene signal from xylene signals increases with the increase of the RF-voltage. On the other hand, the separation between xylene isomers achieves the maxima at the field of 20 kV/cm (1000 V) and then decreases with the increase of the electric field. Based on these observations, the electric field of 20 kV/cm (1000 V), providing the highest resolution and intensive signals, was chosen for the following experiments. The relation between RF and CV will be discussed in detail in chapter 4.

The flow rate of the carrier gas through the detector influences the residence time of the analytes in the ion-filter region, and hence influences the signal intensity and its area. However, no significant influence of the flow rate on the compensation voltage of the monomers was observed (Figure 2.4a) what is predicted by the theory of DMS [12].

The second signal was observed for ethylbenzene and toluene at flow rates of 200 and 250 mL/min. It can be assumed that these signals are related to the dimer formation, since at the lower flow rates the analyte is less diluted with the carrier gas and the higher concentration of the analyte makes the formation of the dimer more probable. The signal with a higher shift (from zero) in the compensation voltage is usually associated with the monomer, whereas the signal with the compensation voltage closer to zero is related to the dimer [13].

The signal of the dimer disappeared at flow rates higher than 250 mL/min. At flow rates above 300 mL/min, the compensation voltages for the analyzed organic compounds are almost constant. Thus, the effect of the flow rate on the compensation voltage is not significant in the range of 300 mL/min to 500 mL/min. A flow rate of 300 mL/min is adopted in the following measurements.

Generally, the detector temperature can have an effect on the intensity of the signal, but should not influence the compensation voltage needed for the ions detection. Furthermore, the compensation voltage is dependent on the

temperature of the drift tube[14] . Sacks et al. have demonstrated on the example of alcohols (C4-C7) that for the miniaturized DMS device the temperature of the sensor has an influence on the compensation voltage[15]. This effect was examined by Krylov et al. and algorithm for the prediction of compensation voltage depending on temperature was proposed[14]. The shift of the compensation voltage can be explained by influence of the temperature on gas density (N), and hence on the value of E/N. In addition the distribution of ion-neutral collision energy, and therefore the ion mobility, is changed[14]. The similar effect, as shown in Figure 2.4b, was observed in this study. The values of compensation voltage versus detector temperature give linear correlation for the analyzed compounds in the range from 80 to 120 ℃.

As already discussed the compounds with higher molecular weights have a smaller shift in the compensation voltages compared to those compounds with lower molecular weights. This observation is valid within the temperature range (80-120 ℃). Moreover, it was found that at lower sensor temperatures the signal resolution of the analyzed compounds is higher than those at higher temperatures (Figure 2.4b).
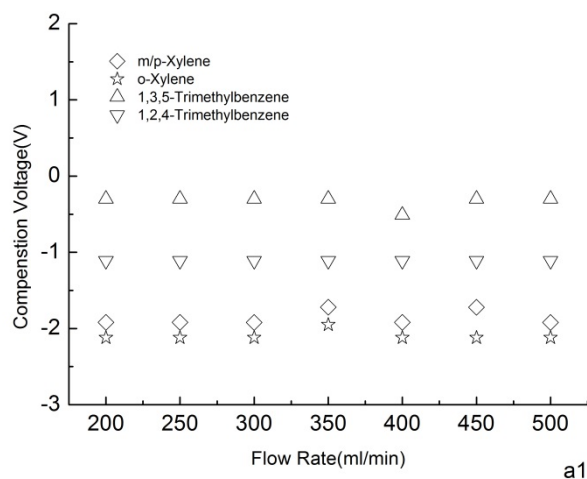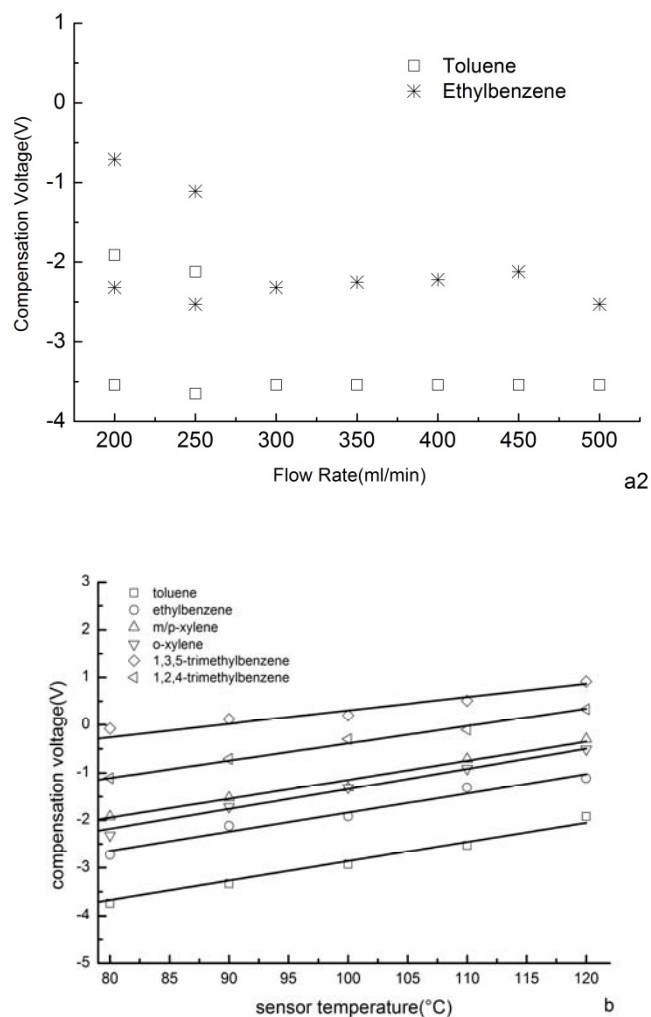
Figure 2.4 Effect of the flow rate (**a1** and **a2**) and sensor temperature (**b**) on the compensation voltages of the analyts

Hence, the following measurements were performed at the electric field of 20 kV/cm (1000V) with a carrier gas flow rate of 300 mL/min and a sensor temperature of 80 ℃.

2.3.3 Quantitative relationships between fingerprint compounds and gasoline in groundwater

The relationship between the DMS signal intensity of the target compounds and the concentration of gasoline in groundwater is shown in Figure 2.5. The signal intensities of seven compounds are plotted versus the concentration of gasoline in groundwater in the range from 29,08 to 72,70 mg/L. In cases of gasoline leaks,

the contaminant concentrations of gasoline in groundwater are usually in this range what allow a fast monitoring of gasoline contaminated groundwater by the described method. Mononuclear aromatic constitute are the main class of hydrocarbons found in water soluble fraction. The total mononuclear aromatics constitute about 89% of the total water soluble fraction of crude oil. BTEX represented 87,6% of the water soluble fraction[16].
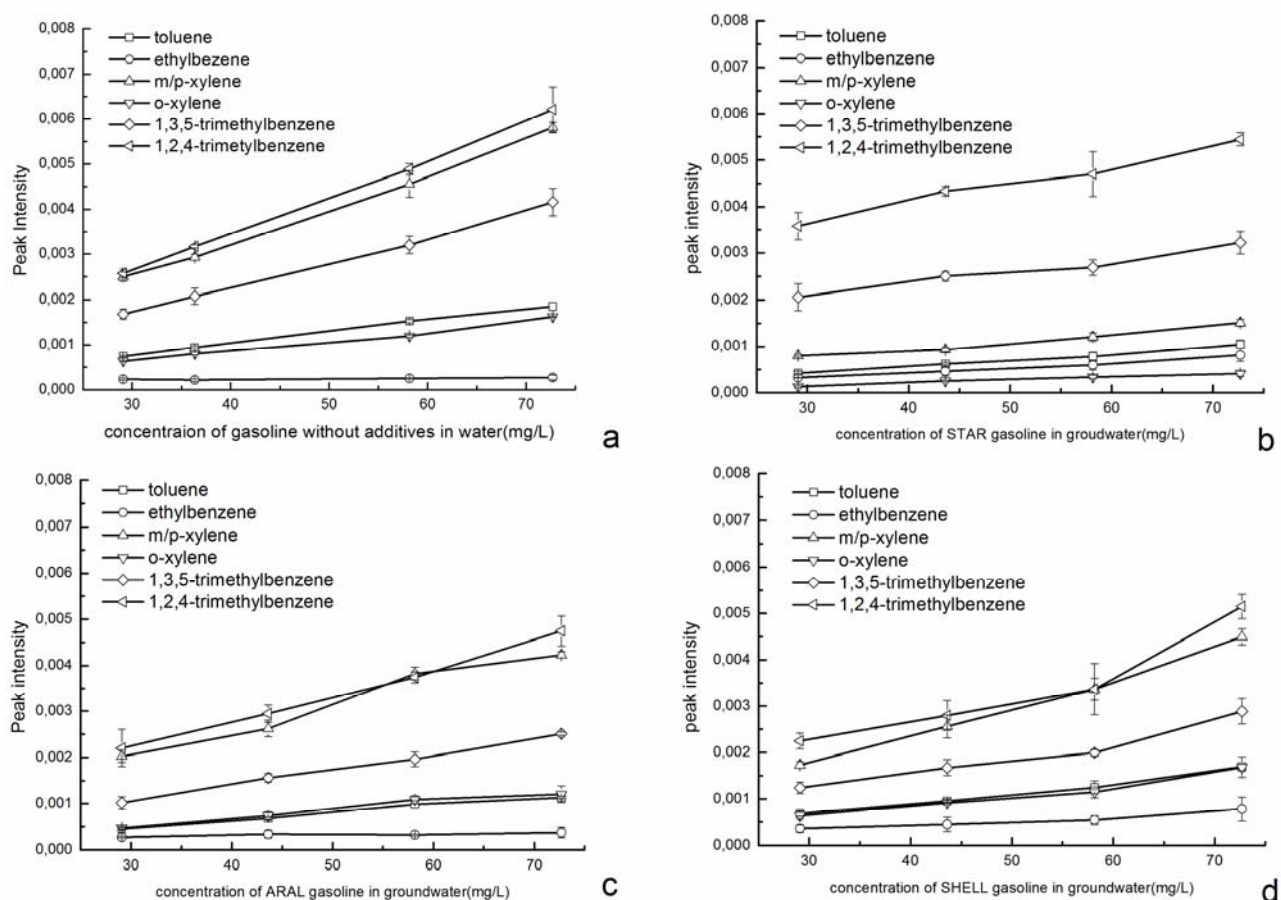
Figure 2.5 Relationship between signal intensities of the fingerprint compounds (toluene, ethylbenzene, m/p-xylene, o-xylene, 1,3,5-trimethylbenzene and 1,2,4-trimethylbenzene) and the concentration of gasoline in groundwater

2.4 Summary

In this work, the feasibility of fingerprint identification of volatile organic compounds in gasoline contaminated groundwater by differential mobility spectrometry was demonstrated.

The method is based on the detection of organic compounds (BTEX) which were found in all analyzed groundwater samples spiked with gasoline. These

compounds give high responses of the DMS detector. Coupling of GC with DMS, which has an own separation ability based on differences in the ion mobilities in the low and high electric fields, gives an advantage by analysis in the presence of a complex matrix. The optimization of the DMS parameters e.g. RF-voltage, carrier gas flow rate and sensor temperature resulted in a further improvement of the compounds separation. The results of this study show the feasibility of GC-DMS for monitoring of gasoline contamination in groundwater.

2.5 References

1.   Haest, P.J., et al., *Containment of groundwater pollution (methyl tertiary butyl ether and benzene) to protect a drinking-water production site in Belgium.* Hydrogeology Journal, 2010. **18**(8): p. 1917-1925.
2.   Anderson, J.W., et al., *Characteristics of Dispersions and Water-Soluble Extracts of Crude and Refined Oils and Their Toxicity to Estuarine Crustaceans and Fish.* Marine Biology, 1974. **27**(1): p. 75-88.
3.   Sauer, T.C. and H.J. Costa, *Fingerprinting of gasoline and coal tar NAPL volatile hydrocarbons dissolved in groundwater.* Environmental Forensics, 2003. **4**(4): p. 319-329.
4.   Kanu, A.B. and C.L.P. Thomas, *The presumptive detection of benzene in water in the presence of phenol with an active membrane-UV photo-ionisation differential mobility spectrometer.* Analyst, 2006. **131**(9): p. 990-999.
5.   U Telgheder, M.M., MA Jochmann,, *Determination of volatile organic compounds by solid-phase microextraction-gas chromatography-differential mobility spectrometry.* International Journal for Ion Mobility Spectrometry, 2009. **12**: p. 123-130.
6.   Baumbach, J.I., et al., *Detection of the gasoline components methyl tert-butyl ether, benzene, toluene, and m-xylene using ion mobility spectrometers with a radioactive and UV ionization source.* Analytical Chemistry, 2003. **75**(6): p. 1483-1490.
7.   Schmidt, T.C., et al., *Analysis of fuel oxygenates in the environment.* Analyst, 2001. **126**(3): p. 405-413.
8.   Eiceman, G.A. and Y. Feng, *Limits of separation of a multi-capillary column with mixtures of volatile organic compounds for a flame ionization detector and a differential mobility detector.* Journal of Chromatography A, 2009. **1216**(6): p. 985-993.
9.   Creaser, C.S., et al., *Ion mobility spectrometry: a review. Part 1. Structural analysis by mobility measurement.* Analyst, 2004. **129**(11): p. 984-994.
10.   Eiceman, G.A., et al., *Micro-machined planar field asymmetric ion mobility spectrometer as a gas chromatographic detector.* Analyst, 2002. **127**(4): p. 466-471.
11.   GA Eiceman, Z.K., *Ion Mobility Spectrometry, second edition.* 2005: American Chemical Society, CRC press.
12.   Buryakov, I.A., et al., *A New Method of Separation of Multi-Atomic Ions by Mobility at Atmospheric-Pressure Using a High-Frequency Amplitude-Asymmetric Strong Electric-Field.* International Journal of Mass Spectrometry and Ion Processes, 1993. **128**(3): p. 143-148.
13.   Miller, R.A., et al., *A novel micromachined high-field asymmetric waveform-ion mobility spectrometer.* Sensors and Actuators B-Chemical, 2000. **67**(3): p. 300-306.
14.   Krylov, E.V., S.L. Coy, and E.G. Nazarov, *Temperature effects in differential mobility spectrometry.* International Journal of Mass Spectrometry, 2009. **279**(2-3): p. 119-125.
15.   Lambertus, G.R., et al., *Silicon microfabricated column with microfabricated differential mobility spectrometer for GC analysis of volatile organic compounds.* Analytical Chemistry, 2005. **77**(23): p. 7563-7571.
16.   Carls, M.G. and S.D. Rice, *Abnormal-Development and Growth Reductions of Pollock Theragra-Chalcogramma Embryos Exposed to Water-Soluble Fractions of Oil.* Fishery Bulletin, 1990. **88**(1): p. 29-37.

3. Rapid separation of BTEX in groundwater by fast gas chromatography

3.1 Introduction

For speciation and quantification of volatile and semivolatile organic compounds, gas chromatography is the most frequently used method. The GC analytical procedures consist essentially of 4 separate steps: sample preparation and injection, separation and detection, GC oven cooling time and re-equilibration, and the data elaboration. The first two steps have generally greater impact on analytical time cost, selectivity, sensitivity, ruggedness, precision, and accuracy. For this reason, both have been subjected to a great deal of development. The reductions in analysis time for these two steps will have economic advantages for application GC on-field -portable instruments.

Considering the GC separation step, a high number of methods have been introduced in the last decades. High-speed gas chromatography (HSGC) has become one of more highly developed techniques to shorten the analysis time of GC in the past few years. At the beginning of the 1960's, Desty presented the potential of small diameter column to be used in separation [1]. Unfortunately, at the beginning, due to the lack of injection systems, a narrow sample band was manually injected onto the capillary column with a good full width at half maximum (FWHM). Other techniques, which include multicapillary columns (MCC)[2], wide-bore columns [3]and short capillary columns [4]were developed and introduced following the primordial narrow internal diameter column experiment. Korytar and Janssen gave an overview of the various methods available for fast GC [5].

HSGC allows rapid, highly selective analysis of a wide range samples. In 1988, van Es separated 4 n-alkane (C6- C9) and 5 other organic components mixture in 0,7 s with high speed narrow bore capillary gas chromatography [6]. With

little loss of resolution, the analysis time for mixtures of VOCs by HSGC is 10 to 60 folds faster than those of traditional GC techniques [7, 8]. The separation of 114 VOCs in water in 8 min is achieved by HSGC-MS[9]. Davis et al detected 6 PAHs in drinking water in 3 min with HSGC, which equipped a 10m length short column and at a high flow rate (5 mL/min) [10]. Hada et al reported determination of 17 pesticides in water in 8,5 min with a fast temperature program by a short microbore column [11]. In other literature reported, the time for separation 17 trizine pesticides and 10 organic phosphate pesticides in water is low to 5 min by a short column with 5m length and 0,1 mm ID [12].

The focus on DMS is to develop a "laboratory-in-the-field" capability to conduct general environmental assessments [13]and a "rapid response monitor" to quickly and accurately detect toxic compounds, such as chemical agents, resulting from leaks or releases. HSGC were utilized for field applications in near real time or "lab in the field". Current et al used HSGC to monitor and assess the performance of a trickle-bed bioreactor designed for the removal of VOCs from air [14]. Bruker company offers a portable GC/MS (Spectra-Trak) as a "real-time" monitor for toxic air, water, and soil pollutants; however, its portability is limited by weight and the need to attach a mechanical pump separately [15, 16]. Baumbach et al introduced a method to on field monitor BTEX in water in 300 sec by multicapillary GC coupled with IMS [17]. The described tool may be advantageously used for emergency field investigations, because it can be operated on-site at relatively small expenditure, and because it provides results within a short time.

As mentioned in chapter 2, the total analysis time for BTEX in groundwater spiked with gasoline is closed to 20 min by conventional GC (60m length column) coupled to DMS. To shorten the analysis time, a short capillary GC column was selected to analyze the target compounds BTEX by GC-MS. Then, this short GC column will be connected into DMS with a homemade interface.

After optimization the operation condition, the detection of BTEX by this GC-DMS system is done.

3.2 Experimental section

3.2.1 GC-MS setup

To shorten the analysis time, a MXT-5 column (12 meter length × 0,28 mm I.D.× 0,25 d$_f$) from RESTEK, USA was used. The parameters of the GC column are listed in Table 3.1. A Trace GC Ultra (S+H Analytik, Mönchengladbach, Germany) equipped with a split/splitless injector is coupled to a DSQ II single quadrupole mass spectrometer (S+H Analytik) equipped with electron impact ionization source. The GC-MS interface temperature was set to 250 ℃ and the ion source temperature was set to 220 ℃. The ionization energy of the ion source was set to 70 eV and the quadrupole was set to scan mode (*m/z*) of 49-180, 6,5 scans/s. Xcalibur 1.4 data system (S+H Analytik) was used for instrument control, data acquisition, and performance evaluation. The temperature program was used in an isotherm mode.

3.2.2 GC-DMS System Setup

Figure 3.1 shows the schematic setup of GC-DMS system.

The SIONEX SVAC DMS (Sionex Corporation, Bedford, MA, USA) equipped with a [63]Ni ion source of 5 mCi, was used. The sensor temperature was set to 80 °C. Nitrogen (99.999 %, Air Liquide, Oberhausen, Germany) was used as carrier gas with a flow rate of 300 mL/min. All data were recorded by microDMx Expert version 2.4.0 software.

Table 3.1: the details of MXT-5 GC column

Type:	MXT-5
Company	RESTEK, USA
Serial-No:	70221
Material:	Siltek® treated stainless steel
Stationary phase:	low polarity phase; crossbond 5% Diphenyl 95% Dimethylpolysiloxane
Length:	12m
Inner diameter(ID):	0,28mm
d_f	0,25 μm
Temp.-Range:	-60 °C to 430 °C

A Shimadzu GC-2014 GC system was used for all analyses. The split/splitless injector operated at 150 ℃. Nitrogen (>99,999% pure) was used as the carrier gas. Separation was performed on a 12m × 0,28mm ID× 0,25 μm d_f MXT-5 GC column. The temperature of GC oven was kept at 80 ℃. A homemade 10-cm-long interface was used to connect the GC and DMS. The temperature of interface was setup at 80 ℃.
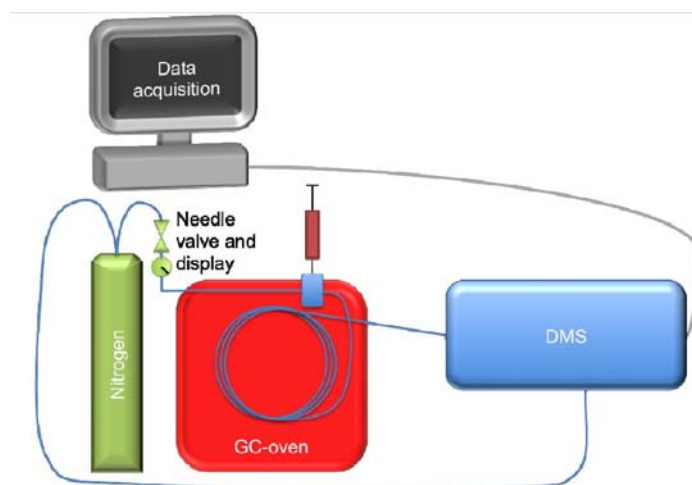

Figure 3.1: schematic setup of GC-DMS

3.2.3 Chemicals

In this work o-xylene(≥99,0%, Fluka Analytical, Steinheim, Germany), p-xylene(≥99,0%, Fluka analytical, Steinheim, Germany), m-xylene(≥99,0%, Fluka, Steinheim, Germany), benzene(99%, AppliChem, Darmstadt, Germany), ethylbenzene (≥99,0%, Fluka, Steinheim, Germany), toluene(99,9%, J.T.Baker, Netherland), MTBE (≥99,5%,Merck, Germany), 1,2,4-trimethylbenzene(98%, Aldrich, Germany) and methanol (99,99%, Fisher Scientific, Germany) were used without further purification.

3.2.4 Data Analysis

OriginLab 9.0 was used to analyze the data recorded by microDMx Expert version 2.4.0 software. Firstly, a 2D diagram was produced (one dimension as retention time of GC; another dimension as compensation voltage detected by DMS) by OriginLab. For quantifying the peak area of target compound, the data at constant compensation voltage dimension was used to generate a chromatogram. Based on the chromatogram, the retention time, peak area, and FWHM are obtained and calculated according to Gauss function by OriginLab 9.0.

According to DIN 32645, the detection limit is defined as the concentration or amount of analyte which can be ascribed to the critical value of a measurement. At the critical value, the content of the analyte can be ascribed to the sample or to the blank. The detection limits are calculated for this method, with the values derived from the calibration curves incorporated in following equation:

$$X_{LOD} = s_x * t_{f,a} * \sqrt{\frac{1}{m} + \frac{1}{n} + \frac{x^2}{Q_{xx}}} \quad \text{(eq. 3.1)}$$

Where n and m are the number of calibration points and measurements, respectively; Q_{xx} and x are the sum of squared deviations and the mean value of the working range; $t_{f,a}$ is the Student's value (at f degrees of freedom and confidence level $\alpha=0,05\%$, f=N-2, P=95%).

The resolution factor (Rs) was calculated using the recommended IUPAC expression [18]:

$$R_S = \frac{2 \times (t_{r2} - t_{r1})}{w_{b1} + w_{b2}} \quad \text{(eq. 3.2)}$$

Where t_{r1} and t_{r2} are the retention times of two analytes and W_{b1} and W_{b2} are the respective widths of each adjacent peak at its base.

3.3 Results and discussion

3.3.1 Choice of MXT-5 GC column

The separation efficiencies of multicapillary column (MCC) and MXT-5 column have been compared. It was found that the separation efficiency of the MCC column was much lower than that of the MXT column, which was able to separate a five substance mixture containing compounds with varying vapor pressures and different retention times. In contrast, the MCC was not able to even completely separate a four substance mixture. Therefore, MXT-5 GC column is used in the following experiment.

General operating requirements for HSGC are easily described from eq. 3.3. This equation gives the retention time t_R of the last component of interest. In this equation, L is the column length, μ is the average carrier gas velocity in the column, and k_n is the retention factor of the last component of interest. Short columns, higher-than-usual carrier gas velocities, and relatively small retention factors can reduce separation times by 1 to 2 orders of magnitude [19].

$$t_R = \frac{L}{u}(k_n + 1) \quad \text{(eq. 3.3)}$$

As shown in Figure 3.1, BTEX can be baseline resolved by MXT-5 column. Dependent on the retention times of these 5 compounds, the peaks are identified by mass spectrometry: 1, benzene, 2, toluene, 3, ethylbenzene, 4, m/p-xylene and 5, o-xylene. The boiling points are 80 °C for benzene, 111 °C for toluene, 136 °C for ethylbenzene, 139 °C for m-xylene, 138 °C for p-xylene and 144 °C for o-xylene, respectively. From the results achieved by using MXT-5 column, the retention times of these target compounds are also positive related to their

boiling points. This result suggests the compounds with lower boiling point will remain less time in GC column, resulting in shorter retention time in chromatogram. Because of the close boiling points and similar physical chemical property of m-xylene and p-xylene, the separation of these two isomers by MXT-5 column was not achieved. According to regulation on water of US EPA and WHO[20], the three xylene isomers being taken account into together, separation is unnecessary.
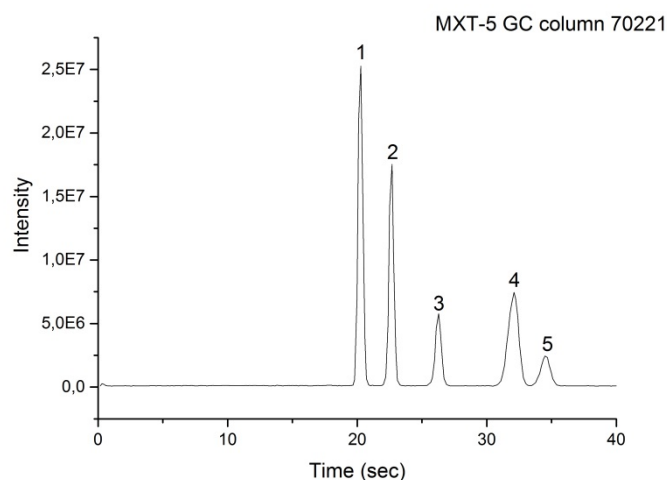

Figure 3.1: BTEX separation by MXT-5 GC column (12m length) detected by MS. Compound identification numbers: 1, benzene, 2, toluene, 3, ethylbenzene, 4,m/p-xylene, 5, o-xylene

As shown in Table 3.2, separation of BTEX in less than 1 min can be achieved by MXT-5 GC column. The retention times are 20,3 sec for benzene, 22,7 sec for toluene, 26,3 sec for ethylbenzene, 32,1 sec for m/p-xylene and 34,5 sec for o-xylene, respectively. Meanwhile, the FWHMs for each peaks are 0,43 sec for benzene, 0,40 sec for toluene, 0,49 sec for ethylbenzene, 0,87 sec for m/p-xylene and 0,74 sec for o-xylene, respectively. There are often discussions as to what can truly be considered "high-speed", "fast GC", "ultra-fast GC". This classification is not academic and still controversial. Dagan and Amira suggested that the speed enhancement factor (SEF) be used to provide definitions for the terms normal (conventional), fast, very fast and ultra-fast GC [21]. The SEF is the increase in speed that can be obtained by using a shorter

column and a higher carrier gas velocity in comparison to the same analysis on a conventional GC column under optimum carrier gas velocity conditions. Otherwise, Van Deursen et al proposed a classification based on the peak widths (2,354σ) and total analysis times[22]. High Speed GC can then be classified as:

> ➤ Fast GC: separation in the minutes range; peak-width, several seconds (FWHM 200-1000ms).
>
> ➤ Very fast GC: separation in the range of seconds; peak width, 30-200ms (FWHM 30-200ms).
>
> ➤ Ultra-fast GC: separation in the sub-second range; peak width, 5-30ms (FWHM 5-30ms).

According to the classification by van Deursen, the method based on MXT-5 GC column can be called as fast GC. The MXT-5 GC column will be used in the following work.

Table 3.2: Retention time (RT) and FWHM of BTEX in chromatogram by MXT-5 GC column

	MXT-5 GC	
	FWHM(sec)	RT (sec)
benzene	0,43	20,3
toluene	0,40	22,7
ethylbenzene	0,49	26,3
m/p-xylene	0,87	32,1
o-xylene	0,74	34,5

3.3.2 Temperature effect on separation by MXT-5 column coupled to MS

The main parameters that govern gas chromatography, in addition to the column material used are the GC temperature and carrier gas linear velocity. As shown in eq. 3.3, the retention factor k_n will influence the retention time. To shorten the retention time, k_n can decrease through increasing column temperature. The GC

oven temperature has a dramatic exponential effect on the speed of analysis. Increasing of the column temperature results in a reduction of the elution time by a factor of about two for each 10 ℃ [23].

Because oven cooling down and equilibration are time-consuming, the time for whole measurement will increase. Moreover, if a fast temperature program is used, the initial oven temperature affects the cool down time more than the final temperature because it usually takes longer for an oven to cool from 100 to 50 ℃ than 300 to 100 ℃. For a field portable device, it is better to cut off the time for cooling down and equilibration. The easiest way to achieve the required conditions for a more rapid elution would be to perform the analysis isothermally. Therefore, if without any special mentioned, the following methods are all used isothermal mode for GC.
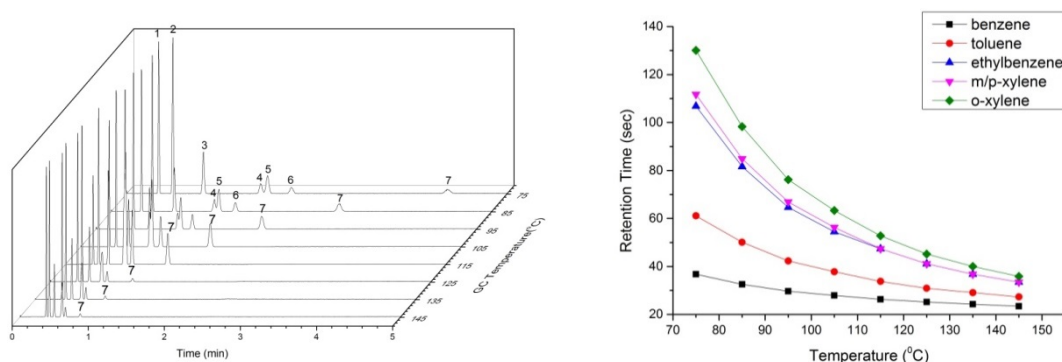

Figure 3.2: effect of temperature on separation by fast GC-MS. Compound identification numbers: 1, MTBE, 2, benzene, 3, toluene, 4, ethylbenzene, 5,m/p-xylene, 6, o-xylene, 7, 1,2,4-trimethylbenzene

The temperature effects on fast GC are shown in Figure 3.2. As shown on chromatogram(left in Figure 3.2), the first and last peaks are MTBE and 1,2,4-trimethylbenzene. The retention times for all compounds decrease with the increasing oven temperature. The compounds with high boiling point are influenced largely by temperature. For instance, the retention time for o-xylene declines rapidly from 130,1 to 48,6 sec when the column temperature increases from 75 to 145 ℃ (in Figure 3.2 right). Due to low boiling points, benzene and toluene eluted from the column very quickly and the retention times did not change largely when the oven temperature changed.

Blumberg et al found that high elution temperature will decrease separation efficiency and will cause greater thermal breakdown of susceptible analytes [24]. In Figure 3.2, when the temperature was above 95 ℃, it failed to separate the three compounds (ethylbenzene, m/p-xylene, o-xylene), resulting in the peaks overlapping.

3.3.3 GC coupled to DMS

3.3.3.1 Optimization of flow rate for GC-DMS

As shown in eq. 3.3, the variable μ in the equation is inversely proportional to t_R. Therefore, μ can be increased to cause a decrease in time of analysis. In Figure 3.3, the effect of the column flow rate on the separation of BTEX mixture is demonstrated. As the GC column flow increases, the elution time proportionally reduces. The total analysis time is from closed to 200 sec at low flow rate of 2 mL/min to less than 60 sec at high flow rate of 10 mL/min. As shown in Figure 3.4, it should be noted that as the flow rate increases, the peak areas of BTEX detected by DMS also intensify. This can be explained by the fact that the compounds, which eluted from the GC column, are mixed with DMS carrier gas N_2 and then are introduced into the DMS detector. When the flow rate of DMS carrier gas is constant, at the same time, the amount of analytes will be introduced into DMS at a higher GC flow rate. Therefore, the signal detected by DMS will intensify at higher GC flow rate.
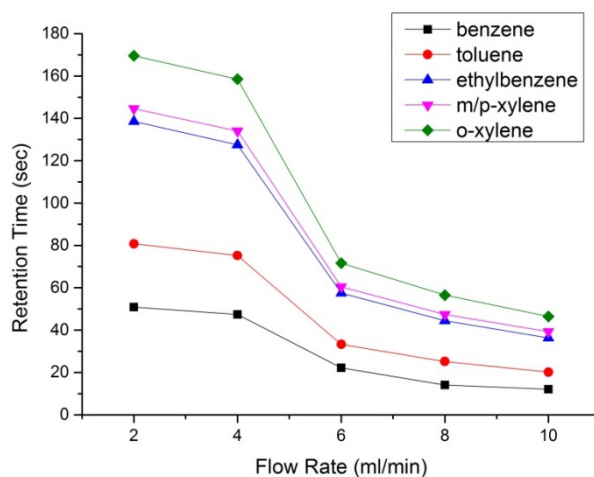

Figure 3.3: the effect of flow rate of GC carrier gas on retention time

Figure 3.3 shows the relation between retention time and flow rate. As the flow rate increases, the retention time declines. However, as shown in Table 3.3, to shorten the time of analysis, the separation efficiencies will be sacrificed. The resolutions of ethylbenzene and m/p-xylene at flow rate above 6 mL/min are low. This can be explained by that use of high carrier gas flow rate reduces column elution temperature and partition time between gas and stationary phase [21, 25, 26]leading to loss of separation efficiencies. Ethylbenzene and m/p-xylene formed almost a single peak in chromatogram. Blumberg et al estimated that operation at $\mu= 2\mu_{opt}$ causes a 25% loss in separation efficiency and 12% loss in Rs [27].
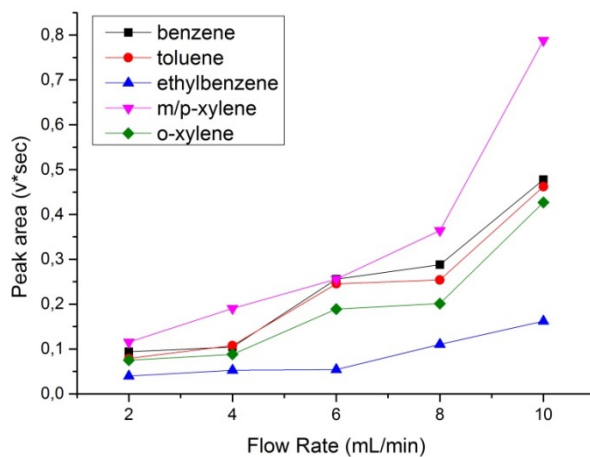

Figure 3.4: the effect of flow rate of GC carrier gas on peak area of BTEX

Table 3.3: resolution at different flow rate

GC Flow Rate(mL/min)	Rs (ethylbenzene and m/p-xylene)	Rs(m/p-xylene and o-xylene)
2	1,20	4,26
4	1,19	3,46
6	1,10	3,02
8	1,00	2,21
10	0,65	1,92

3.3.3.2 Optimization of parameters of detector ^{63}Ni-DMS

The compensation voltage (CV) is employed to compensate for ion drift under different electric field. As a result, a subset of ions can pass through the device. Therefore, the CV value reflects ion properties under varying electric field and thus it is orthogonal unique to each ion. When ^{63}Ni is used as ionization source, reactant ions are very important for formation of product ions. Thus, in the following part, associated with the intensity of reactant ion peak (RIP), CV value of reactant ions described as the position of RIP is used to evaluate the condition of the device.
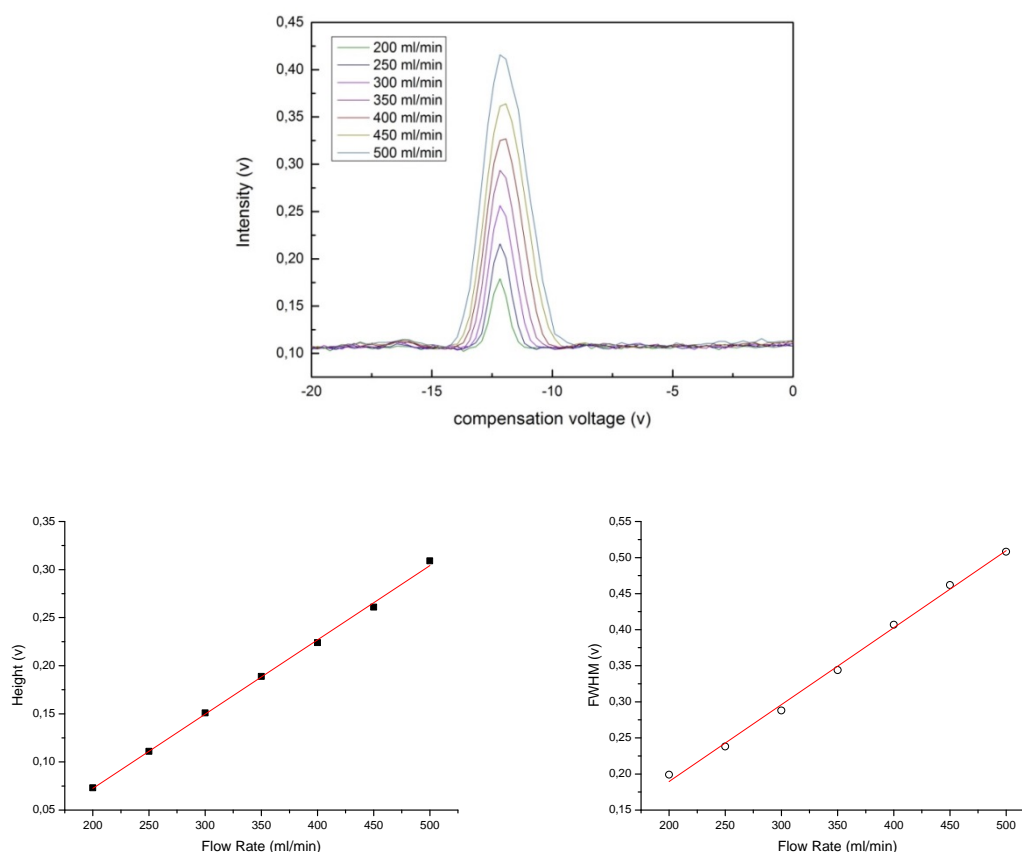

Figure 3.5: effect of flow rate on compensation voltage of RIP at 80 °C and 1000 V (RF)

Theoretically, the flow rate of DMS carrier gas will lead to the shifts in intensity of RIP, but slightly change the RIP position [28]. As shown in Figure 3.5, the principal RIP was observed at -12,2 V. Additionally, when carefully observing the peak shape of different flow rates, it is found that the right tailing part of the peak moves more largely than the left half part, but the entire peak shifts not

very significantly to less negative in compensation voltage. This can be explained that with flow rate increasing, the displacement of ions in ion filter region reduces and hence the absolute value of the compensation voltage needed to correct the trajectory of the ion reduces [29].

The flow rate of the carrier gas affects both peak intensity described as peak height and peak area. As the flow rate increases from 200 to 500 mL/min, the peak height of RIP intensifies from 0,073 to 0,309V. These findings suggest that the high flow rate of the carrier gas will strengthen the signal of RIP. Under a certain range of flow rate, the diffusion, ion neutralization and annihilation processes play key roles to loss of ions. Thus, the increasing flow rate will shorten the residence time of ions in ion filter electrodes, which enhances the number of ions survived through the ion filter region. As a result, the intensity of ions will increase. Miller reported that the curve of peak intensity is as a function of flow rate below the flow rate of 3 L/min and then saturates or begins to decrease at high flow rate [29]. In this case, since the range of the flow rate of DMS adjusted is from 200 to 500 mL/min, the effect of high flow rate above 500 mL/min on RIP cannot be studied. Otherwise, the peak width (described as full width at half maximum, FWHM) increases from 0,199 to 0,508V as the increase of the carrier gas flow from 200 to 500 mL/min. In addition, both curves of FWHM are as proportional function to flow rate (as shown in Figure 3.5) in the range of 200 to 500 mL/min. In literature [30], six target compounds used for testing the effect of flow rate on DMS detector, it was found that at flow rates above 300 mL/min, the values of CVs for the analyzed organic compounds are almost constant and the effect of the flow rate on the CVs for the target compounds is not significant in the range of 300 mL/min to 500 mL/min. Consequently, taking account to results related to effect of flow rate on RIP in this work and on target compounds in previous work together, a flow rate of 300 mL/min was also adopted in the following experiment.

There are two distinct ways of temperature influencing the ion mobility in electric fields. First, the drift gas density will be influenced by temperature, leading to change field contribution to ion kinetic energy. Moreover, gas temperature changes the ion and neutral kinetic energy distributions and hence changes the distribution of ion neutral collision energies and the ion mobility [31]. The effect of the temperature on compensation voltage of target organic compounds was studied in chapter 2. In this section, the sensor temperature influencing the compensation voltage and intensity of the RIP was studied. As shown in Figure 3.6, the plots of temperature and compensation voltage of the RIP were recorded at 5 temperature points (80 ℃, 90 ℃, 100 ℃, 110 ℃, 120 ℃) at a fixed RF voltage of 1000 V. The CV shifts into more negative region obviously and the intensities of RIP decline when increasing temperature from 80 ℃ to 120 ℃.
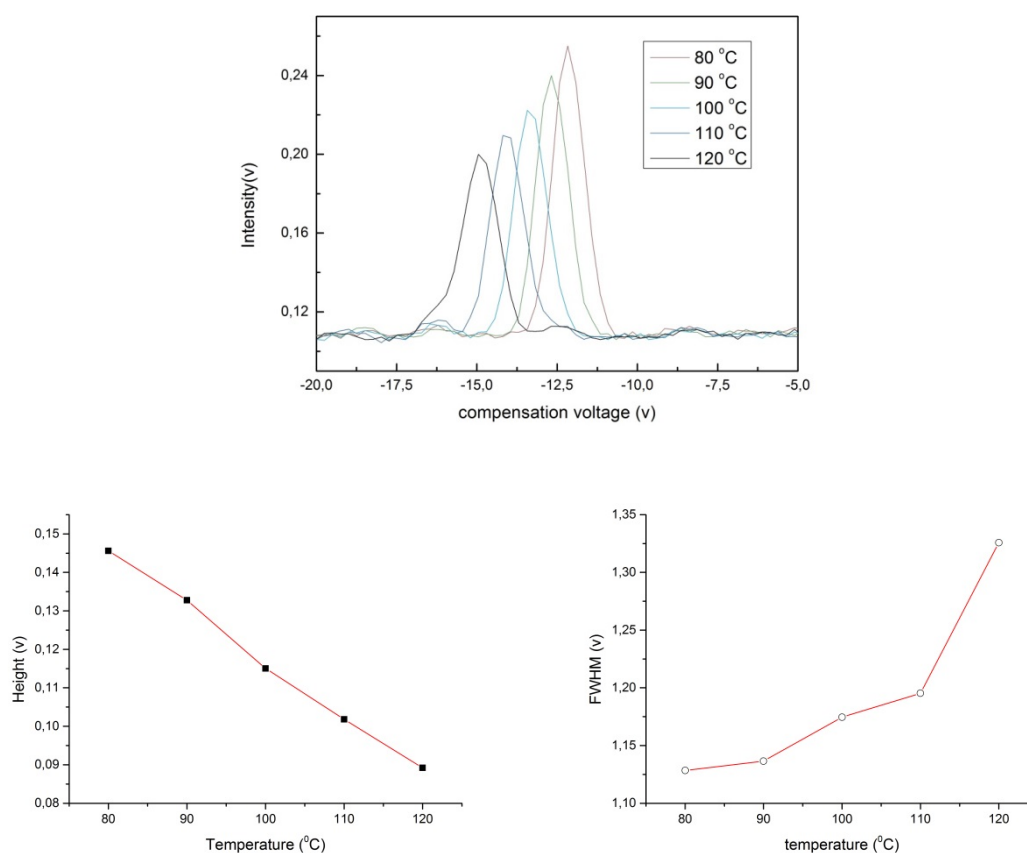

Figure 3.6: sensor temperatures of DMS influences the RIP at 1000 V (RF) and flow rate of 300 mL/min

As shown in Figure 3.7, the CV of RIP shifts to more negative value when RF voltage increases. Moreover, the intensity of RIP decreases as the increasing of RF voltage obviously. At the RF value of 1200 V, the RIP disappeared. This phenomenon can be explained as follows. When at a high RF voltage field, the ions of RIP drift largely toward one of the electrode plate, leading to large displacement of ions in the ion filter region. As a result, a large magnitude of CV needs to offset the drift trajectory, allowing the ions to remain in equilibrium inside the filter gap and eventually to pass the ion filter region. Meanwhile, the number of ions that survive through the ion filter region decreases at a high RF field.
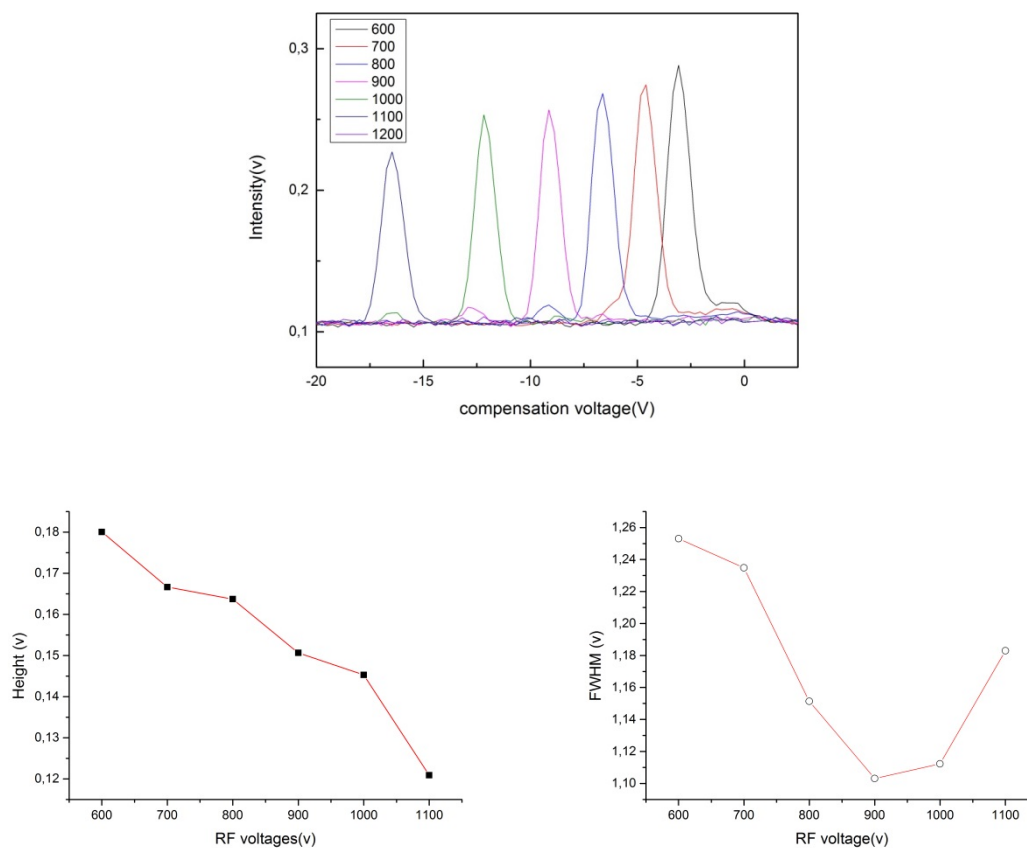

Figure 3.7: the effect of RF voltage on the RIP at 300 mL/min and 80 ℃

When the elution of the compounds, the intensity of a product ion peak grows with a corresponding decrease in intensity of the RIP until a maximum for the GC elution profile is reached. After this, the intensity of the product ions decreases, leading to an increase of RIP until eventually reaching the original

intensity. To balance the intensity and CV, 1000 V was used as RF voltage in the following experiment.

3.3.3.3 Characterization of GC-^{63}Ni-DMS

After optimization of the temperature and the flow rate for GC and DMS, the characterization of GC-^{63}Ni-DMS system including calibration curves and detection limits of target compounds were shown in Figure 3.8 and Table 3.4.

Table 3.4: Characterization of GC-^{63}Ni-DMS

Compounds	Retention time (sec)	Compensation voltage (V)	Detection limits (mg/L)
Benzene	44,1	-6,2	201,8
Toluene	55,2	-3,6	50,3
Ethylbenzene	74,4	-2,7	9,5
m-Xylene	77,4	-2,2	6,2
p-Xylene	77,4	-2,2	8,5
o-Xylene	86,5	-2,3	4,8

According to DIN 32645, the detection limits of target compounds in groundwater are shown in Table 3.4. The detection limits achieved by this method are higher than those of the lab based standardized methods by GC-MS and GC-FID. However, the concentrations of most contaminant cases are in the range of mg/L [17]. Additionally, to improve the sensitivity of this system, UV lamp will be used in the following chapter.
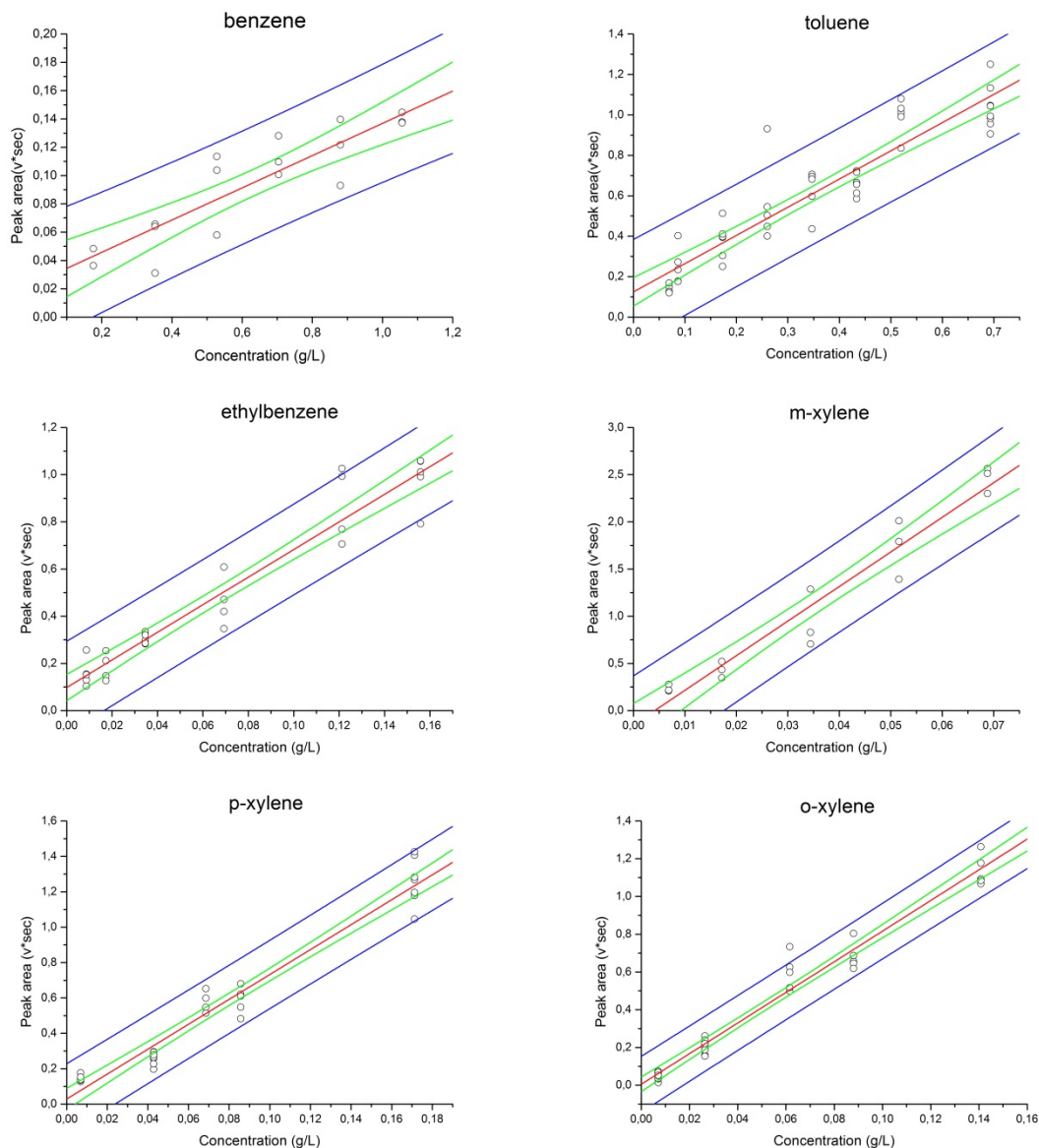
Figure 3.8: calibration curves of GC-^{63}Ni-DMS system for target compounds

3.4 Summary

A short column MXT-5 was selected and utilized for separating the target compounds (BTEX) in groundwater. The analysis time is less than 2 min. After being coupled to DMS equipped with ^{63}Ni, The detection limits of target compounds in groundwater are 201,8 mg/L for benzene, 9,53 mg/L for ethylbenzene, 50,31 mg/L for toluene, 6,20 mg/L for m-xylene, 8,53 mg/L for p-xylene, and 4,76 mg/L for o-xylene, respectively, by GC-^{63}Ni-DMS. The detection limits are higher than the MCLs regulated by WHO (0,01 mg/L for benzene, 0,7 mg/L for toluene, 0,3 mg/L for ethylbenzene and 0,5 mg/L for total xylene).

The next chapter, in order to improve the sensitive, the ^{63}Ni ionization source will be replaced by krypton lamp. The performance of GC-UV-DMS will be discussed.

3.5 References

1.   Dekker, M., *Advances in Chromatography*. 1965, New York.

2.   van Lieshout, M., et al., *A practical comparison of two recent strategies for fast gas chromatography: Packed capillary columns and multicapillary columns.* Journal of Microcolumn Separations, 1999. **11**(2): p. 155-162.

3.   van Deursen, M., et al., *Fast gas chromatography using vacuum outlet conditions.* Journal of Microcolumn Separations, 2000. **12**(12): p. 613-622.

4.   Bicchi, C., et al., *Conventional inner diameter short capillary columns: an approach to speeding up gas chromatographic analysis of medium complexity samples.* Journal of Chromatography A, 2001. **931**(1-2): p. 129-140.

5.   Korytar, P., et al., *Practical fast gas chromatography: methods, instrumentation and applications.* Trac-Trends in Analytical Chemistry, 2002. **21**(9-10): p. 558-572.

6.   Vanes, A., et al., *Sample Enrichment in High-Speed Narrow Bore Capillary Gas-Chromatography.* Journal of High Resolution Chromatography & Chromatography Communications, 1988. **11**(12): p. 852-857.

7.   Sacks, R., H. Smith, and M. Nowak, *High-speed gas chromatography.* Analytical Chemistry, 1998. **70**(1): p. 29a-37a.

8.   Klemp, M., A. Peters, and R. Sacks, *High-Speed Gc Analysis of Vocs - Sample Collection and Inlet Systems .1.* Environmental Science & Technology, 1994. **28**(8): p. A369-A376.

9.   George, C., *High-speed analysis of volatile organic compounds in environmental samples using small-diameter capillary columns and purge-and-trap GC-MS systems.* Lc Gc North America, 2001. **19**(6): p. 578-+.

10.   Davis, S.C., A.A. Makarov, and J.D. Hughes, *Supersonic molecular beam hyperthermal surface ionisation coupled with time-of-flight mass spectrometry applied to trace level detection of polynuclear aromatic hydrocarbons in drinking water for reduced sample preparation and analysis time.* Rapid Communications in Mass Spectrometry, 1999. **13**(4): p. 247-250.

11.   Hada, M., et al., *Trace analysis of pesticide residues in water by high-speed narrow-bore capillary gas chromatography-mass spectrometry with programmable temperature vaporizer.* Journal of Chromatography A, 2000. **874**(1): p. 81-90.

12.   Vreuls, R.J.J., J. Dalluge, and U.A.T. Brinkman, *Gas chromatography-time-of-flight mass spectrometry for sensitive determination of organic microcontaminants.* Journal of Microcolumn Separations, 1999. **11**(9): p. 663-675.

13.   Mcdonald, W.C., et al., *Developments and Applications of Field Mass Spectrometers.* Environmental Science & Technology, 1994. **28**(7): p. A336-A343.

14.   Current, R.W., E.I. Kozliak, and A.J. Borgending, *Monitoring biodegradation of VOCs using high speed gas chromatography with a dual point sampling system.* Environmental Science & Technology, 2001. **35**(7): p. 1452-1457.

15.   Eckenrode, B.A., *The application of an integrated multifunctional field-portable GC/MS system.* Field Analytical Chemistry and Technology, 1998. **2**(1): p. 3-20.

16.   Baykut, G. and J. Franzen, *Mobile Mass-Spectrometry - a Decade of Field Applications.* Trac-Trends in Analytical Chemistry, 1994. **13**(7): p. 267-275.

17.   Walendzik, G., J.I. Baumbach, and D. Klockow, *Coupling of SPME with MCC/UV-IMS as a tool for rapid on-site detection of groundwater and surface water contamination.* Analytical and Bioanalytical Chemistry, 2005. **382**(8): p. 1842-1847.

18.   IUPAC, *compendium of chemical terminology.* second ed. 1997.

19.   Mastovska, K. and S.J. Lehotay, *Practical approaches to fast gas chromatography-mass spectrometry.* Journal of Chromatography A, 2003. **1000**(1-2): p. 153-180.

20.   Available from: http://www.edstrom.com/Resources.cfm?doc_id=167.

21.   Dagan, S. and A. Amirav, *Fast, very fast, and ultra-fast gas chromatography-mass spectrometry of thermally labile steroids, carbamates, and drugs in supersonic molecular beams.* Journal of the American Society for Mass Spectrometry, 1996. **7**(8): p. 737-752.

22.   van Deursen, M.M., et al., *Evaluation of time-of-flight mass spectrometric detection for fast gas chromatography.* Journal of Chromatography A, 2000. **878**(2): p. 205-213.

23.   Dagan, S. and A. Amirav, *Fast, High-Temperature and Thermolabile Gc Ms in Supersonic Molecular-Beams.* International Journal of Mass Spectrometry and Ion Processes, 1994. **133**(2-3): p. 187-210.

24.   Blumberg, L.M. and M.S. Klee, *Optimal heating rate in gas chromatography.* Journal of Microcolumn Separations, 2000. **12**(9): p. 508-514.

25.   Kochman, M., et al., *Fast, high-sensitivity, multipesticide analysis of complex mixtures with supersonic gas chromatography-mass spectrometry.* Journal of Chromatography A, 2002. **974**(1-2): p. 185-212.

26.   Amirav, A., A. Gordin, and N. Tzanani, *Supersonic gas chromatography/mass spectrometry.* Rapid Communications in Mass Spectrometry, 2001. **15**(10): p. 811-820.

27.   Blumberg, L.M., T.A. Berger, and M. Klee, *Constant Flow Versus Constant-Pressure in a Temperature-Programmed Gas-Chromatograph.* Hrc-Journal of High Resolution Chromatography, 1995. **18**(6): p. 378-380.

28.   Buryakov, I.A., et al., *A New Method of Separation of Multi-Atomic Ions by Mobility at Atmospheric-Pressure Using a High-Frequency Amplitude-Asymmetric Strong Electric-Field.* International Journal of Mass Spectrometry and Ion Processes, 1993. **128**(3): p. 143-148.

29.   Miller, R.A., et al., *A MEMS radio-frequency ion mobility spectrometer for chemical vapor detection.* Sensors and Actuators a-Physical, 2001. **91**(3): p. 301-312.

30.   Feng Liang, K.K., Andriy Kuklya,Ursula Telgheder *Fingerprint identification of volatile organic compounds in gasoline contaminated groundwater using gas chromatography differential ion mobility spectrometry.* International Journal for Ion Mobility Spectrometry, 2012. **15**: p. 169-177.

31.   Krylov, E.V., S.L. Coy, and E.G. Nazarov, *Temperature effects in differential mobility spectrometry.* International Journal of Mass Spectrometry, 2009. **279**(2-3): p. 119-125.

4. Comparative determination of BTEX by GC coupled to DMS equipped with radioactive [63]Ni and UV lamp

4.1 Introduction

Radioactive ionization sources, corona or partial discharge ionization, photoionization, laser ionization, surface ionization, electrospray ionization and some other techniques are commonly used as ionization methods [1, 2]. For IMS, the radioactive [63]Ni is the usual source of ionizing electrons, due to high efficiency for many analytes and no power requirement [3]. Polar and nonpolar compounds can be ionized and be detected by [63]Ni-IMS or [63]Ni-DMS. The efficiency of detection for many analytes is largely depending on chemical ionization reactions of one or more molecular properties, such as ionization potential, electron affinity, proton transformation. Unfortunately, the detection limits of [63]Ni-DMS for BTEX are high and linear working ranges are limited. Additionally, there are very strict regulatory on the use of radioactive material. For obvious reasons it would be highly advantageous to replace the radioactive source with other ionization ways like atmospheric pressure photoionization (APPI).

In 1983, Baim used photoionization at atmospheric pressure equipped to ion mobility spectrometry[4]. After that, in 1980s, Eiceman reported a series of pioneer works on photoionization IMS[5-7]. The applications have been recently published [8-12]. Baumbach et al detected ethanol and 1- propanol in the concentration range between 1 and 100 ppmv by UV-IMS[8]. Borsdorf et al analyzed sets of structural isomeric and stereoisomeric non-polar hydrocarbons (saturated and unsaturated cyclic hydrocarbons and aromatic hydrocarbons) using a novel miniature DMS equipped with APPI[9]. A comparative study of analysis of halogenated compounds by APPI-IMS-MS and APPI-DMS was also done by Borsdorf [10]. Real time monitoring of MTBE, BTX in water and nitrogen is achieved by MCCs coupled to IMS equipped with UV ionization

source[11]. Cheng et al developed a dopant-assisted negative photoionization source for IMS equipped with commercial VUV krypton lamp and evaluated its capabilities for detection of common explosives like trinitrotoluene (TNT) [12]. Noble gas resonance lamps have long been used as standard equipment in GC photoionization detectors operating at atmospheric pressure[13]. The normal carrier gases like N_2 and He, having ionization energies much higher than the lamp photon energies, provide no ions in competition with target analytes. The greater part of the studies operated in APPI were performed with a krypton lamp. It can produce photons of 10,03 and 10,64 eV in a 4:1 ratio[14]. Because most analytes have lower ionization energy (IE) values than the photon's energy but commonly used solvents and carrier gases present in the source (He, N_2, etc.) have higher IE, krypton was selected to be ionization source. Besides krypton, xenon and argon were also used[15]. In the early years of photoionization, Locke et al used xenon as ionization source [16]. It penetrates deeply but lower energy of produced photons. Argon produces more energetic photons than krypton, leading to produce more abundant molecular ions than krypton [15]. Krypton lamp produces a better signal to noise ratio at a low flow rate, whereas argon are better at high flow rates. The gas phase IE and proton affinity (PA) values of target compounds are listed in Table 4.1.

Table 4.1: gas phase IE and PA values of BTEX and carrier gas [17, 18]

	IE(eV)	PA(kJ/mol)	Argon (eV)	Krypton (eV)	Xenon (eV)
Nitrogen	15,58	493,8	11,7	10,03	8,4
Water	12,62	691,0		10,64	
Oxygen	12,07	421,0		(4:1)	
Benzene	9,24	750,4			
Toluene	8,83	784,0			
Ethylbenzene	8,77	789,9			
m-Xylene	8,55	812,1			
p-Xylene	8,44	794,4			
o-Xylene	8,56	796,0			

In this section, the ionization behaviors of BTEX in DMS equipped with two differential ionization sources [63]Ni and krypton lamp will be discussed. After coupling to GC, the calibration curves and detection limits of BTEX detected by GC-UV-DMS were done.

4.2 Experimental section

4.2.1 Chemicals and sample preparation

The chemicals such as o-xylene(≥99,0%, Fluka Analytical, Steinheim, Germany), p-xylene(≥99,0%, Fluka analytical, Steinheim, Germany), m-xylene(≥99,0%, Fluka, Steinheim, Germany), benzene(99%, AppliChem, Darmstadt, Germany), ethylbenzene (≥99,0%, Fluka, Steinheim, Germany), toluene(99,9%, J.T.Baker, Netherland), and methanol (≥99,99%, Fisher Scientific, Germany) were used without further purification.

In order to obtain the calibration curves and detection limits, clean groundwater spiked with different concentrations of the pure chemicals was used.

4.2.2 DMS description

A set-up of the DMS (SIONEX, SVAC) with the photoionization source is shown in Figure 4.1. The dimensions of the electrodes are as follows: length 15,0 mm; width 3,0 mm; and distance apart 0,50 mm. The volume between the plates is 22,5 mm^3. The residence time of an ion in the analytical section is about 0,405 ms at a gas flow rate of 300 mL/min. Positive and negative ions formed in the source are carried together by N_2 between two parallel electrodes and then detected by Faraday plates.
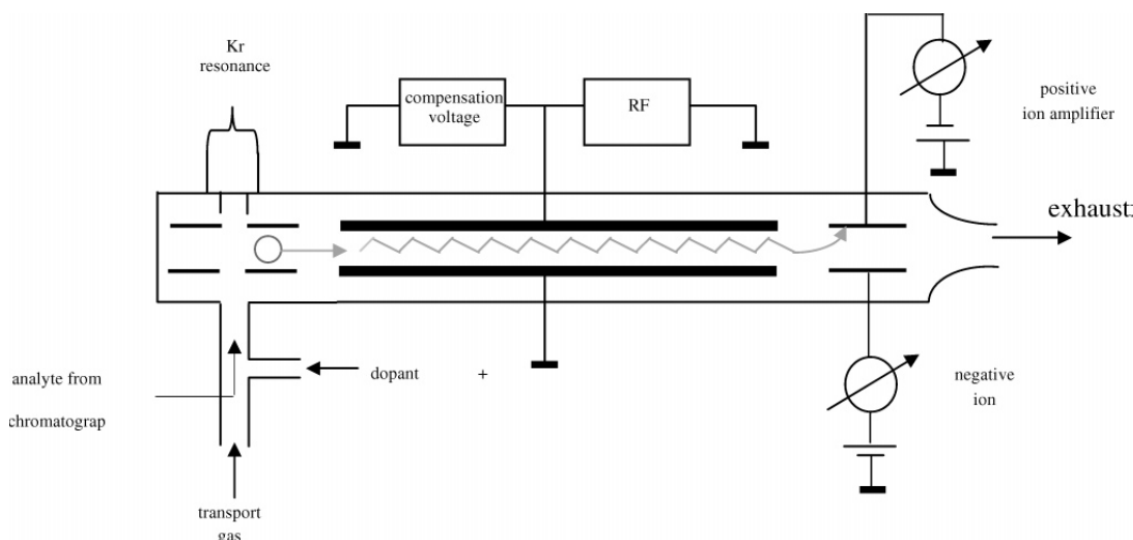
Figure 4.1: Differential mobility spectrometer with a krypton resonance UV lamp as ionization source. For RF and CV measurement, the analyte was directly introduced into DMS without any dopant [19]

The ions pass in the gas stream through the small gap between the two filter electrodes. A strong asymmetric waveform RF electric field of 1,18 MHz is applied on the separating plates perpendicular to the direction of gas flow. As shown in Figure 4.2, the profile of the waveform has equal integral above, high field, and below, low filed, the zero line. Asymmetric field (E_{high}=30000 V/cm and E_{low}=-7200 V/cm) can be generated when the maximum difference between the filter plates (spaced 0,5mm apart) is +1500 V[19].

For APPI method, a miniature krypton discharge lamp with a MgF_2 window (CPI, Santa Rosa, CA) provides photons with energies of 10,03 eV and 10,64 eV with a ratio of 4:1. The light is directed down through a tube with inner diameter (4mm). The analytes are ionized and transported into the separation regions by carrier gas (N_2). For radioactive method, a [63]Ni radioactive source was used.
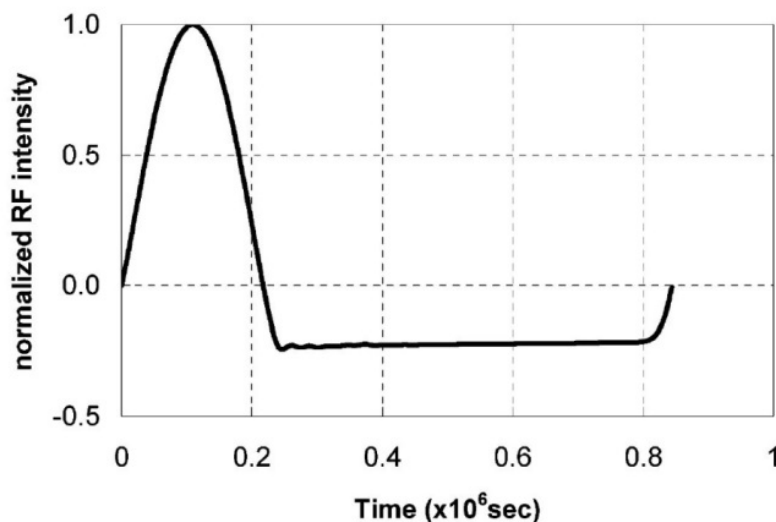
Figure 4.2: Asymmetric waveform of SIONEX SVAC electric field. The integrals above and below the 0 line are equal [19]

4.2.3 Data acquisition and processing

Combinations of separation voltage (SV) and compensation voltage (CV) fields allow the target ion trajectory to pass straight through the analytical region without colliding with the electrodes. Consequently, by scanning or fixing SV and CV, DMS can be operated in the following modes. Firstly, a particular SV and CV combination can be selected, which can continuous filtrate particular ion species. Secondly, when SV is fixed and CV scanned, linear DMS spectra can be recorded. Thirdly, a full differential mobility scan can be recorded when the SV and CV are both synchronized and scanned.

To know the ion species of BTEX ionized by different ionization sources ([63]Ni and UV lamp), the third mode was used; the SV from 500 to 1500 V and CV are both synchronized and scanned. A full differential mobility scan can be obtained. The topographic plots with compensation voltage vs. separation voltages can disclose ion transformations with changes in RF voltage. The compensation voltage was scanned from -20 to 5V for [63]Ni-DMS and from -10 to 4,5 V for UV-DMS.

When DMS coupled to GC, the second mode is used, the SV being fixed and CV being scanned. Under this mode, chromatogram at different CV can be

obtained. In order to do the calibration curves, the peak areas of BTEX in chromatogram are obtained by integration.

In DMS, ion separation occurs through the field dependence of ion mobility, represented by the $\alpha(E/N)$. In $K(E/N)=K_0(1+\alpha(E/N))$, where K_0 is the ion mobility at low of standard conditions and $K(E/N)$ is the ion mobility for particular ion species as a function of electric field amplitude. The $\alpha(E/N)$ can also be described as $\alpha(E/N)=\Delta K/K_0$. It is determined by the relative change in ion mobility between low and high electric field conditions. It is very important for ion species identification dependent on the magnitude and sign of alpha function. The alpha function can be calculated by the RF waveform and the compensation voltage. The detail about alpha function calculation is described in chapter 1. In this work, for the actual waveform shown in Figure 4.2, the real field form factors were determined as $<f^2(t)>=0,236, <f^3(t)>=0,111, <f^5(t)>=0,103$ by literatures [20, 21].

All data are recorded and stored for positive ions simultaneously as excel format by commercial software provided by Sionex SVAC and are analyzed by OriginLab 9.0.

4.3 Results and discussion

4.3.1 Generation of ions by UV and [63]Ni

4.3.1.1 Positive ions generated by UV ionization

In UV-DMS, in the absence of analytes, the DMS spectrum represented a flat baseline. This can be explained that all the main components of the carrier gas N_2 with trace water or other gases, have ionization energies higher than the maximum photon energy of the krypton lamp, no ions were produced. As shown in Figure 4.3, when introduction of a constant flow of analytes, at low RF field below 600 V, as expected, the CVs for all compounds are very close to 0 V. The CVs move to more negative positon with increasing amplitude of RF voltage from 600 to 1200 V.

The signal intensity at peak maximum decreased as the RF increased from 500 to 1500 V. Nazarov et al observed the signal intensity at peak maximum initially increased slightly as the amplitude of RF increased from 0 to 400 V[19]. Then the values of RF increase from 500 to 1500 V, the signal intensity at peak maximum declined. Above results are in consistent with those reported by Nazarov et al.
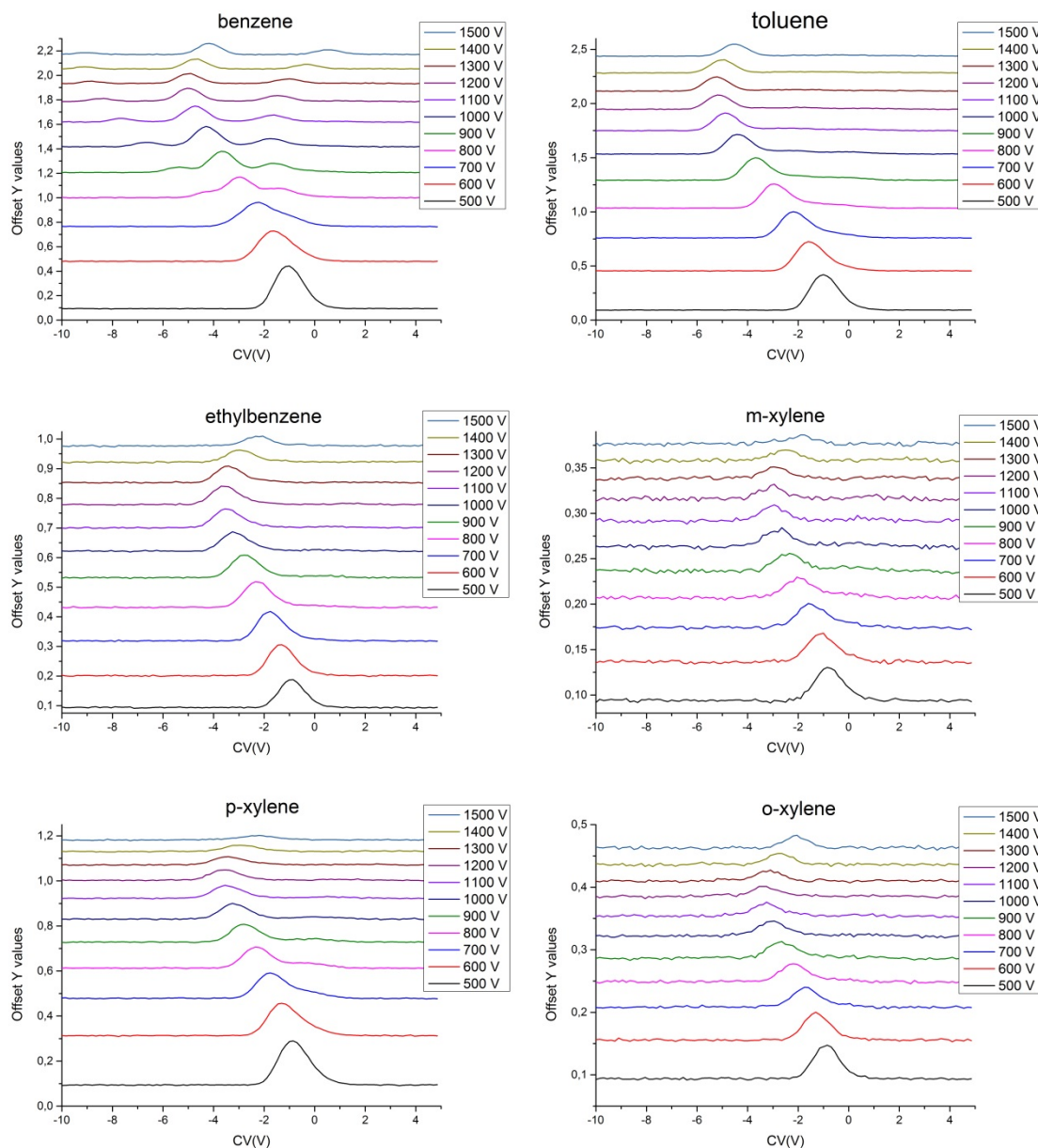

Figure 4.3: plots of compensation voltage versus RF voltage for BTEX by UV-DMS

As shown in Figure 4.3, except benzene, all other aromatic hydrocarbons analyzed have single peaks. This can probably be attributed to ions related to

monomer ion (M^+). The plots of compounds (toluene, ethylbenzene, xylene) are not found the dimer cation, hydrated proton or hydrated combiner. This findings are in a good agreement with those reported by Borsdorf [9].

The plot of benzene is the only one, which has three peaks at high RF voltage. This indicates that a series of reactions occur after benzene ionized by UV. There are at least three ions formed. The peak in the middle is the benzene cation ($C_6H_6^+$) as described mechanism in eq. 4.1.

$$C_6H_6 + hv \rightarrow C_6H_6^+ + e^- \quad \text{(eq. 4.1)}$$
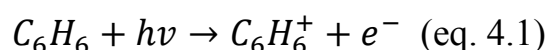
There are several possibilities for the formation of ions after benzene ionized by UV. The first possibility of formation of the peak with the most negative CV is benzene-water cation by the reaction of the benzene cation with water vapor as described in eq. 4.2. The water vapor may be from the carrier gas.

$$C_6H_6^+ + nH_2O \rightarrow C_6H_6^+(H_2O)_n \quad \text{(eq. 4.2)}$$
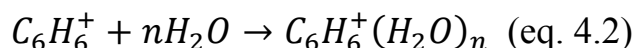
The thermodynamics of the stepwise hydration of the benzene cation has been studied by Ibarhim et al[22]. The standard enthalpy and entropy changes of clustering reactions with the first two water molecules are, respectively, -9,0 kcal/mol and -19,5 kcal/mol for one water clustering and -8,0 kcal/mol and -18,9 kcal/mol for two water clustering. Solca et al[23] estimated the binding energy of the first water molecule with benzene$^+$ as 59±13 kJ/mol, which is in good agreement with other literature [22]. The calculated ratio of the benzene cation and its monohydrate at 350 K in the presence of 1 ppmv of water is $1:2\times10^{-5}$. The ratios of the di and trihydrate of the benzene cation at 350 K for 1ppmv of water vapor are $1: 2\times10^{-10}$ and $1:7\times10^{-16}$.

At a high water concentration of 1300 ppmv, the estimated ratio of the bare, mono, di, and trihydrated of the benzene cation is $1:3\times10^{-2}: 3\times10^{-4}: 2\times10^{-6}$. The formation of the hydrated proton may occur through the following eq. 4.3:

$$C_6H_6^+(H_2O)_n \rightarrow C_6H_5 + (H_2O)_nH^+ \quad \text{(eq. 4.3)}$$
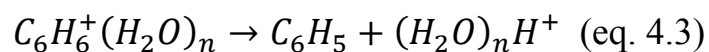
Although with the higher concentration of water vapor the equilibrium ratio of the trihydrate is very small, its reaction to form the hydrated proton occurs with high efficiency.

However, at a low water concentration (n≤3), the formation of the hydrated proton derived from the hydrated benzene cation may be not possible [22]. Therefore, in Fiugure 4.3, the peak with most negative CV may be $C_6H_6^+(H_2O)_n$ not the hydrate proton or other protonated species via the hydrated proton.

Once a benzene monomer cation is produced, charge resonance (CR) interaction with a neighboring neutral molecule produces a stable dimer, $(C_6H_6)_2^+$.

$$C_6H_6 + C_6H_6^+ \rightarrow (C_6H_6)_2^+ \quad (eq.\ 4.4)$$
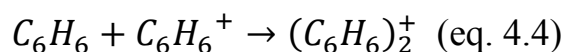
Generally, the bonding in van der Waals complexes arises from electrostatic, polarization, dispersion, charge transfer and short-range repulsion interactions. The binding energy of the dimer cation is nearly one order of magnitude larger than that of the neutral dimer. This was attributed to a strong charge transfer resonance interaction in the dimer ion, i.e. the charge is delocalized over both benzene rings [24].

Rusyniak et al reported that isomerization of the benzene radical cation occurs to generate the fulvene cations[25]. Assuming a usual factor of 10^{14} s^{-1}, an activation energy E_a(fulvene$^+$→benzene$^+$) >24,3 kcal/mol was calculated. Considering the 12,2 kcal/mol difference between ΔH^o_f (benzene$^+$) and ΔH^o_f (fulvene$^+$), E_a(benzene$^+$ → fulvene$^+$)>36,5 kcal/mol. Assuming the factors between 10^{13} and 10^{15} s^{-1}, the lower limit of E_a is between 34,4 and 38,6 kcal/mol. The fulvene$^+$ is formed during the electron impact ionization of benzene in the electron impact ion source rather than by collisions with helium atoms during ion injection. The electron impact ionization source is at a fixed electron energy ranging from 300 to 100 eV. Therefore, although fulvene having a lower ionization energy (8,36 eV), the isomeric fulvene ion cannot be formed since the isomerization barrier is larger than 1,6 eV and there are no possible

fragment ions by UV lamp. Therefore, the peak with less compensation voltage is belong to benzene dimer cation $(C_6H_6)_2{}^+$ not fulvene cations.

4.3.1.2 Positive ion spectra by ^{63}Ni ionization

As described in Table 4.1, the PAs for BTEX are 750,4 kJ/mol for benzene, 784,0 kJ/mol for toluene, 789,9 kJ/mol for ethylbenzene, 812,1 kJ/mol for m-xylene, 794,4 kJ/mol for p-xylene and 796,0 kJ/mol for o-xylene, respectively. The PAs for BTEX are larger than water, which has a PA value of 691,0 kJ/mol. This means the following reaction can occur:

$$M + (H_2O)_n H^+ \rightarrow MH^+ + nH_2O \quad \text{(eq. 4.5)}$$

The mechanism on formation of $(H_2O)_nH^+$ is described by [26-28]. The n is governed by temperature and moisture level. The plots of compensation voltage and RF voltage in ^{63}Ni radioactive ionization mode are shown in Figure 4.4. At RF = 500 V, there is only one peak in the spectrum at each compound since this voltage is insufficient for ion separation. As RF increases, the peak of $(H_2O)_nH^+$ is separated and moves to more negative position in CV axis. After that, it disappears when RF voltage is larger than 1100 V. All protonated monomers MH^+ except $(C_6H_6)H^+$ and protonated toluene begin to be separated from the reactant ions at RF=600 V. The protonated benzene and toluene can be separated from RIP at 700 V. As the RF increases from 600 to 1100 V, the separation resolution of protonated molecules and reactant ions increase. Both compensation voltages for reactant ions and product ions move to more negative. Meanwhile, the intensity of both reactant ions and product ions decline when the RF increases. This is understood to be a loss in transmission efficiency, for differential mobility spectrometers with planar configurations, through neutralization by collisions of ions on walls of the analyzer. Increases in separation voltage lead to increases in collisions for ions not in the center of the flow channel of the analyzer. The decrease in intensity is generally less for heavier, less mobile ions [29].
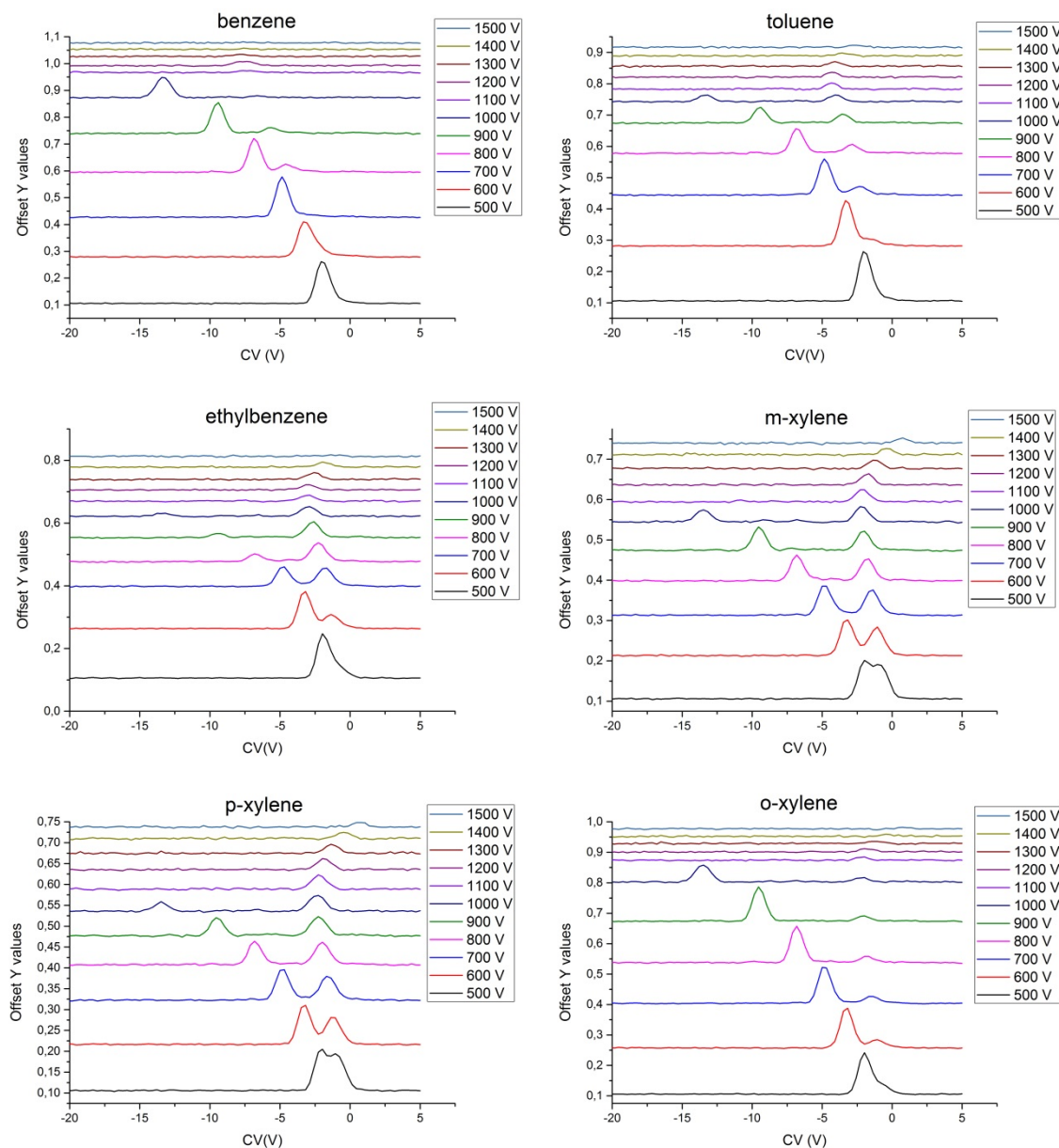
Figure 4.4: plots of compensation voltage versus RF voltage for BTEX by ^{63}Ni-DMS

Another possible reason is that the activated MH$^+$ decomposes due to the combination of thermal energy and the energy acquired from the separation field. Ion decomposition in the separation field is brought about by the conversion of translational energy acquired from acceleration in the field into internal energy. The high separation field will cause the decompositions of MH$^+$ [29]. When RF voltage increases from 1100 to 1400 V, the compensation voltages for product ions move back to less negative and close to zero.

Eiceman et al described the ion chemistry of 1,4-dimethylpyridine (DMP) that occurs in [63]Ni ionization mode, which is operated at atmospheric pressure[30]. The protonated molecule $(DMP)H^+$ is first formed by proton transfer from the reactant ion $(H_2O)_nH^+$ and subsequently the proton bound dimer $(DMP)_2H^+$ may form by association of $(DMP)H^+$ with DMP at sufficiently elevated vapor concentrations. However, in Figure 4.4, no protonated dimers of BTEX can be found. This may be explained that the concentrations of BTEX analyzed are lower than those required to form protonated dimers. It is suitable to use the protonated product ions to quantify the concentrations of target compounds.

4.3.2 Alpha functions for BTEX detected by UV-DMS and [63]Ni-DMS

Due to the different ionization mechanism of UV and [63]Ni, different ions will be produced by UV and [63]Ni. Normally, mass spectrometry was used to be coupled with DMS to identify the ions[31]. However, the ions may be lost and transform to other ions due to reduced pressure. Therefore, mathematical calculation like alpha function was introduced to provide another way to investigate ions in DMS.

At a fixed temperature and gas density N, the ion mobility and the average drift velocity can be approximated as follows:

$$K(E/N)=K_0(1+\alpha(E/N)) \quad (eq.\ 1.5)$$

Alphas are reported in units of Td^{-2n} (1 Td = 1×10^{-17} V/cm^2) and have no further physical meaning. The nonlinear dependence of K, determined by alpha values, is used to classify ions in three group (A,B,C) [32, 33]. For A-type ions, mobility increases monotonically over small regions with E/N and α_2 and α_4 are >0. For C-type ions, both α_2 and α_4 are <0, in this case the ion mobility decreases monotonically with E/N. B-type ions exhibit a maximum since $\alpha_2 > 0$ and $\alpha_4 < 0$. The actual values for alpha coefficients are shown in Table 4.2. All ions of BTEX including protonated monomers and monomers exhibited $\alpha_2 > 0$ and $\alpha_4 < 0$. These ions can be classified as B-type.

Table 4.2: values for Alpha parameters for ions of BTEX by [63]Ni and krypton UV lamp

	[63]Ni-DMS		UV-DMS	
	α_2 (1/Td^2)	α_4 (1/Td^4)	α_2 (1/Td^2)	α_4 (1/Td^4)
Benzene	1,39E-04	-1,64E-08	8,26E-05	-7,10E-09
Toluene	8,87E-05	-7,94E-09	8,43E-05	-7,20E-09
Ethylbenzene	4,93E-05	-5,15E-09	6,05E-05	-4,38E-09
m-xylene	4,05E-05	-2,90E-09	4,46E-05	-2,91E-09
p-xylene	4,35E-05	-3,33E-09	6,10E-05	-4,43E-09
o-xylene	4,06E-05	-2,99E-09	5,73E-05	-4,00E-09

The plots of alpha function for BTEX ionized by [63]Ni with the electric fields are shown in Figure 4.5. When E/N < 60 Td, the alpha values of protonated monomers for benzene and ethylbenzene increase as the E/N increases. When the E/N > 60 Td, the alpha values decline as the E/N increases. The protonated monomers like benzene, toluene and ethylbenzene exhibited a significantly B type alpha curves.

The trend of increase for alpha values of protonated monomers as the increase of E/N is negative related to molecular mass. As shown in Figure 4.5, the alpha value of protonated benzene increase fastest with the increase of E/N , followed by toluene, then ethylbenzene and xylene, which having the same molecular mass. Krylov et al reported the similar trend for protonated monomer for ketones. Interestingly, the alpha curves for three xylene isomers are quite similar [31]. This may be explained that the compounds with the same functional group, protonated monomers of a single type, have the similar dependence of coefficients of mobility on electric fields.

The plots for alpha function for BTEX ions detected by UV-DMS with the electric fields are shown in Figure 4.6. The ions of BTEX ionized by UV are different from these ionized by [63]Ni. As mentioned above, benzene monomer, dimer and $C_6H_6^+(H_2O)_n$ were found in the experiment. In order to compare the behavior of ions with other compounds, only the alpha values of monomers are calculated. Slope of alpha versus E/N were monotonic from 0 to 90 Td for

ethylbenzene, m-xylene, p-xylene, o-xylene. Benzene and toluene showed plots with an inversion of slope above 75 V. Interestingly, the alpha plot for [m-xylene]$^+$ is significantly distinct from the other two xylenes, with $\alpha_2=4{,}46E^{-05}$ and $\alpha_4=-2{,}91E^{-09}$. This means that the behavior of [m-xylene]$^+$ in the asymmetric high electrical field will be different with [p-xylene]$^+$ and [o-xylene]$^+$. However, the overlapping peak between m-xylene and p-xylene was still found. As mentioned in section 1.6, three main errors were introduced in measurements for alpha function. The approximate combined error may be 10 %. Practically, alpha was expressed as tow polynomial terms. However, this approximation algorithm may lose more information of the behavior of ions in DMS. Therefore, the investigation of alpha function calculation is still needed.
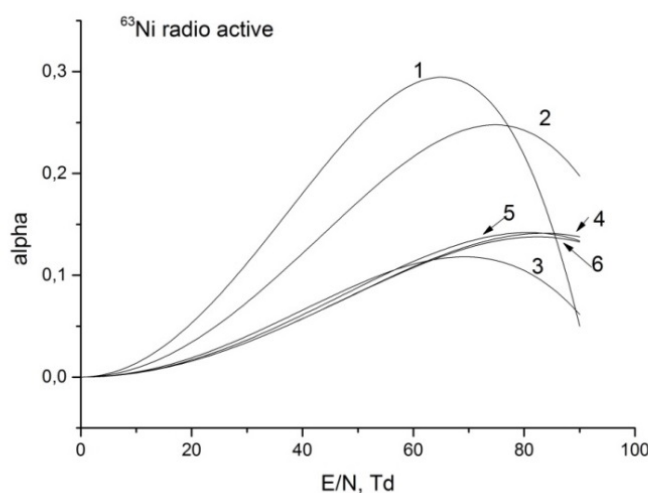

Figure 4.5: plots of α(E/N) for BTEX (protonated monomers) vs. electric field, ionization source ^{63}Ni, 1, [benzene]H$^+$ 2, [toluene]H$^+$, 3, [ethylbenzene]H$^+$, 4, [m-xylene]H$^+$, 5, [p-xylene]H$^+$, 6, [o-xylene]H$^+$, temperature 80 ℃, flow rate 300 ml/min
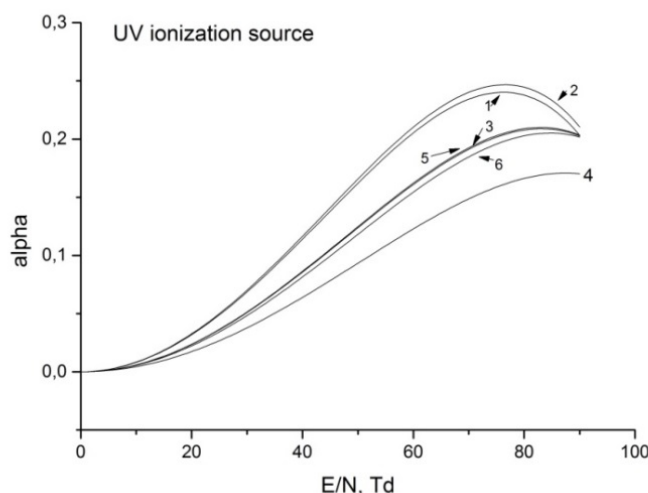
Figure 4.6: plots of $\alpha(E/N)$ for BTEX (monomer ion) vs. electric field, ionization source UV lamp, 1, [benzene]$^+$ 2, [toluene]$^+$, 3, [ethylbenzene]$^+$, 4, [m-xylene]$^+$, 5, [p-xylene]$^+$, 6, [o-xylene]$^+$, temperature 80 ℃, flow rate 300 mL/min

4.3.3 Comparison of GC-[63]Ni-DMS and GC-UV-DMS

Eiceman and Vandiver quantified response curves of aromatic hydrocarbons by photoionization and compared these events to radioactive ionization [6]. As discussed in chapter 3, increased product ion intensity was accompanied by decreased reactant ion intensity in a regular even fashion for each aromatic hydrocarbon in [63]Ni mode. The chemical ionization response for target compounds was limited by available reactant ions.

Table 4.3: Characterization of GC-[63]Ni-DMS and GC-UV-DMS

Compounds	Retention time (sec)	Compensation voltage (V)		Detection limits (mg/L)		MCLs by WHO(mg/L)
		UV	[63]Ni	UV	[63]Ni	
Benzene	44,1	-5,9	-6,2	0,08	201,80	0,01
Toluene	55,2	-3,2	-3,6	0,15	50,31	0,7
Ethylbenzene	74,4	-2,1	-2,7	0,12	9,53	0,3
m-Xylene	77,4	-1,3	-2,2	0,15	6,20	0,5
p-Xylene	77,4	-2,1	-2,2	0,16	8,53	(total xylene)
o-Xylene	86,5	-1,7	-2,3	0,16	4,76	

The calibration curves of BTEX in groundwater detected by GC-[63]Ni-DMS are shown in chapter 3. R^2 for benzene and toluene are 0,77 and 0,86, respectively. This means that the signals of [benzene]H$^+$ and [toluene]H$^+$ are not stable.

However, the R^2 for calibration curves of other compounds like ethylbenzene, xylene isomers are above 0,93, which is acceptable. This can be explained that the benzene and toluene are very sensitive for the concentration of water vapor. As shown in Table 4.1, the PAs of benzene and toluene are 750,4 eV and 784,0 eV, respectively, which are lower than other compounds. In Figure 4.7, the R^2 for calibration curves of benzene and toluene obtained by GC-UV-DMS are 0,99 and 0,97, respectively, which are quite linear correlations. Due to the different ionization mechanisms on benzene and toluene induced by [63]Ni and UV, the ions without proton may be more stable at a certain water vapor. In [63]Ni mode, the kinetics of ion cluster formation are fast enough for changes in water concentration to exert a significant effect on the differential mobility of ions[34]. Kanu and Thomas obtained quantitative responses to benzene in water over the concentration range 6 to 177 µg/cm^3 with linear correlations with R^2 values ranging from 0,97 to 0,99 by UV photoionization differential mobility spectrometer [35].

Detection limits of BTEX in groundwater by GC-[63]Ni-DMS and GC-UV-DMS are listed in Table 4.3. The detection limits of BTEX detected by GC-[63]Ni-DMS are in the range from 4,8 to 201,8 mg/L. The detection limits of TEX detected by GC-UV-DMS are 0,15 mg/L for toluene, 0,12 mg/L for ethylbenzene, 0,15 mg/L for m-xylene, 0,16 mg/L for p-xylene, 0,16mg/L for o-xylene, respectively, which are 30 to 330 fold lower than those obtained by [63]Ni-DMS. The detection limit for benzene obtained by GC-UV-DMS is 0,08 mg/L, which is more than 2500 folds improved over GC-[63]Ni-DMS. The detection limits for all target compounds except benzene by GC-UV-DMS are below the maximum contamination levels (MCLs) recommended by WHO. The detection limit for benzene by GC-UV-DMS is also acceptable, which is closed to the MCL of benzene in drinking water by WHO. Moreover, the concentrations of most contaminant cases are in the range of mg/L[36].
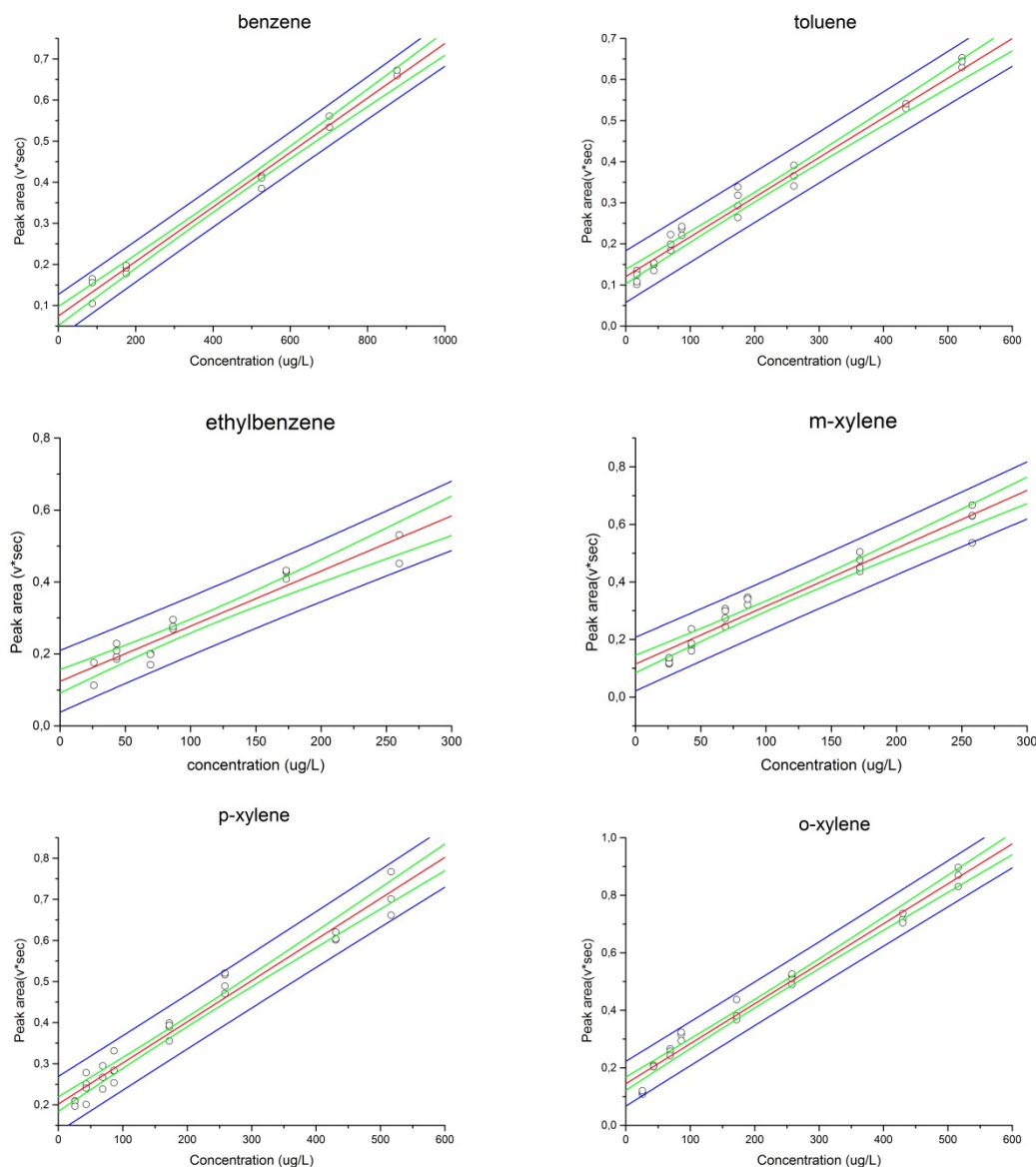
Figure 4.7: calibration curves of GC-UV-DMS system for target compounds

4.4 Summary

In this chapter, firstly, the behaviors of BTEX ionized by two different ionization ways were studied by DMS. The pronated monomer of target compounds are predominated ions produced through chemical reaction with reactant ions via [63]Ni. Otherwise, all compounds are directly ionized to monomer ions by UV photoionization. Besides $[C_6H_6]^+$, $[C_6H_6]_2^+$ and $C_6H_6^+(H_2O)_n$ were found and separated by DMS by using UV ionization source. In order to characterize the ions produced by [63]Ni and UV, alpha functions for the protonated monomers and monomers ions of target compounds were

calculated. Depending on the α_2 and α_4 values, all the ions (both protonated monomers and monomers ions) can be classified as B-type ions.

The calibration curves and detection limits for BTEX detected by GC-UV-DMS were calculated, respectively. The detection limits of BTEX detected by GC-UV-DMS are low to 0,08 mg/L. Except benzene, the detection limits of other compounds TEX are below the MCLs regulated by WHO. However, all data obtained in this chapter by using clean groundwater spiked with pure compounds. The matrix effect of the complicated real groundwater contaminated by gasoline is unknown.

4.5 References

1. Stlouis, R.H. and H.H. Hill, *Ion Mobility Spectrometry in Analytical-Chemistry.* Critical Reviews in Analytical Chemistry, 1990. **21**(5): p. 321-355.
2. Baumbach, J.I. and G.A. Eiceman, *Ion mobility spectrometry: Arriving on site and moving beyond a low profile.* Applied Spectroscopy, 1999. **53**(9): p. 338a-355a.
3. Preston, J.M., F.W. Karasek, and S.H. Kim, *Plasma Chromatography of Phosphorus Esters.* Analytical Chemistry, 1977. **49**(12): p. 1746-1750.
4. Baim, M.A., R.L. Eatherton, and H.H. Hill, *Ion Mobility Detector for Gas-Chromatography with a Direct Photo-Ionization Source.* Analytical Chemistry, 1983. **55**(11): p. 1761-1766.
5. Leasure, C.S., et al., *Photoionization in Air with Ion Mobility Spectrometry Using a Hydrogen Discharge Lamp.* Analytical Chemistry, 1986. **58**(11): p. 2142-2147.
6. Eiceman, G.A. and V.J. Vandiver, *Charge-Exchange in Binary-Mixtures of Polycyclic Aromatic-Hydrocarbons Using Photoionization Ion Mobility Spectrometry.* Analytical Chemistry, 1986. **58**(11): p. 2331-2335.
7. Eiceman, G.A., M.E. Fleischer, and C.S. Leasure, *Sensing of Petrochemical Fuels in Soils Using Headspace Analysis with Photoionization-Ion Mobility Spectrometry.* International Journal of Environmental Analytical Chemistry, 1987. **28**(4): p. 279-296.
8. Sielemann, S., et al., *Detection of alcohols using UV-ion mobility spetrometers.* Analytica Chimica Acta, 2001. **431**(2): p. 293-301.
9. Borsdorf, H., E.G. Nazarov, and R.A. Miller, *Atmospheric-pressure ionization studies and field dependence of ion mobilities of isomeric hydrocarbons using a miniature differential mobility spectrometer.* Analytica Chimica Acta, 2006. **575**(1): p. 76-88.
10. Borsdorf, H., E.G. Nazarov, and R.A. Miller, *Time-of-flight ion mobility spectrometry and differential mobility spectrometry: A comparative study of their efficiency in the analysis of halogenated compounds.* Talanta, 2007. **71**(4): p. 1804-1812.
11. Baumbach, J.I., et al., *Detection of the gasoline components methyl tert-butyl ether, benzene, toluene, and m-xylene using ion mobility spectrometers with a radioactive and UV ionization source.* Analytical Chemistry, 2003. **75**(6): p. 1483-1490.
12. Cheng, S.S., et al., *Dopant-Assisted Negative Photoionization Ion Mobility Spectrometry for Sensitive Detection of Explosives.* Analytical Chemistry, 2013. **85**(1): p. 319-326.
13. Good, A., D.A. Durden, and P. Kebarle, *Ion-Molecule Reactions in Pure Nitrogen and Nitrogen Containing Traces of Water at Total Pressures 0.5-4 Torr Kinetics of Clustering Reactions Forming H+(H2o)N.* Journal of Chemical Physics, 1970. **52**(1): p. 212-&.
14. Robb, D.B. and M.W. Blades, *Factors affecting primary ionization in dopant-assisted atmospheric pressure photoionization (DA-APPI) for LC/MS.* Journal of the American Society for Mass Spectrometry, 2006. **17**(2): p. 130-138.
15. Short, L.C., S.S. Cai, and J.A. Syage, *APPI-MS: Effects of mobile phases and VUV lamps on the detection of PAH compounds.* Journal of the American Society for Mass Spectrometry, 2007. **18**(4): p. 589-599.
16. Locke, D.C., B.S. Dhingra, and A.D. Baker, *Liquid-Phase Photo-Ionization Detector for Liquid-Chromatography.* Analytical Chemistry, 1982. **54**(3): p. 447-450.
17. Raffaelli, A. and A. Saba, *Atmospheric pressure photoionization mass spectrometry.* Mass Spectrometry Reviews, 2003. **22**(5): p. 318-331.
18. Available from: http://webbook.nist.gov/chemistry/.
19. Nazarov, E.G., et al., *Miniature differential mobility spectrometry using atmospheric pressure photoionization.* Analytical Chemistry, 2006. **78**(13): p. 4553-4563.

20.   Krylov, E.V., E.G. Nazarov, and R.A. Miller, *Differential mobility spectrometer: Model of operation.* International Journal of Mass Spectrometry, 2007. **266**(1-3): p. 76-85.

21.   Krylov, E.V., *Pulses of special shapes formed on a capacitive load.* Instruments and Experimental Techniques, 1997. **40**(5): p. 628-631.

22.   Ibrahim, Y., et al., *Stepwise hydration and multibody deprotonation with steep negative temperature dependence in the benzene(center dot+)-water system.* Journal of the American Chemical Society, 2004. **126**(40): p. 12766-12767.

23.   Solca, N. and O. Dopfer, *IR spectrum of the benzene-water cation: direct evidence for a hydrogen-bonded charge-dipole complex.* Chemical Physics Letters, 2001. **347**(1-3): p. 59-64.

24.   Morokuma, K., *Why Do Molecules Interact - Origin of Electron Donor-Acceptor Complexes, Hydrogen-Bonding, and Proton Affinity.* Accounts of Chemical Research, 1977. **10**(8): p. 294-300.

25.   Rusyniak, M., et al., *Mass-selected ion mobility studies of the isomerization of the benzene radical cation and binding energy of the benzene dimer cation. Separation of isomeric ions by dimer formation.* Journal of Physical Chemistry A, 2003. **107**(38): p. 7656-7666.

26.   Carr, T.W., *plasma chromatography.* 1984, New York: Plenum Press. 95.

27.   Sunner, J., M.G. Ikonomou, and P. Kebarle, *Sensitivity Enhancements Obtained at High-Temperatures in Atmospheric-Pressure Ionization Mass-Spectrometry.* Analytical Chemistry, 1988. **60**(13): p. 1308-1313.

28.   Carroll, D.I., et al., *Identification of Positive Reactant Ions Observed for Nitrogen Carrier Gas in Plasma Chromatograph Mobility Studies.* Analytical Chemistry, 1975. **47**(12): p. 1956-1959.

29.   An, X., et al., *Gas phase fragmentation of protonated esters in air at ambient pressure through ion heating by electric field in differential mobility spectrometry.* International Journal of Mass Spectrometry, 2011. **303**(2-3): p. 181-190.

30.   Ewing, R.G., et al., *The kinetics of the decompositions of the proton bound dimers of 1,4-dimethylpyridine and dimethyl methylphosphonate from atmospheric pressure ion mobility spectra.* International Journal of Mass Spectrometry, 2006. **255**: p. 76-85.

31.   Krylov, E., et al., *Field dependence of mobilities for gas-phase-protonated monomers and proton-bound dimers of ketones by planar field asymmetric waveform ion mobility spectrometer (PFAIMS).* Journal of Physical Chemistry A, 2002. **106**(22): p. 5437-5444.

32.   Purves, R.W., et al., *Mass spectrometric characterization of a high-field asymmetric waveform ion mobility spectrometer.* Review of Scientific Instruments, 1998. **69**(12): p. 4094-4105.

33.   Shvartsburg, A.A., S.V. Mashkevich, and R.D. Smith, *Feasibility of higher-order differential ion mobility separations using new asymmetric waveforms.* Journal of Physical Chemistry A, 2006. **110**(8): p. 2663-2673.

34.   Krylova, N., et al., *Effect of moisture on the field dependence of mobility for gas-phase ions of organophosphorus compounds at atmospheric pressure with field asymmetric ion mobility spectrometry.* Journal of Physical Chemistry A, 2003. **107**(19): p. 3648-3654.

35.   Kanu, A.B. and C.L.P. Thomas, *The presumptive detection of benzene in water in the presence of phenol with an active membrane-UV photo-ionisation differential mobility spectrometer.* Analyst, 2006. **131**(9): p. 990-999.

36.   Walendzik, G., J.I. Baumbach, and D. Klockow, *Coupling of SPME with MCC/UV-IMS as a tool for rapid on-site detection of groundwater and surface water contamination.* Analytical and Bioanalytical Chemistry, 2005. **382**(8): p. 1842-1847.

5. Determination of BTEX in real contaminated groundwater samples by GC-UV-DMS

5.1 Introduction

In many countries, the groundwater is always used as drinking water source in which the allowable amounts of the BTEX is very low due to their serious adverse impact on human health. European Union (EU) legislated the strictest maximum contamination level for benzene in drinking water as 0,001 mg/L, which is lower than that (0,01 mg/L) recommended by World Health Organization (WHO). Meanwhile, US EPA presented a medium level (0,005 mg/L for benzene) between WHO and EU. For the other compounds (toluene, ethylbenzene, xylene-total), there is no regulation in EU. Otherwise, US EPA regulated 1,0 mg/L for toluene, 0,7 mg/L for ethylbenzene, and 10 mg/L for total-xylene, respectively. In comparison with US EPA, WHO recommended a more strict regulation on TEX, 0,7 mg/L for toluene, 0,3 mg/L for ethylbenzene and 0,5 mg/L for total xylene[1-3].

Uncontrolled release of gasoline into aquatic environment will result in contamination groundwater, particularly the underground storage tank leak. A slow leak from a 10.000 gallon gasoline storage tank virtually undetectable to station operator is still quite hazardous to groundwater supplies. For instance, according to water quality guideline of WHO, a spill of 10 gallons of gasoline (only 0,1 % of the 10.000 gallon tank) will contaminate approximately 230 million liters drinking water [2].

There are two ways to analyze the BTEX in groundwater. One is on site method and another is on lab method. Analyses of BTEX in water are usually carried out by gas chromatography using a flame ionization detector (GC-FID) or electrolytic conductivity detectors (GC-ECD)[4-6]. Ji et al evaluated a portable gas chromatography–microflame ionization detection (portable GC-FID) coupled to headspace solid-phase microextraction (HS-SPME) for the field analysis of BTEX in water samples [6].The detection limits found were lower

than 1,5 µg/L, which was enough sensitive to detect the BTEX in water samples. The optimized method was applied to the field analysis of BTEX in wastewater samples. Recent decade, gas chromatography mass spectrometry (GC-MS) is becoming increasingly common [7-9]. Laaks et al presented a novel in-tube extraction device (ITEX) for headspace sampling coupled to GC/MS analysis of BTEX in aqueous samples [7]. The detection limits of 1 to10 ng/L were achieved for volatile organic compounds (VOCs), which is much lower than demands by regulatory limit values. Kamal and Klein estimated BTEX in groundwater sample by using GC-MS, after standardization of this technique for advancement towards purification check of water samples in the petro-polluted regions of the soil [8]. Jia et al analyzed BTEX in water by using SPME-GC-MS. The detection limits of BTEX are in the range of 0,001 to 0,009 mg/L [9]. In addition, other methods are reported to detect BTEX in water [10, 11]. Karlowatz et al detected and quantified simultaneous the environmentally relevant analytes benzene, toluene, and the three xylene isomers in water by reflection mid-infrared spectroscopy [10]. Wittkamp and Tilotta described a new method for determining BTEX in water combining SPME and spontaneous Raman spectroscopy. The detection limits using the most intense Raman bands are in the 1-4 ppm range and produce relative standard deviations of 3-9% [11]. However, the methods mentioned above are time consuming. As described in chapter 3 and chapter 4, the analysis time by GC-DMS is less than 2 min and the detection limits are low to ppb. However, until now, it is still unclear whether the concentrations of BTEX detected by GC-UV-DMS are closed to the actual concentrations in the sample.

In this chapter, 17 groundwater samples are collected in a natural gas field in Rotenburg an der Wümme, northen Germany. These samples are analyzed by the developed method (GC-UV-DMS) and reference lab method, respectively. The results obtained by GC-UV-DMS were evaluated.

5.2 Experimental section

5.2.1 Groundwater sampling

The groundwater samples are collected from a natural gas field in Rotenburg an der Wümme, northern Germany. The volume of each sample is 250 mL. There is a variety of these samples. The natural gas is fed continuously throughout the whole year. The groundwater located in 5000 meters. The groundwater samples contain a number of ingredients as follows: strongly fluctuating high salinity, iron and manganese, oxygen, petroleum hydrocarbons, heavy metals such as mercury, sediment, and microorganisms. The composition of the water of a reservoir varies over the year. This water is stored for short period under anaerobic, usually covering natural gas to the respective bore. When the containers are full, bring a tanker off the water and drive it to the repressing in an old disused bore. However, the sediment prior to repress, hydrocarbons, iron and manganese must be removed from the water. The samples are supplied either from such a plant influent raw water or they are according to the different steps of the plant was taken. There are as follows:

1, deposition of sediments and free phase in a lamella occurs a coagulation of fine droplets of hydrocarbons to phase.

2, for the separation of sediment, precipitated iron and manganese. Here also occurs a coagulation of fine droplets of hydrocarbons to phase.

3, coagulation disperses fine droplets of hydrocarbons to free phase by high performance membranes called coalescing.

5.2.2 Chemicals

Chemicals like o-xylene(≥99,0%, Fluka Analytical, Steinheim, Germany), p-xylene(≥99,0%, Fluka analytical, Steinheim, Germany), m-xylene(≥99,0%, Fluka, Steinheim, Germany), benzene(99%, AppliChem, Darmstadt, Germany), ethylbenzene (≥99,0%, Fluka, Steinheim, Germany), toluene(99,9%, J.T.Baker, Netherland), methanol (≥99,99%, Fisher Scientific, Germany) were used without further purification.

5.2.3 Determination of BTEX in groundwater by reference method

ITEX GC-MS Instruments and Parameters: All analyses were performed using a Trace GC Ultra (S+H Analytik, Mönchengladbach, Germany) coupled to a DSQ II single quadrupole mass spectrometer (S+H Analytik). The GC was equipped with a split/splitless injector (SSL), and a Combi-PAL autosampler (Axel Semrau, Sprockhövel, Germany). Compound separation was performed on a Restek Rtx-V MS column (medium polar, proprietary modified phase) with 60 m length, 0,32 mm i.d., and 1,8 μm film thickness (Restek,Bad Homburg, Germany).

The MS was set to electron ionization (EI) with an ionization energy of 70 eV in scan mode (m/z) 49 to 180, 6,5 scans/s. The MS transfer line was set to 250 ℃; the ion source temperature was 220 ℃.

For the GC measurement, the injector temperature of the Optic 3 was set to 280 ℃ in splitless mode. The temperature program for oven was set up as follows. Firstly, the oven temperature was set to 40 ℃ for 1 min, then heated up to 130 ℃ with 4 ℃/min and to 200 °C with 10 ℃/min, then holding at 200 ℃ for 10 min. The flow rates for column and injector were set up as follows. The column flow was raised to a constant flow of 1,5 mL/min, the split was opened at 20 mL/s, and the trap was heated to 250 °C with a heating rate of 30 ℃/s.

The parameters and conditions of ITEX are described in detail by [7].

Instrument control, data acquisition, and evaluation were performed by the Xcalibur 1.4 data system (S+H Analytik).

The real groundwater samples are diluted to 10.000 times for analysis of ethylbenzene and xylene by ITEX-GC-MS. Meanwhile, the real samples are diluted to 1000.000 times for analysis of benzene and 100.000 times for analysis of toluene. The calibration solutions are prepared by spiking clean groundwater

with BTEX standard solutions, which are prepared through dissolving BTEX chemical into methanol.

5.2.4 GC-UV-DMS measurement

The instrument of GC-UV-DMS was described in chapter 4. To analyze the groundwater, the real samples were diluted to 100 times for analysis of ethylbenzene and xylene, 500 times for quantifying toluene, as well as 1000 times for analysis of benzene. 500 µl headspace air was directly injected into GC-UV-DMS system. In order to eliminate the matrix effect, the calibration curves were obtained by spiking clean and contaminated groundwater samples with standard solution of BTEX.

5.2.5 Data analysis

OriginLab 9.0 was used to analyse the data recorded by microDMx Expert version 2.4.0. Firstly, a 2D diagram was produced (one dimension as retention time of GC; another dimension as compensation voltage detected by DMS) by OriginLab. For quantifying the peak area of target compound, the data at fix compensation voltage dimension was used to generate a chromatogram. The details are described in chapter 4.

To compare the results obtained by GC-UV-DMS and reference method, F-test, one of statistical models of analysis of variance (ANOVA), was used by OriginLab 9.0.

5.3 Results and Discussion

5.3.1 Characterization of GC-UV-DMS

Figure 5.1 shows five chromatographs at different characterized compensation voltages for BTEX. The order of the peaks is as follows: 1, benzene, 2, toluene, 3, ethylbenzene, 4, m/p-xylene, 5, o-xylene (from left to right).
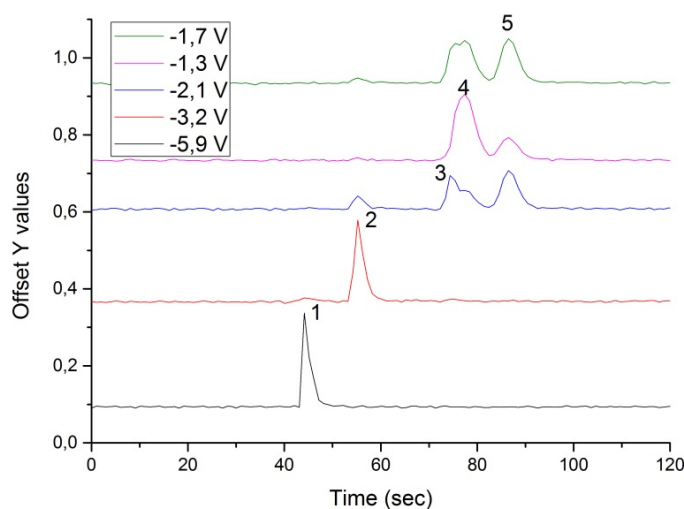
Figure 5.1: Chromatograph of BTEX in real sample: 1, benzene, 2, toluene, 3, ethylbenzene, 4, m/p-xylene, 5, o-xylene
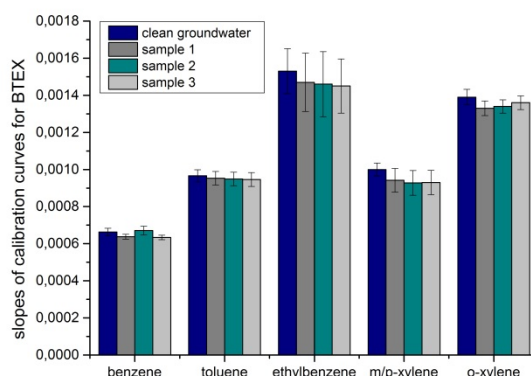

Figure 5.2: slopes of BTEX for calibration curves obtained from clean groundwater and three real samples spiked with different concentrations of BTEX

Methods for monitoring BTEX levels in real groundwater samples are relatively complicated due to strong matrix effect. In order to eliminate the matrix effect, three real groundwater samples spiked with the standard solutions were prepared and analyzed by GC-UV-DMS. The calibration curves and the slopes of calibration curves are shown in Figure 5.2 and Figure 5.3. The slopes of three calibration curves are in good agreement with that obtained from clean groundwater in chapter 4. Therefore, the calibration curves obtained in chapter 4 can be used to quantify the real samples without considering the matrix effect.

It should be clarified that the slopes for calibration curves of m and p-xylene are combined together, because the two peaks are not separated (as shown in Figure 5.1). Otherwise, in chapter 4, the calibration curves of these two compounds are obtained separately, because the standard solutions used to calibrate were prepared by single compound instead of mixture. The slope of calibration curve of p-xylene obtained in chapter 4 was listed as m/p-xylene in Figure 5.2.
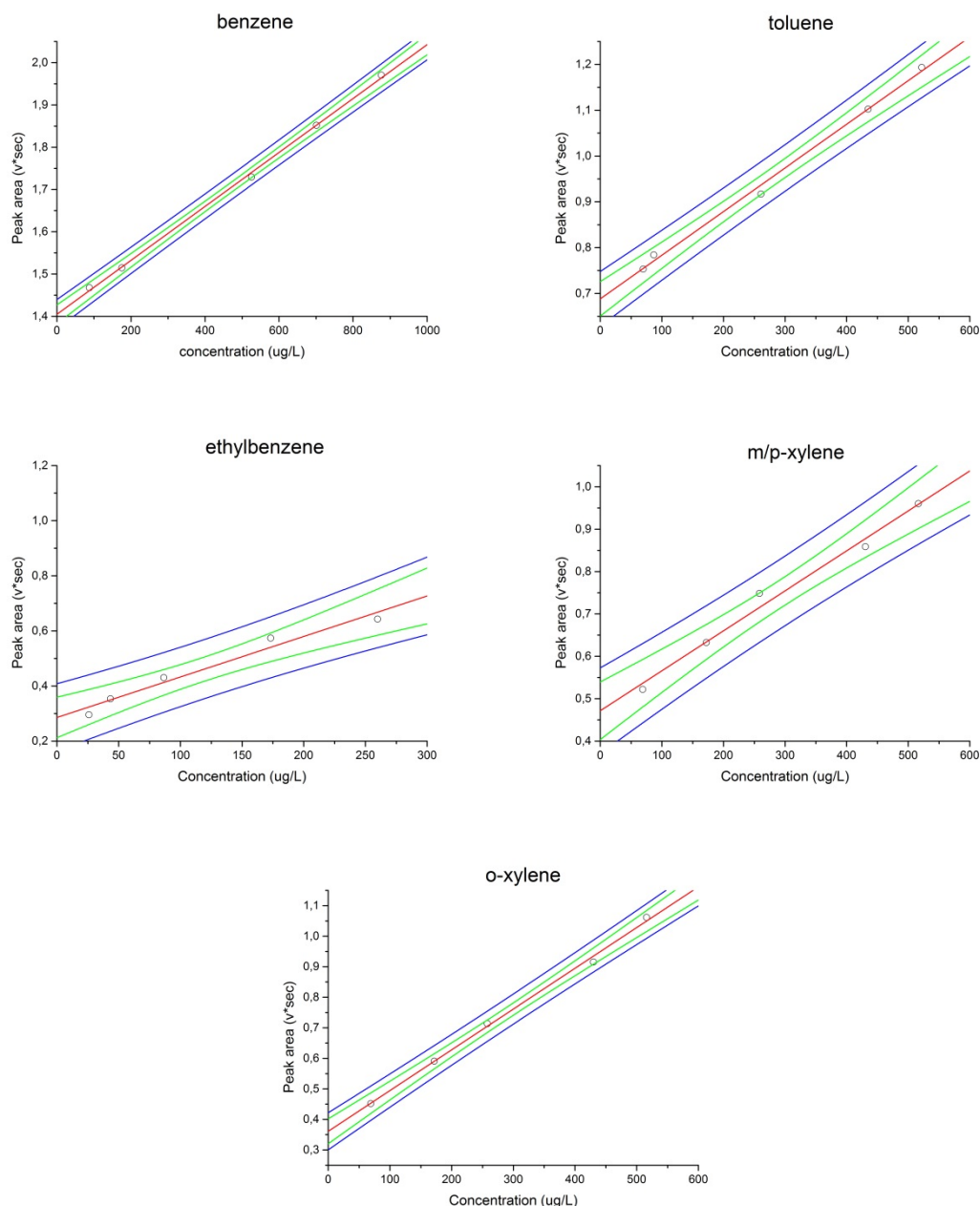
Figure 5.3: calibration curves for BTEX in real contaminated groundwater spiked with standards by GC-UV-DMS

5.3.2 Application to groundwater studies

The analysis results of 17 groundwater samples collected from a natural gas field in Rotenburg an der Wümme, northern Germany are shown in Figure 5.4 to 5.8. These results revealed that BTEX concentrations are within the range from 2,0 to 616,9 mg/L. The concentrations were in general much higher than the MCLs of BTEX regulated by WHO[2].

In Figure 5.4, the concentrations of benzene were in the range from 133,8 to 616,9 mg/L. These concentrations were much higher than the MCLs regulated by EU, US and WHO [1-3]. All data points were used to do F-test (Table 5.1). At the 0,05 level, the mean concentrations of quantified by the two different analytical procedures are significantly different. The F value is 5,31, larger than the critical value of 4,17. This may be explained by the fact that the concentrations of benzene vary largely in different real groundwater samples.
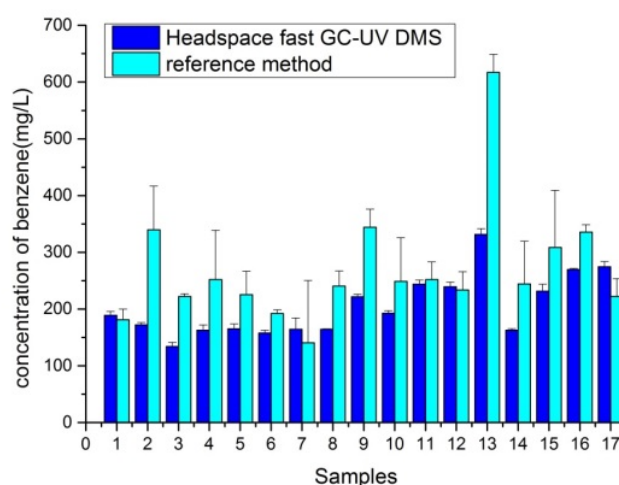

Figure 5.4: concentrations of benzene in groundwater contaminated by gasoline obtained by the application of two distinct analytical methods (GC-UV-DMS and reference method).

Table 5.1: ANOVA results of the comparison for the concentrations of benzene detected by GC-UV-DMS and reference method

	Degree of freedom(f)	Sum of Squares	Mean Square	F Value	Prob>F	Critical of F Value
Between groups	1	37182,71	37182,71	5,31	0,027	4,17
Within groups	32	223736,56	6991,77			
Total	33	260919,27				

In Figure 5.5, the concentrations of toluene were within the range from 29,9 to 116,3 mg/L, which are much higher than the MCLs regulated by US and WHO [1, 2]. The concentrations of toluene quantified by GC-UV-DMS are in a good agreement as that obtained by reference method. The F value is 0,044, below the critical value of 4,17 (Table 5.2).
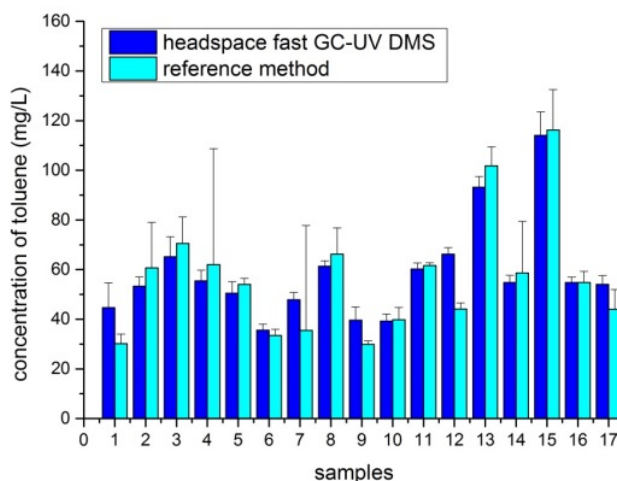

Figure 5.5: concentrations of toluene in groundwater contaminated by gasoline obtained by the application of two distinct analytical methods (GC-UV-DMS and reference method).

Table 5.2: ANOVA results of the comparison for concentrations of toluene detected by GC-UV-DMS and reference method

	Degree of freedom(f)	Sum of Squares	Mean Square	F Value	Prob>F	Critical of F Value
Between groups	1	20,71	20,71	0,044	0,835	4,17
Within groups	32	15069,41	470,92			
Total	33	15090,12				

In Figure 5.6, the concentrations of ethylbenzene were in the range from 2,0 to 9,8 mg/L. The measured concentrations were much higher than the MCLs regulated by US and WHO [1, 2].As shown in Table 5.3, the concentrations of ethylbenzene quantified by the two different analytical procedures are in good agreement. The F value is 0,85, below the critical value of 4,17.
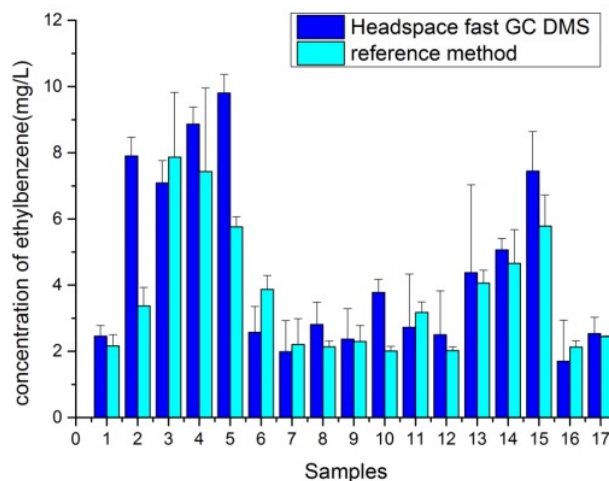

Figure 5.6: concentrations of ethylbenzene in groundwater contaminated by gasoline obtained by the application of two distinct analytical methods (GC-UV-DMS and reference method).

Table 5.3: ANOVA results of the comparison for concentration of ethylbenzene detected by GC-UV-DMS and reference method

	Degree of freedom(f)	Sum of Squares	Mean Square	F Value	Prob>F	Critical of F Value
Between groups	1	4,67	4,67	0,85	0,36	4,17
Within groups	32	175,46	5,48			
Total	33	180,14				

In Figure 5.7 and 5.8, the concentrations of xylene were in the range from 2,4 to 26,5 mg/L. Meanwhile, the concentrations of xylene quantified by the two distinct methods(GC-UV-DMS and reference method) are within good agreement. As shown in Table 5.4 and Table 5.5, the F values for m/p-xylene and o-xylene are 0,024 and 0,082, respectively. Both F values are below the critical value of 4,17.
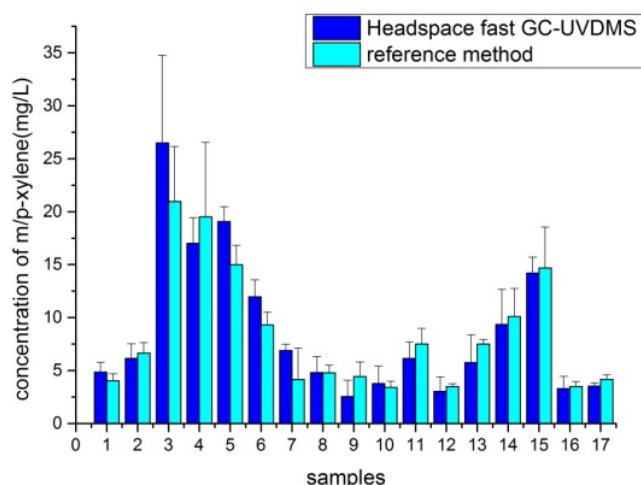

Figure 5.7: concentrations of m/p-xylene in groundwater contaminated by gasoline obtained by the application of two distinct analytical methods (GC-UV-DMS and reference method).
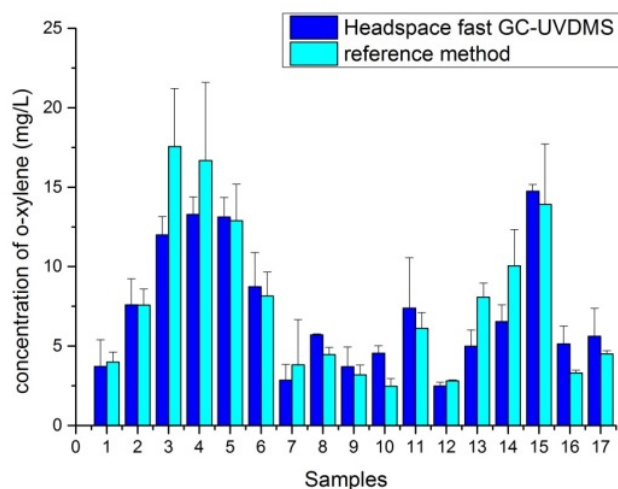
Figure 5.8: concentrations of o-xylene in groundwater contaminated by gasoline obtained by the application of two distinct analytical methods (GC-UV-DMS and reference method).

Table 5.4: ANOVA results of the comparison for concentrations of m/p-xylene detected by GC-UV-DMS and reference method

	Degree of freedom(f)	Sum of Squares	Mean Square	F Value	Prob>F	Critical of F Value
Between groups	1	0,97	0,97	0,024	0,88	4,17
Within groups	32	1269,37	39,67			
Total	33	1270,33				

Table 5.5: ANOVA results of the comparison for concentrations of o-xylene detected by GC-UV-DMS and reference method

	Degree of freedom(f)	Sum of Squares	Mean Square	F Value	Prob>F	Critical of F Value
Between groups	1	1,62	1,62	0,082	0,78	4,17
Within groups	32	633,73	19,80			
Total	33	635,35				

5.3.3 Concentrations of BTEX in groundwater by GC-UV-DMS

Total dissolved BTEX concentrations (sum concentration of benzene, toluene, ethylbenzene, and the xylene isomers) in 17 groundwater samples collected at the monitoring wells are shown in Figure 5.9. The lowest concentration in sample 6 is 216,5 mg/L and the sample 13 presents the highest concentration of 439,9 mg/L. In all samples, benzene exhibits the highest concentration, followed by toluene. The ethylbenzene and xylene exhibit the lowest concentration. This can be explained by the fact that the difference in solubility and degradation for these six compounds. In comparison with other compounds, benzene has high water solubility as 1700 mg/L (25 ℃), followed by toluene with 515 mg/L, ethylbenzene with 152 mg/L and xylene with 172 mg/L[12]. Some literatures [13-15] reported that toluene is the easiest BTEX compound to degrade, followed by the xylenes. Benzene and ethylbenzene are the most difficult to degrade. If degradation were occurring, toluene concentrations would be the first to decrease.
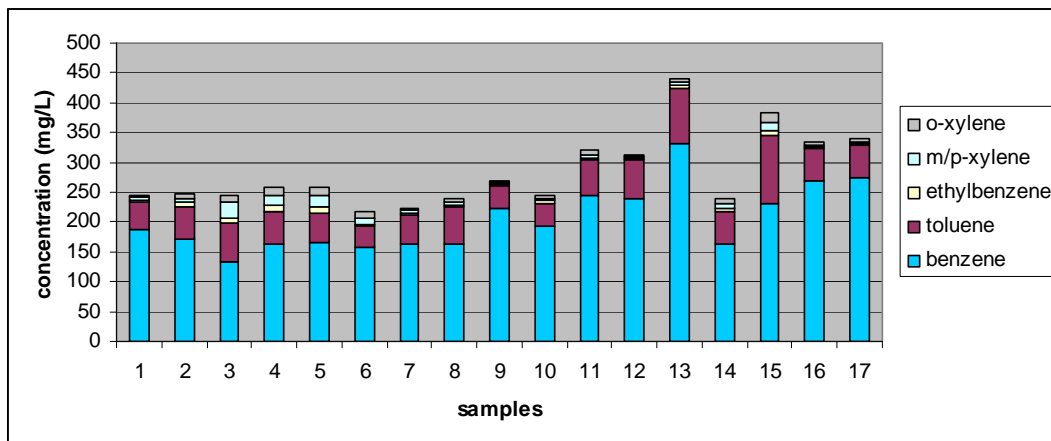
Figure 5.9: Total concentrations of BTEX in real groundwater samples detected by GC-UV-DMS

A high correlation was observed between the concentration of ethylbenzene, m/p-xylene and o-xylene (as shown in Figure 5.10). These results indicate that these pollutants exhibit similar behavior in the field. Keer et al also reported the similar phenomenon found in the groundwater obtained from a contaminated site located in the industrial area of Belgium [16].
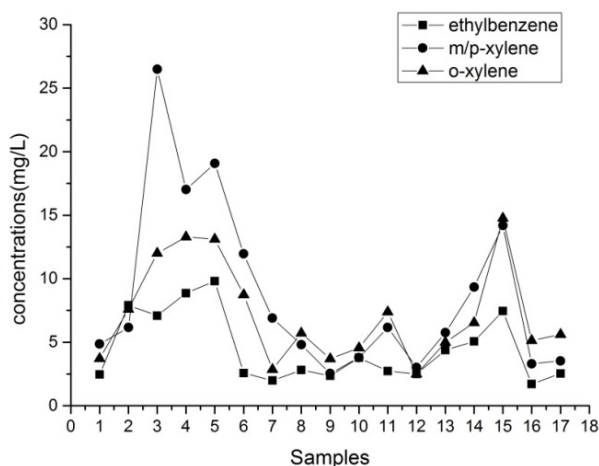

Figure 5.10: correlation between concentrations of ethylbenzene, m/p-xylene and o-xylene

In order to know more details about the contamination detected by GC-UV-DMS, the statistical properties of BTEX concentrations in the 17 groundwater samples are calculated in Figure 5.11. In one chart, the left part is the data and a lognormal distribution and the right part is the box chart including the mean value, median value, maximum and minimum value and standard deviation (SD).

According to WHO's regulation, the concentrations of total xylene were put together. The mean values for 17 real samples are 204,4 mg/L for benzene, 58,2 mg/L for toluene, 4,5 mg/L for ethylbenzene and 15,9 mg/L for total xylene, respectively. Additionally, the median values are 188,7 mg/L for benzene, 54,8 mg/L for toluene, 2,8 mg/L for ethylbenzene and 10,7 mg/L for total xylene, respectively. All concentrations of BTEX are higher than the guidelines of drinking water recommended by WHO. Interestingly, among the BTEX compounds, benzene had the widest distribution and a high degree of variability. The arithmetic mean value for benzene is greater than the median value. The levels of toluene, ethylbenzene, and xylene compounds in the real samples also exhibited the similar results. The lognormal distribution of BTEX shows that there are more samples with lower values than these with high concentrations. This finding is quite good agreement with others [17].
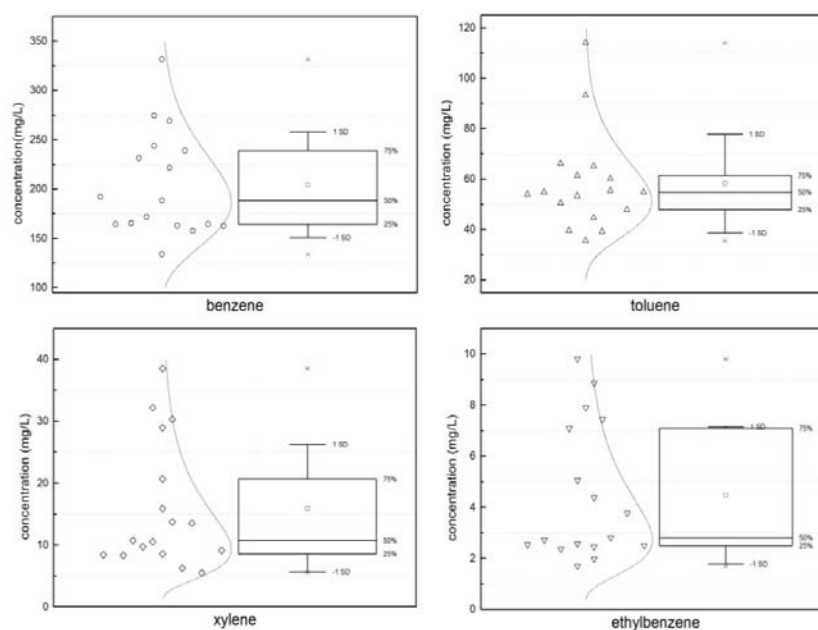

Figure 5.11: The statistical properties of individual BTEX concentration in contaminated groundwater (arithmetic mean, median)

In order to obtain more information from the environmental viewpoint, the results were compared with others reported in different regions. The data is shown in Table 5.6. The results for benzene in real groundwater samples are

higher than that reported by other literatures [12, 16, 18]. The concentrations of toluene are in the range reported in Belgium, but higher than that reported in Brazil and Jordan. The similar results for xylene are obtained. Note that in literature [16], they combined ethylbenzene and m/p-xylene together. However, in these results for 17 groundwater samples, only xylene was put together. In order to compare the results, the concentrations of ethylbenzene and xylene were summed together. These results for ethybenzene and total xylene are in good agreement with that reported in literature [16]. Therefore, the results for BTEX obtained by this method are in good agreement with that reported in Belgium, but significant different in comparison with other regions like Brazil and Jordan. Therefore, the results obtained by GC-UV-DMS can also provide the geological meanings.

Table 5.6: comparison of the concentrations of BTEX in different sites

	these samples mean values(mg/L)	Brazil, Pires do Rego et al [18](mg/L) maximum values	Jordan, Kuisi et al[12](mg/L) mean values	Belgium, Van Keer et al [16](mg/L) range
benzene	204,4	8,12	0,0017	0,06-11,6
toluene	58,2	3,03	0,0021	0,007-62,0
ethylbenzene	4,5	9,09	0,0016	0,011-22,8(ethylbenzene + m/p-xyelene)
Total xylene	15,9	3,60	0,0012	0,003-4,5 (o-xylene)

5.4 Summary

Seventeen real groundwater samples contaminated by gasoline were analyzed by GC-UV-DMS and the concentrations of BTEX were quantified. In comparison

with reference method, the results except benzene obtained by GC-UV-DMS are in good agreement with those by reference method.

The concentrations of BTEX in real groundwater samples differ largely. In this case, the groundwater samples collected are high contaminated by gasoline. In comparison with the results by other literatures, the groundwater contamination is largely depending on the behavior of BTEX in groundwater and the region. The data obtained by GC-UV-DMS can provide more information on contamination. Thus, further investigations are necessary to extend the knowledge on site by GC-UV-DMS.

5.5 References

1.   Available from: http://www.edstrom.com/Resources.cfm?doc_id=167.
2.   Organization, W.H., *Drinking Water Quality: Third Edition incorporating the First and Second Addenda.* 2008: Geneva.
3.   Union, C.o.t.E., *Council Directive 98/83/EC on the Quality of Water Intended for Human Consumption.* 1998.
4.   *Volatile organic compounds by gas chromatography mass spectrometry (GC/MS) Method 8260B.* 1996.
5.   *Aromatic and halogenated volatiles by gas chromatography using photoionization and/or electrolytic conductivity detectors. Method 8021B.* 1996.
6.   Ji, J., et al., *Field analysis of benzene, toluene, ethylbenzene and xylene in water by portable gas chromatography-microflame ionization detector combined with headspace solid-phase microextraction.* Talanta, 2006. **69**(4): p. 894-899.
7.   Laaks, J., et al., *In-Tube Extraction of Volatile Organic Compounds from Aqueous Samples: An Economical Alternative to Purge and Trap Enrichment.* Analytical Chemistry, 2010. **82**(18): p. 7641-7648.
8.   M.A. Kamal and P. Klein, *Estimation of BTEX in groundwater by using gas chromatography-mass spectrometry.* Saudi Journal of Biological Sciences, 2010. **17**: p. 205-208.
9.   Jin-ping, J., et al., *Improvement of the determination method of benzene, toluene, ethylbenzene and xylene (BTEX) in water using activated carbon fiber solid-phase microextraction/ gas chromatography-mass spectrometry(GC-MS).* Chinese Journal of Chromatography, 2002. **20**(1): p. 63-65.
10.   Karlowatz, M., M. Kraft, and B. Mizalkoff, *Simultaneous quantitative determination of benzene, toluene, and xylenes in water using mid-infrared evanescent field spectroscopy.* Analytical Chemistry, 2004. **76**(9): p. 2643-2648.
11.   Wittkamp, B.L. and D.C. Tilotta, *Determination of Btex Compounds in Water by Solid-Phase Microextraction and Raman-Spectroscopy.* Analytical Chemistry, 1995. **67**(3): p. 600-605.
12.   Al Kuisi, M., et al., *Potential Occurrence of MTBE and BTEX in Groundwater Resources of Amman-Zarqa Basin, Jordan.* Clean-Soil Air Water, 2012. **40**(8): p. 808-816.
13.   Kuhn, E.P., et al., *Anaerobic Degradation of Alkylated Benzenes in Denitrifying Laboratory Aquifer Columns.* Applied and Environmental Microbiology, 1988. **54**(2): p. 490-496.
14.   Edwards, E.A., et al., *Anaerobic Degradation of Toluene and Xylene by Aquifer Microorganisms under Sulfate-Reducing Conditions.* Applied and Environmental Microbiology, 1992. **58**(3): p. 794-800.
15.   Cozzarelli, I.M., J.S. Herman, and M.J. Baedecker, *Fate of Microbial Metabolites of Hydrocarbons in a Coastal-Plain Aquifer - the Role of Electron Acceptors.* Environmental Science & Technology, 1995. **29**(2): p. 458-469.
16.   Van Keer, I., et al., *Limitations in the use of compound-specific stable isotope analysis to understand the behaviour of a complex BTEX groundwater contamination near Brussels (Belgium).* Environmental Earth Sciences, 2012. **66**(2): p. 457-470.
17.   Cho, I.H., et al., *Risk Assessment Before and After Solar Photocatalytic Degradation of BTEX Contaminated Groundwater at a Gas Station Site in Korea.* Environmental Progress, 2008. **27**(4): p. 447-459.
18.   do Rego, E.C.P. and A.D.P. Netto, *PAHs and BTEX in groundwater of gasoline stations from Rio de Janeiro City, Brazil.* Bulletin of Environmental Contamination and Toxicology, 2007. **79**(6): p. 660-664.

6. Simulation of on-site conditions for determination of BTEX in groundwater

6.1 Introduction

Rapid, reliable and on site systems to monitor groundwater are needed to test on field and validate the function in a complicated working environment. However, it is difficult for us to find a workplace, which is contaminated by gasoline, to do this. Therefore, a simulation system on lab is used to test the developed method.

The availability of fast on-field systems in polluted regions is needed to detect diffusion of BTEX in contaminated groundwater[1]. Therefore, the study of spill of BTEX in groundwater has to be carried out to evaluate. Due to the fact that only headspace sample of real groundwater is introduced and analyzed by GC-UV-DMS, the diffusion rates of BTEX from water to air are very important to know for monitoring the contaminated groundwater.

Several contaminant transport models were introduced[2]. Dilling et al simulated the natural environmental desorption process in the laboratory to estimate the persistence of low molecular weight chlorinated hydrocarbons in natural water [3]. Theoretically, the flux of exchange of VOCs between air and water is based on two factors. One factor is the degree of disequilibrium between the air and water concentration. Another factor is a mass transfer coefficient [4].There are three theoretical models to estimate the mass transfer coefficient : 1) two film model [5, 6] 2) the penetration model [7], 3) the surface renewal model [8]. One of the basic theories of mass transfer will be described in section 6.2.

In this chapter, on field conditions to monitor the behavior of BTEX diffusion from water to air were simulated. Several factors such as temperature, tube length, and matrix effect affecting the diffusion were studied by GC-UV-DMS.

6.2 Mass transfer Theory

Based on the classical two-film mass transfer model[9], an expression for the volatilization rate of a chemical C from water is

$$-\frac{d[C]}{dt} = k_v\,[C]\ \ \text{(eq. 6.1)}$$

Where k_v is the volatilization rate constant of chemical C. The volatilization rate constant k_v is expressed in terms of the mass transfer rates of the substance across liquid- and gas-phase boundary layers. The general expression for k_v is

$$k_v = \frac{1}{L}\left[\frac{1}{k_l} + \frac{RT}{H_c k_g}\right]^{-1}\ \ \text{(eq. 6.2)}$$

Where k_v is the volatilization rate constant (s^{-1}); L is the length of tube; k_l is the liquid-film mass transfer coefficient (cm/h); R is the gas constant (8,314472(15) J $K^{-1}mol^{-1}$); T is the temperature; H_c is the Henry's law constant (atm L mol^{-1}); and k_g is the gas film mass transfer coefficient (cm/h).

The relative importance of the liquid and gas phase resistances can be assessed as follows:

$$\frac{R_l}{R_g} = \left(\frac{H}{RT}\right)\frac{k_g}{k_l}\ \ \text{(eq. 6.3)}$$

where R_l and R_g are mass transfer resistances from liquid phase and gas phase, respectively. According to Mackay and Leinonen's recommendation [10], when $R_l/R_g \geq 20$, corresponding to the $H_c > 4,8$ [atm L mol^{-1}], the liquid phase resistance dominates. As shown in Table 6.1, all the compounds studied in this work satisfy this definition of liquid-phase control.

6.3 Experimental section

6.3.1 Temperature effect experiment

The glass tube with an inner diameter 10 cm and length 0,5 m was kept at a constant temperature of 25 °C. After putting the 10mL groundwater spiked with BTEX standard solution in the tube, the tube was closed with Parafilm and

aluminum foil. Every 30 min, 200 µl air at the top of tube was analyzed by GC-UV-DMS.

As shown in Figure 6.1, a homemade Liebig condenser with an inner diameter 2,4 cm and length 0,5 m was used to study the diffusion of BTEX at 10 ℃. The tap water flushed from the inlet of condenser and constantly to keep the temperature of the condenser at 10 ℃. After putting the 10mL groundwater spiked with BTEX inside of condenser, the condenser was closed with Parafilm on both sides. Every 30 min, 200 µL air at the top of condenser was analyzed by GC-UV-DMS.
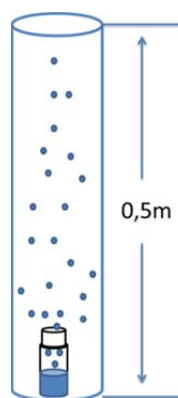
Figure 6.1: Simulation system 0,5 m glass tube used to keep a constant temperature of 10 ℃

Table 6.1: properties of BTEX[11]

	Henry's constant (atm L/mole, 25 ℃)	Vapor pressure (Torr,25℃)	Air conversion factor at 25 ℃ 1ppm(v/v)=mg/m^3	Solubility in water (mg/L, 25℃)	Molecular weight (g/mol)
benzene	5,56	95,2	3,19	1800	78,11
toluene	6,63	28,4	3,77	470	92,14
ethylbenzene	7,88	9,6	4,34	150	106,17
m-xylene	7,34	8,3	4,34	160	106,16
p-xylene	7,66	8,84	4,34	180	106,16
o-xylene	5,20	6,6	4,34	175	106,16

6.3.2 Matrix effect experiment

The real contaminated groundwater samples are very complicated. These samples contain a number of ingredients like sediment and dissolved salinity. The matrix will influence the diffusion of BTEX in groundwater. Therefore, to simulate the matrix effect, three grams soil or sand were added to the groundwater spiked targets compounds. Then the samples were put at the bottom of the simulation tube. Every 30 minutes, 200 µl headspace at the top of simulation tube was injected into the GC-UV-DMS.

6.3.3 Chemicals and sample preparation

In this work, o-xylene(≥99,0%, Fluka Analytical, Steinheim, Germany), p-xylene(≥99,0%, Fluka analytical, Steinheim, Germany), m-xylene(≥99,0%, Fluka, Steinheim, Germany), benzene(99%, AppliChem, Darmstadt, Germany), ethylbenzene (≥99,0%, Fluka, Steinheim, Germany), toluene(99,9%, J.T.Baker, Netherland), and methanol (≥99,99%, Fisher Scientific, Germany) were used without further purification.

To detect the mass transfer rate of BTEX, the clean groundwater was spiked with pure chemicals in constant concentrations (438 mg/L for benzene, 261 mg/L for toluene, 130 mg/L for ethylbenzene, 129 mg/L for m/p-xylene and 132 mg/L o-xylene).

To observe the diffusion of BTEX in real contaminated groundwater samples, the real contaminated groundwater samples from a natural gas field in Rotenburg an der Wümme were used.

6.3.4 GC-DMS analysis

A Shimadzu GC-2014 GC system was used for all analysis. The split/splitless injector operated at 150 ℃. Nitrogen (>99,999% pure) was used as the carrier gas at a 3 mL/min flow rate. Separation was performed on a 12m × 0,28mm × 0,25 µm MXT-5 GC column. The GC oven was kept at 120 ℃.

A DMS equipped with krypton UV lamp was coupled to GC with a homemade interface, which can be kept at 80 °C. The sensor temperature of DMS was setup at 80 °C. Nitrogen was used as carrier gas for DMS with a constant flow rate of 300 mL/min.

6.4 Results and discussion

According to the methods recommend by Roberts and Dändllker[12], values of the mass transfer rate constant, k_v, were determined as follows:

$$-ln\left[\frac{C_L(t)}{C_L(0)}\right] = k_v\ (t - t_0)\ \ \text{(eq. 6.4)}$$

This equation is changed to the function of the signal intensity (I) with time (t):

$$I(t) = ae^{k_v t} + b\ \ \ \text{(eq. 6.5)}$$

where a and b are constants, the I(t) is signal intensity and t is time.

The signal intensity is calculated from the peak area of target compounds in the chromatogram obtained by GC-UV-DMS.

6.4.1 Tube length selection

The tube length is one of the important factors to monitor the diffusion of BTEX from groundwater to gas. Two type glass tubes with same inner diameter 10 cm and with different length (0,5m, 1,0m) were used. The kinetic curves and k_v values are shown in Figure 6.2 and Table 6.2, respectively. These values are larger than these of 1m tube. To simplify the simulation condition and save the analysis time, the 0,5 m length tube was used as a simulation system in the following experiment.

Table 6.2: the k_v of BTEX at different tube length(25 ℃)

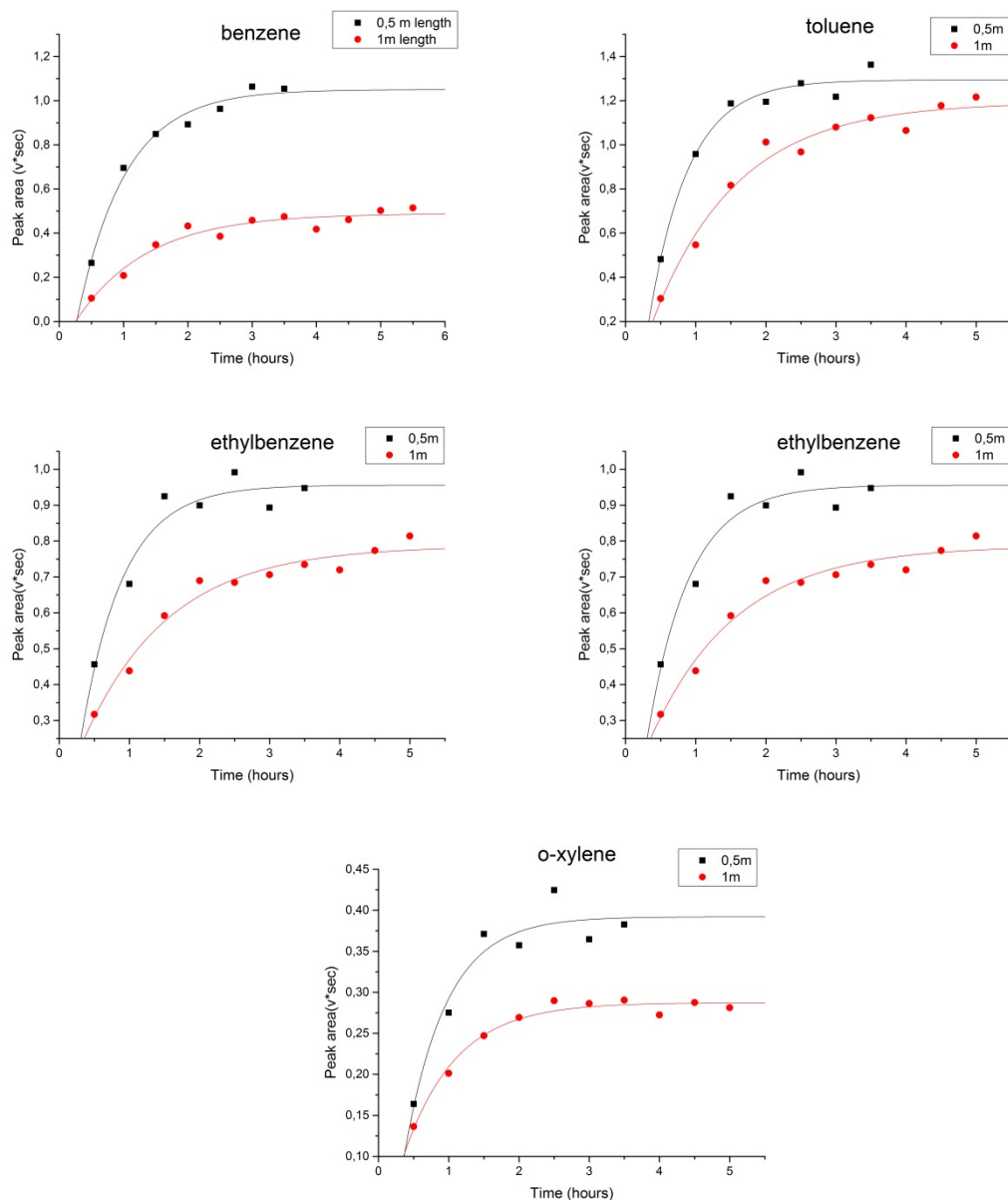|	k_v,(s^{-1}),1m tube length	k_v,(s^{-1}), 0,5m tube length
benzene	2,50E-04±0,34E-04	3,69E-04±0,65E-04
toluene	2,31E-04±0,38E-04	4,93E-04±0,56E-04
ethylbenzene	2,27E-04±0,42E-04	4,67E-04±0,18E-04
m/p-xylene	2,74E-04±0,36E-04	4,97E-04±0,15E-04
o-xylene	2,46E-04±0,39E-04	4,71E-04±0,47E-04

Figure 6.2: diffusion of BTEX in simulation tubes with different lengths

6.4.2 Temperature effect on diffusions of BTEX

As shown in eq. 6.2, temperature influences the mass transfer factor. Therefore, the effect of temperature (10 ℃ and 25 ℃) on the diffusion of BTEX was studied. The results are shown in Figure 6.3. The results show that the equilibrium time for BTEX at 25 ℃ is about 1,75 hours, shorter than that at 10 ℃, which are more than 2,5 hours. This result indicates that the higher temperature can speed up the mass transfer of BTEX from water to gas phase.

The mass transfer coefficients are also calculated and shown in Table 6.3. As expected, the values of k_v are larger at higher temperature than those obtained at lower temperature.

From eq. 6.2, if assuming that the H_c is fixed, the k_v decrease as the temperature increases. However, the change of T can lead to the change of H_c. Thus, from this equation, it is difficult to explain the result that k_v decreases when the temperature decreases. Therefore, another explanation based on the two film model will be introduced as follows.

Based on the classical two film theory, the transfer through a boundary layer is by molecular diffusion, because the fluid in the boundary layer is stagnant. Then the diffusion process can be described by Fick's law in one dimension, where the flux of the chemical $N(g\ cm^{-2}\ h^{-1})$ is

$$N = -D\frac{\partial C}{\partial z} \text{ (eq. 6.6)}$$

Where D is the diffusion coefficient and z is the vertical distance. If the concentration gradient $\partial C/\partial z$ is constant within the boundary layer, the equation can be changed as

$$N = k_v \Delta C \quad \text{(eq. 6.7)}$$

The mass transport coefficient k_v has the units of velocity and is

$$k_v = D/\delta \text{ (eq. 6.8)}$$

where δ is the boundary layer thickness.

The diffusion coefficient is dependent on the temperature and the viscosity of the solution [13]. The thickness of the stagnant film at gas-liquid interface decreases and the diffusion coefficient increase as viscosity decrease, when the temperature increases. Both effects lead to an increase of k_v [14] .

The signal intensity of BTEX at 10 ℃ is larger than that at 25 ℃. Because the volume of simulation tube used at 10 ℃ is smaller than that used at 25 ℃. In order to keep the temperature of 10 ℃, a homemade Liebig condenser with an inner diameter 2,4 cm and length 0,5 m was used. Otherwise, the glass tube with an inner diameter 10 cm and length 0,5 m was used at 25 ℃. As shown in eq. 6.2,

the k_v is only related with the length of tube. Therefore, the k_v will not be influenced by the tube inner diameter.

Table 6.3: the k_v of BTEX at different temperatures

	$k_{v,}(s^{-1})$,10 °C	$k_{v,}(s^{-1})$,25 °C
benzene	2,23E-04±0,44E-04	3,69E-04±0,65E-04
toluene	2,49E-04±0,48E-04	4,93E-04±0,56E-04
ethylbenzene	2,73E-04±0,20E-04	4,67E-04±0,18E-04
m/p-xylene	2,51E-04±0,30E-04	4,97E-04±0,15E-04
o-xylene	3,07E-04±0,35E-04	4,71E-04±0,47E-04
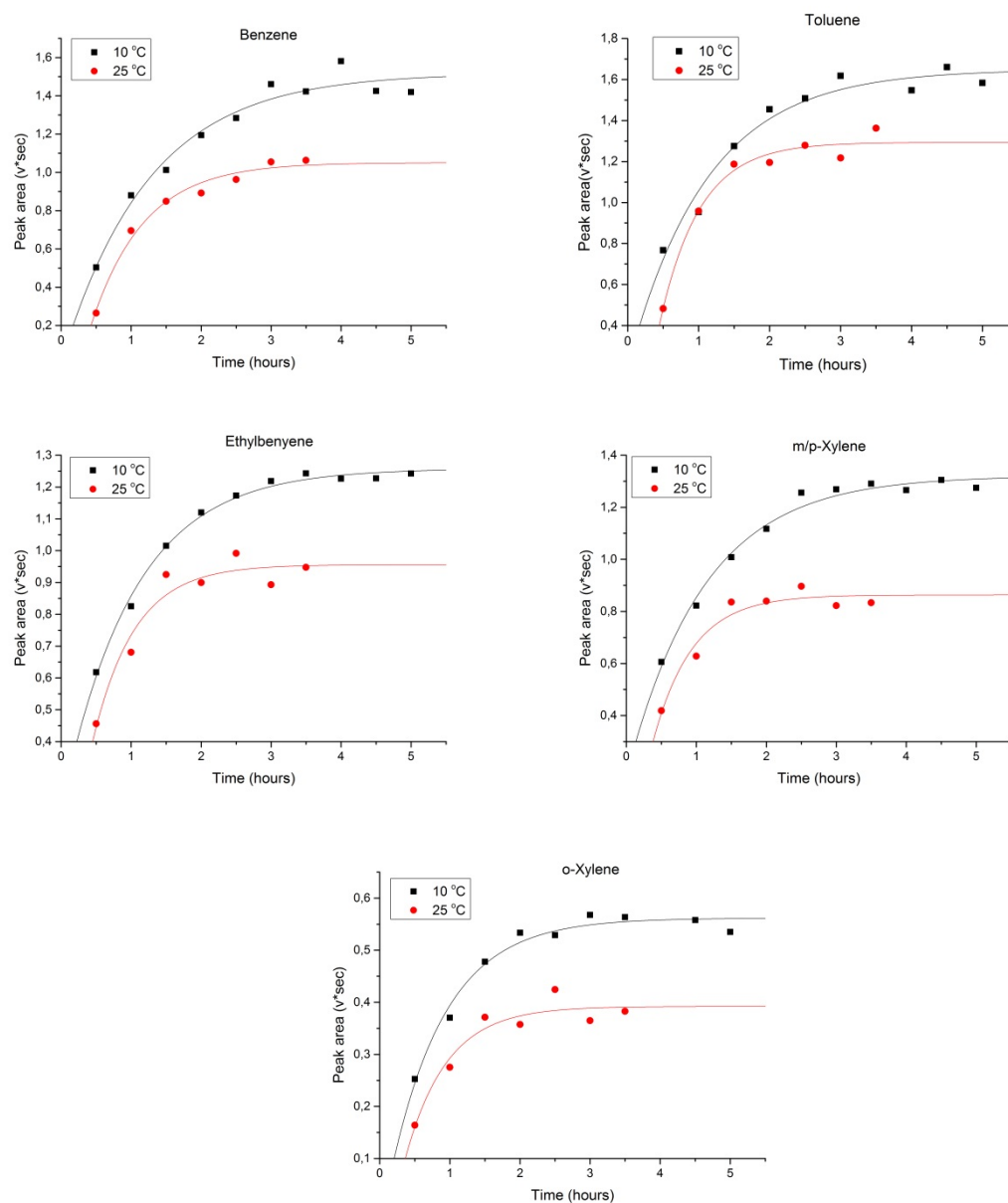
Figure 6.3: Temperature effect on diffusion of BTEX (10 °C and 25 °C)

6.4.3 Matrix effect on diffusion of BTEX

Principally, the diffusion of BTEX from groundwater will be influenced by the matrix. In this work, the effects of soil and sand on diffusion of BTEX were done at 25 °C and the results are shown in Figure 6.4. The times for BTX reaching the equilibration are between 1,5 to 2,5 hours when the solutions are mixed with soil or sand, respectively. In comparison with Figure 6.3, the equilibration time for ethylbenzene is about 1,75 hours without soil and sand at 25 °C. The equilibrium time of BTEX in groundwater with soil or sand is longer than that in groundwater. This finding reveals that the soil and sand can slow down the diffusion and mass transfer of BTEX from water to gas.

Ferreira et al [14] reported the solid particles can increase or decrease k_v, depending on the solids loading, size and their surface properties. The solid particles can increase k_v by enhancing turbulence at the gas-liquid interface and inducing surface renewal. Otherwise, the solid particles can limit the diffusion path, blocking the available area for mass transfer and decrease k_v [15, 16].

The k_v of BTEX from water to gas with soil or sand are calculated and the results are shown in Table 6.4. The k_v of BTEX decreases when the solution containing soil or sand. The values of k_v of BTEX are quite similar for soil and sand. This means that the soil and sand may have the similar effect on the mass transfer of BTEX in groundwater. This phenomenon will be explained as follows.

The transfer between the atmosphere and bodies of water plays a key role on the transport of many organic compounds in environment. Henry's law constant (H_c) describes the equilibrium partitioning between gaseous and aqueous phases. As shown in eq. 6.2, the mass transfer rate will be influenced by Henry's law constant (H_c). Principally, the k_v declines as the H_c decreases.

Theoretically, in water containing sand or soil, VOCs are adsorbed on the surface of these solids (S) and the partition coefficient (K_s, L/mg) of the VOCs

between the solids and the aqueous phase can be expressed, respectively, as follows [17]:

$$C_g \overset{H_c}{\leftrightarrow} C_w \overset{K_S}{\leftrightarrow} S - bound \; VOC \quad \text{(eq. 6.9)}$$

$$K_S = \frac{S - bound \; VOC}{C_w} = \frac{C_s/[S]}{C_w} \quad \text{(eq. 6.10)}$$

where C_s and S are the solid-bound VOC and solid concentrations, both based on the liquid phase volume. The total VOC concentration C_T in the water containing S is

$$C_T = C_w + C_s \quad \text{(eq. 6.11)}$$

In this system, the sorption phenomenon for the specific VOCs can be described as follows:

$$C_g \overset{H'_c}{\leftrightarrow} C_T \quad \text{(eq. 6.12)}$$

And the H_c' can be expressed as follows:

$$H'_c = \frac{C_g}{C_T} = \frac{C_g}{(C_w + C_s)} = H_c \frac{1}{1 + K_s[S]} \quad \text{(eq. 6.13)}$$

Jin and Chou found that the high mixed liquor suspended solid concentrations should result in a lower H_c for hydrophobic VOCs such as toluene and p-xylene, while higher mixed liquor suspended solid concentrations in a higher H_c for hydrophilic VOCs such as methanol and isopropanol [18]. In this result, the soil and sand can reduce the H_c of hydrophobic BTEX, resulting in the k_v declines. This means that the equilibrium time of BTEX in solution mixed with soil or sand will be longer than that without matrix.

Table 6.4: k_v of BTEX in different matrix (soil and sand)

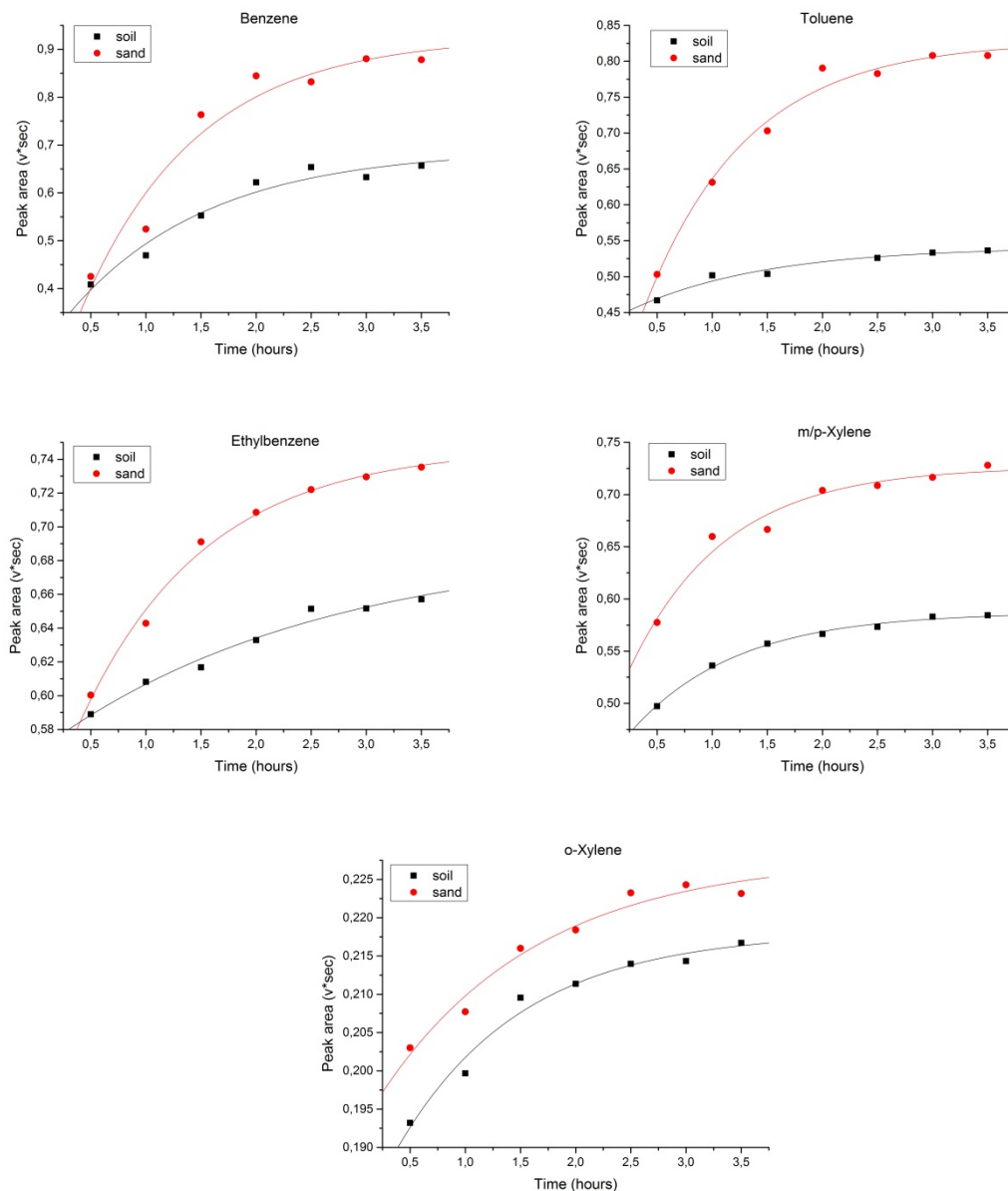|	k_v,(s^{-1}),soil	k_v,(s^{-1}),sand	k_v,(s^{-1})
benzene	2,21E-04±0,33E-04	2,65E-04±0,24E-04	3,69E-04±0,35E-04
toluene	2,30E-04±0,37E-04	3,00E-04±0,50E-04	4,93E-04±0,56E-04
ethylbenzene	1,91E-04±0,51E-04	2,45E-04±0,34E-04	4,67E-04±0,18E-04
m/p-xylene	2,92E-04±0,29E-04	3,21E-04±0,28E-04	4,97E-04±0,15E-04
o-xylene	2,46E-04±0,39E-04	1,96E-04±0,46E-04	4,71E-04±0,47E-04

Figure 6.4: the matrix (sand and soil) effect on diffusion of BTEX in water

6.4.4 BTEX diffusion in real samples

The clean groundwater spiked with BTEX was used in the above experiment. As mentioned in chapter 4, the real contaminated groundwater samples are very complicated, which contain a number of ingredients eg. strongly fluctuating high salinity, iron and manganese, oxygen, petroleum hydrocarbons, heavy metals such as mercury, sediment, and microorganisms. Compared with the real samples, the solution used in simulation experiment is much simpler. The diffusion of BTEX may be influenced by other matrix compounds not only soil or sand. Therefore, it is very necessary to check the diffusion of BTEX in real

groundwater samples. The results of diffusion of BTEX in the real groundwater samples detected by GC-UV-DMS were shown in Figure 6.5, 6.6, 6.7. The values of k_v (in Table 6.5) and equilibration time of BTEX in real groundwater are closed to the results in simulation condition of soil and sand.

Table 6.5: k_v of BTEX in different real samples

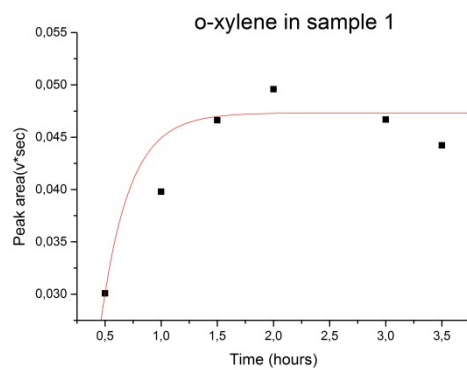|	k_v (s⁻¹), in sample 1	k_v (s⁻¹), in sample 2	k_v (s⁻¹), in sample 3
benzene	2,18E-04±0,63E-04	3,27E-04±0,23E-04	3,43E-04±0,62E-04
toluene	2,97E-04±0,54E-04	2,34E-04±0,34E-04	1,74E-04±0,56E-04
ethylbenzene	2,07E-04±0,51E-04	2,12E-04±0,63E-04	2,32E-04±0,35E-04
m/p-xylene	3,04E-04±0,16E-04	2,51E-04±0,56E-04	3,03E-04±0,57E-04
o-xylene	2,10E-04±0,34E-04	2,22E-04±0,45E-04	1,87E-04±0,35E-04
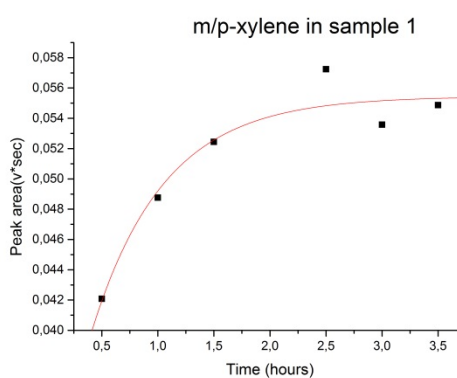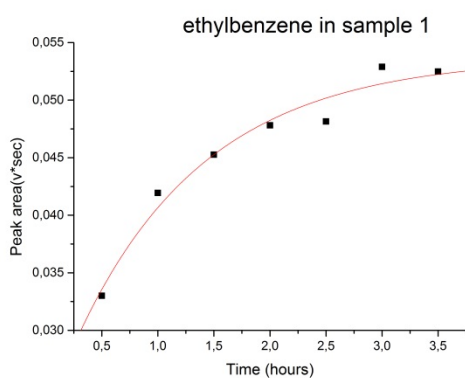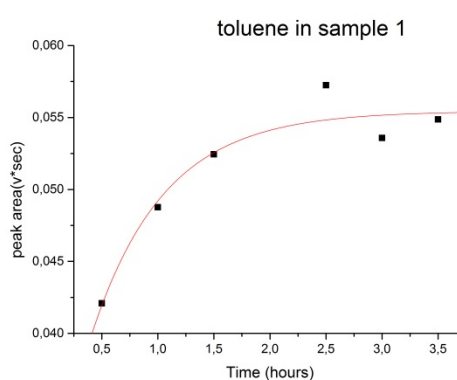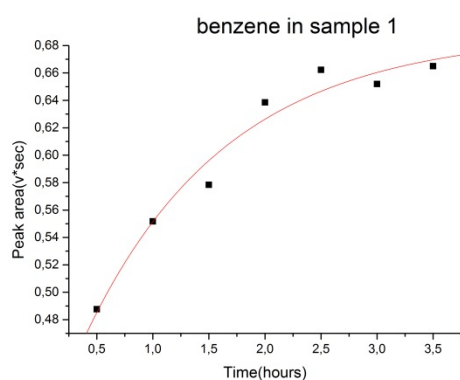
Figure 6.5: diffusion of BTEX in real groundwater (sample 1) collected from northern Germany
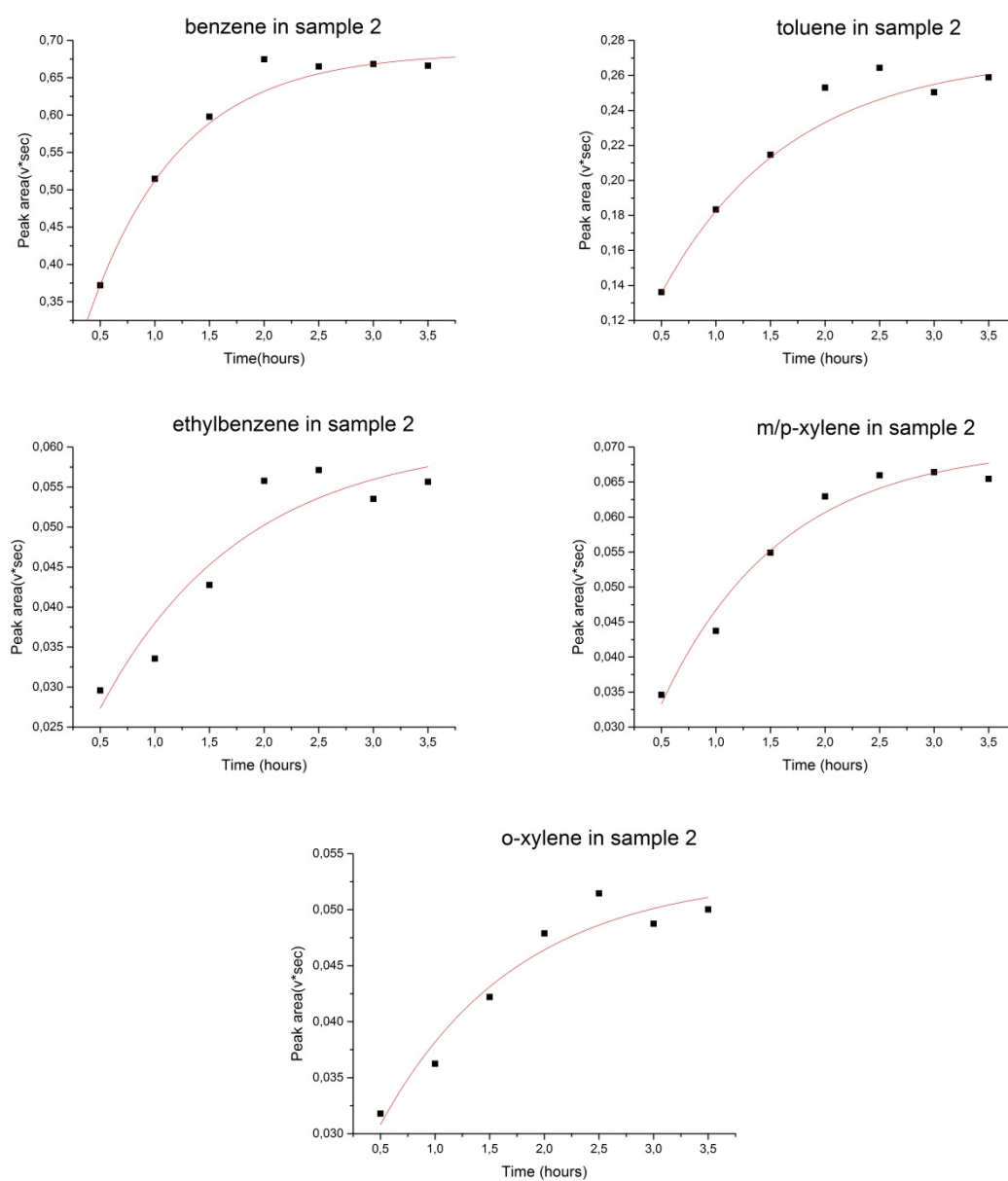
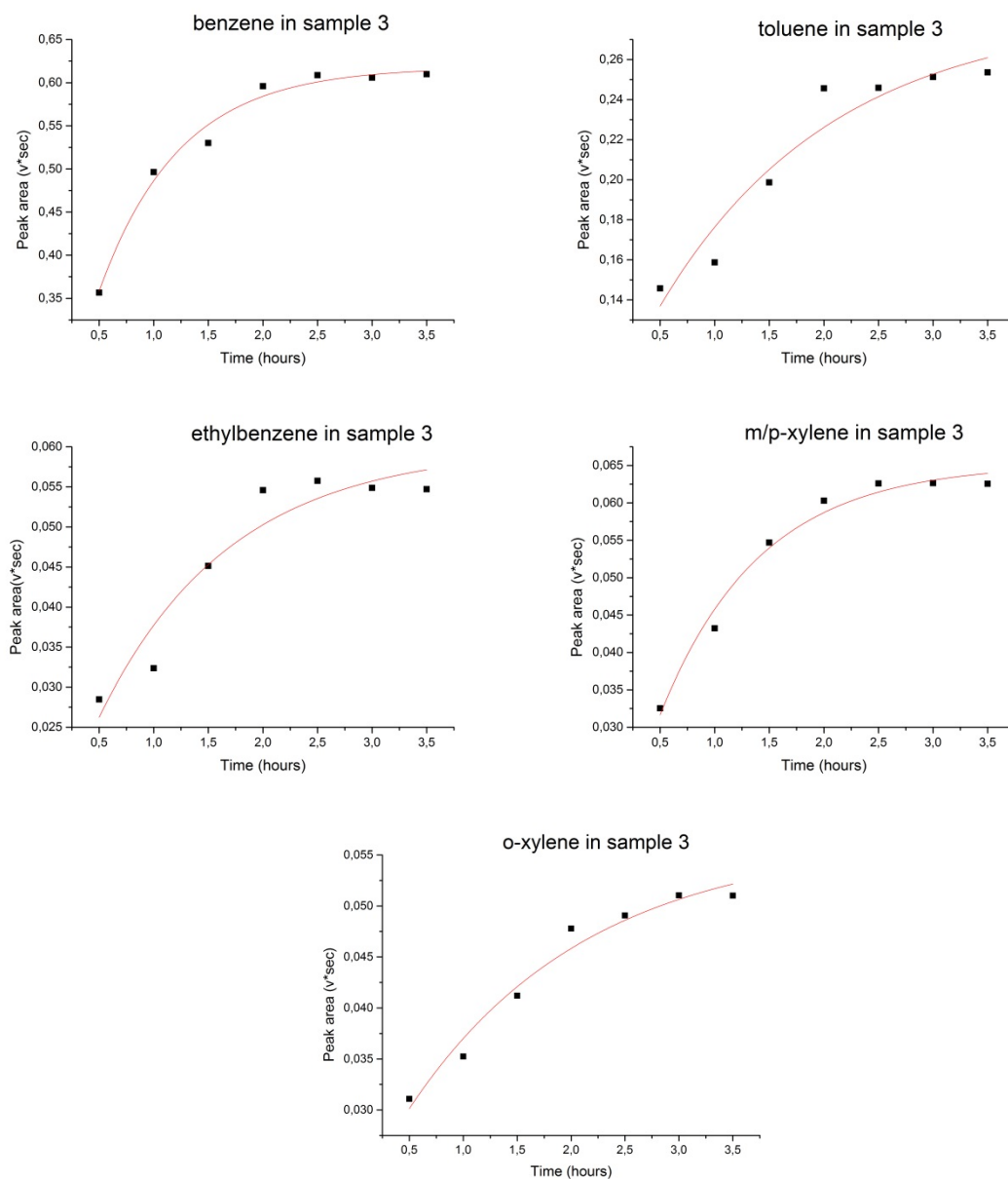Figure 6.6: diffusion of BTEX in real groundwater (sample2) collected from northern Germany

Figure 6.7: diffusion of BTEX in real groundwater (sample3) collected from northern Germany

6.5 Summary

In this chapter, the results of diffusion of BTEX in groundwater were studied by GC-UV-DMS. To simulate the on field condition, simulation tube length was selected and the temperature influencing the diffusion was investigated. In a 0,5 m simulation system, as expected, the values of k_v for target compounds increase as the temperature increases.

Meanwhile, another factor matrix such as sand and soil influencing the diffusions of BTEX were also studied. The k_v of BTEX decline when the solution mixed with sand or soil, which is in a good agreement with that reported in literature. Finally, the real gasoline contaminated groundwater samples were studied by GC-UV-DMS. The equilibration times of BTEX in real groundwater samples are closed to those simulated, about 1,5 to 2,0 hours.

These results reveal that this method based on GC-UV-DMS is feasible to be applied as a system to on-site monitor the groundwater in future.

6.6 References

1.	Mohacsi, A., Z. Bozoki, and R. Niessner, *Direct diffusion sampling-based photoacoustic cell for in situ and on-line monitoring of benzene and toluene concentrations in water.* Sensors and Actuators B-Chemical, 2001. **79**(2-3): p. 127-131.

2.	Clifford K. Ho, R.C.H., Mark W. Jenkins, Daniel A. Lucero, Michael T. Itamura, and a.P.R. Michael Kelley. *Microchemical Sensors for In-Situ Monitoring and Characterization of Volatile Contaminants.* in *the 2001 International Containment and Remediation Technology Conference and Exhibition.* 2001. Orlando, Florida.

3.	Wendell L. Dilling, Nancy B. Tefertiller, and G.J. Kallos, *Evaporation rates and reactivities of methylene chloride, chloroform, 1,1,1-trichloroethane, trichloroethylene, tetrachloroethylene, and other chlorinated compounds in dilute aqueous solutions.* Environ. Sci. Technol., 1975. **9**(9): p. 833–838.

4.	Bidleman, T.F. and L.L. Mcconnell, *A Review of Field Experiments to Determine Air-Water Gas-Exchange of Persistent Organic Pollutants.* Science of the Total Environment, 1995. **159**(2-3): p. 101-117.

5.	Whitman, W.G., *The two-film theory of gas adsorption.* Chem. Metall. Eng., 1923. **29**: p. 146-148.

6.	Liss, P.S. and P.G. Slater, *Flux of Gases across Air-Sea Interface.* Nature, 1974. **247**(5438): p. 181-184.

7.	Higbie, R., *the rate of adsorption of a pure gas into a still liquid during short periods of exposure.* Trans. Am. Inst. Chem. Eng, 1935. **31**: p. 365-389.

8.	Danckwerts, P.V., *Gas Absorption Accompanied by Chemical Reaction.* Aiche Journal, 1955. **1**(4): p. 456-463.

9.	Smith, J.H., D.C. Bomberger, and D.L. Haynes, *Prediction of the Volatilization Rates of High-Volatility Chemicals from Natural-Water Bodies.* Environmental Science & Technology, 1980. **14**(11): p. 1332-1337.

10.	Mackay, D. and P.J. Leinonen, *Rate of Evaporation of Low-Solubility Contaminants from Water Bodies to Atmosphere.* Environmental Science & Technology, 1975. **9**(13): p. 1178-1180.

11.	Mackay, D., et al., *Handbook of Physical-Chemical Properties and Environmental Fate for Organic Chemicals.* 2006, Boca Raton: CRC press.

12.	Roberts, P.V. and P.G. Dandliker, *Mass-Transfer of Volatile Organic Contaminants from Aqueous-Solution to the Atmosphere during Surface Aeration.* Environmental Science & Technology, 1983. **17**(8): p. 484-489.

13.	Bruces, E.P. and P.O.C. John. M. Prausnitz and John, *The properties of gases and liquids. Fifth Edition,.* 2000: McGraw-Hill.

14.	Ferreira, A., et al., *Temperature and solid properties effects on gas-liquid mass transfer.* Chemical Engineering Journal, 2010. **162**(2): p. 743-752.

15.	Yang, W.G., et al., *Experimental study on gas-liquid interfacial area and mass transfer coefficient in three-phase circulating fluidized beds.* Chemical Engineering Journal, 2001. **84**(3): p. 485-490.

16.	Ozkan, O., et al., *Effect of inert solid particles at low concentrations on gas-liquid mass transfer in mechanically agitated reactors.* Chemical Engineering Science, 2000. **55**(14): p. 2737-2740.

17.	David, M.D., N.J. Fendinger, and V.C. Hand, *Determination of Henry's law constants for organosilicones in acutal and simulated wastewater.* Environmental Science & Technology, 2000. **34**(21): p. 4554-4559.

18.	Lin, J.H. and M.S. Chou, *Temperature effects on Henry's law constants for four VOCs in air-activated sludge systems.* Atmospheric Environment, 2006. **40**(14): p. 2469-2477.

7. Conclusion and outlook

7.1 General conclusion

Traditional methods for detecting gasoline related compounds in groundwater are expensive and time consuming. A few monitoring systems exist, but they do not attempt to quantify or characterize the contaminants. This work presents the development of a fast monitoring system based on differential ion mobility spectrometry that can be used to monitor gasoline related compounds in groundwater.

Firstly, BTEX were selected as fingerprint substances. These compounds give a high response on the DMS detector. Therefore, even low concentrations of the gasoline in the groundwater can be detected. After the optimization, it is possible to detect the selected compounds in the range of the usual contaminant concentrations of gasoline in groundwater.

Secondly, a short column MXT-5 was utilized for separating the target compounds (BTEX) in groundwater. The analysis time is less than 2 min. After being coupled to DMS equipped with ^{63}Ni, the detection limits of target compounds in groundwater are 201,80 mg/L for benzene, 9,53 mg/L for ethylbenzene, 50,31 mg/L for toluene, 6,20 mg/L for m-xylene, 8,53 mg/L for p-xylene, and 4,76 mg/L for o-xylene, respectively. The detection limits are higher than that the MCLs regulated by WHO (0,01 mg/L for benzene, 0,7 mg/L for toluene, 0,3 mg/L for ethylbenzene and 0,5 mg/L for total xylene).

Thirdly, in order to improve the detection limits and the sensitivity, a krypton UV lamp is utilized as ionization source instead of ^{63}Ni. The detection limits of BTEX determined by GC-UV-DMS are 0,15 mg/L for toluene, 0,12 mg/L for ethylbenzene, 0,15 mg/L for m-xylene, 0,16 mg/L for p-xylene, 0,16 mg/L for o-xylene, respectively, which are 30 to 330 folds lower than those for ^{63}Ni-DMS. However, the detection limit of benzene is 0,08 mg/L, which is above the MCL recommended by WHO.

Finally, the GC-UV-DMS is used to analyze the concentrations of BTEX in 17 real groundwater samples collected from contaminated sites. In comparison with the reference method, the results of EXT obtained by GC-UV-DMS are in good agreement with those obtained by reference method. However, the mean concentration of benzene obtained by GC-UV-DMS is lower than that obtained by reference method. To simulate the on field condition, the factors influencing the diffusion such as temperature, matrix component are discussed. In a 0,5 m simulation system, the mass transfer k_v of target compounds increase as the temperature increase. Meanwhile, the k_v of BTEX decline when groundwater containing sand or soil. Additionally, the results of diffusion of BTEX in real contaminated groundwater samples were presented by GC-UV-DMS.

The results reveal that the method based on GC-UV-DMS is feasible to be applied as a fast system to monitor the groundwater. The whole analysis time is less than 2 min. Moreover, the detection limits for ETX are lower than the MCLs of WHO. However, there are still several problems to overcome. The dynamic ranges of the determination of BTEX are limited. The detection limit for benzene is higher than that regulated by WHO. The mean concentration of benzene in real groundwater detected by GC-UV-DMS is lower than that obtained by reference method.

7.2 Outlook

The present study on GC-UV-DMS could be applied as a fast device for monitoring groundwater routinely. However, there are still some problems to overcome in future, which are listed as follows:

1, the ionization sources for DMS is one of the key factors influencing the sensitivity of target compounds such as BTEX. For example, the device equipped with krypton lamp has lower detection limit than that with [63]Ni, but high energy consumption. For portable device, the balance between the sensitivity and power consumption should be achieved.

2, the dynamic ranges of BTEX are limited. Furthermore, the detection limit of benzene is 0,08 mg/L, higher than the MCL recommended by WHO. In order to implement this technique as portable device, the dynamic ranges and detection limit for benzene should be improved.

3, all results in this thesis are obtained in lab without any on site analysis. To evaluate the feasibility of DMS to be used as on field system. The on-site test should be done in future.

Publication List:

F. Liang, K. Kerpen, A. Kuklya, U. Telgheder, Fingerprint identification of volatile organic compounds in gasoline contaminated groundwater using gas chromatography differential mobility spectrometry, *International journal of ion mobility spectrometry*, 2011,15(3), 169-177

Posters and Presentations

F. Liang, K. Kerpen, A. Kuklya, U. Telgheder, (oral presentation) Fast onsite determination of gasoline related compounds in groundwater by differential mobility spectrometry *4th Tagung von ion mobility spectrometry*, 2011, Berlin, Germany

F. Liang, K. Kerpen, A. Kuklya, U. Telgheder,(poster) Fast onsite determination of gasoline related compounds in groundwater by differential mobility spectrometry. *WWEM 2012*, Telford, England

F. Liang, K. Kerpen, A. Kuklya, U. Telgheder, (poster) Detection of BTEX in groundwater by Differential Mobility Spectrometry, *SPI-Water Conference, 2012*, Brussels, Belgium

F. Liang, K. Kerpen, A. Kuklya, U. Telgheder, (poster) Fast determination of gasoline related compounds in groundwater by MicroAnalyzer, *ANAKON 2013*, 2013, Essen, Germany

F. Liang, K. Kerpen, A. Kuklya, U. Telgheder, (oral presentation) Fast determination of gasoline related compounds in groundwater by fast GC-UV-DMS *Water: the greatest global challenge*, 2013, Dublin, Ireland

F. Liang, K. Kerpen, A. Kuklya, U. Telgheder, (poster) Fast determination of BTEX in groundwater by fast GC-UV-DMS, *22th International conference on ion mobility spectrometry 2013*, 2013, Boppard, Germany

LEBENSLAUF

Persönliche Daten

Name · · · · · · · · · · · · · · · · Feng Liang
Email-Adresse: · · · · · · · · · · feng.p.liang@gmail.com
Familienstand · · · · · · · · · · · verheiratet
Staatsangehörigkeit · · · · · · · chinesisch
Geburtsdaten und Ort: · · · · · · 14.10.1981 in Jiangsu, China

Schulische Ausbildung/Studium

09.2000 – 06.2004	Bachelor in Bioscience, Studium an Nanjing Normal University, Jiangsu, China Thesis:"determination of organic compounds in medicinal herb by high performance liquid chromatograph"
09.2004 – 06.2007	Master in Chemie, Studium an University of Chinese Academy of Sciences, Beijing, China Thesis:"the behavior of nanoparticles in airborne $PM_{2,5}$"
11.2010-	PhD student im Bereich der Chemie an der Universität Duisburg-Essen, Essen Thema:"fast monitor of gasoline related compounds in groundwater"

Berufliche Erfahrungen

01.08.2007 - 30.07.2008	wiss. Mitarbeiter am Pasteur Institut in Shanghai, Chinese Academy of Sciences, Shanghai, China
01.08.2008 – 30.07.2010	wiss. Mitarbeiter am Shanghai Institut für Angewandte Physik, Chinese Academy of Sciences, Shanghai, China
01.10.2010 – 30.09.2013	Marie Curie Early Stage Researcher bei IWW Rheinisch-Westfälisches Institut für Wasserforschung gemeinnützige GmbH, Mülheim an der Ruhr, Deustchland

Erklärung

Hiermit versichere ich, dass ich die vorliegende Arbeit mit dem Titel

„Fast determination of gasoline related compounds in groundwater by differential ion mobility spectrometry"

selbst verfasst und keine außer den angegebenen Hilfsmitteln und Quellen benutzt habe, und dass die Arbeit in dieser oder ähnlicher Form noch bei keiner anderen Universität eingereicht wurde.

Essen, im Januar,2014